FACULDADE DE ENGENHARIA DA UNIVERSIDADE DO PORTO

Optimization of an airplane wing representative structure for vibration and buckling

Tiago António da Silva Soares

Dissertation submitted to Faculdade de Engenharia da Universidade do Porto for the degree of:
Master in Mechanical Engineering

Supervisor: Carlos Alberto Conceição António (Cathedratic professor)

Co-supervisor: Pedro Manuel Leal Ribeiro (Associate professor)

Porto, October 2022

Optimization of an airplane wing representative structure for vibration and buckling

Tiago António da Silva Soares

Dissertation submitted to Faculdade de Engenharia da Universidade do Porto for the degree of:
Master in Mechanical Engineering

Porto, October 2022

Abstract

The design of composite structures for the aerospace industry is a multidisciplinary task, involving several coupled domains, which increases significantly the development time. Besides that, the necessity to comply with too many requirements in order to establish the system's performance makes that design even more complicated. The aerospace industry has strict rules regarding the design of those structures, mainly because they are high-responsibility applications. Therefore, each individual design must be validated by suitable tests, which are, normally, time-consuming. Multidisciplinary optimization procedures became an alternative over time, because they are capable of considering several domains simultaneously and the interaction between them as well, satisfying design constraints taking into account one or more objectives.

In this report, an airplane wing representative structure provided by the Cardiff School of Engineering is scrutinized. An evolutionary-based algorithm, genetic one, is applied in order to maximise the fundamental natural frequency and the critical buckling load of the representative structure, under several prescribed constraints and altering only the plies' orientations or thicknesses. An artificial neural network is used to predict the output values necessary for the application and development of the genetic algorithm, reducing the number of FEM simulations needed, using Abaqus® software. The genetic procedure is used both for optimising the ANN's configuration and to achieve the desired maximised ω_1 or P_{crit} value.

Firstly, the structure is optimised regarding its fundamental natural frequency, ω_1, by changing the plies' orientations and afterwards adding the thicknesses as design variables. The structure's vibration amplitude may excessively increase if the excitation frequencies are close to the important ones in the excitation spectrum, particularly for lower-damping structures, which may damage other components or even cause human casualties. The maximisation of the first natural frequency of vibration is a means of avoiding this issue when the first mode of vibration dominates the response. For each individual optimization procedure, the relative importance of each design variable on the variance of the output response is calculated based on the first order *Sobol* indices. Moreover, an analytical approach based on the *Rayleigh-Ritz* method is provided in order to predict the natural frequencies of the composite stiffened panel.

Due to the unpredictability of a certain structure pos-buckling, the airplane wing representative structure is also optimised with regard to its critical buckling load. Therefore, the structure's loading spectrum can be enlarged without compromising its performance and safety. The plies' angles and thicknesses of the composite panel are conveniently modified. Furthermore, the linear aggregation method is used to consider the minimisation of the structure's weight as an additional objective. The *Lévy*'s method is applied to formulate an approach capable of determining the buckling loads of a composite panel, owing to its ease of implementation.

Keywords: Composite laminate, Artificial neural network, Uniform design method, Genetic algorithm, Fundamental natural frequency, Critical buckling load.

Resumo

O projeto de estruturas compósitas para a indústria aeroespacial é uma tarefa multidisciplinar, envolvendo vários domínios acoplados, o que aumenta significativamente o tempo de desenvolvimento. Além disso, a necessidade de cumprir com muitos requisitos para estabelecer o desempenho do sistema torna esse projeto ainda mais complicado. A indústria aeroespacial possui regras rígidas no que diz respeito ao projeto dessas estruturas, principamente por se tratarem de aplicações de alta responsabilidade. Consequentemente, cada projeto individual deve ser validado por testes adequados, que são, normalmente, demorados. Procedimentos de otimização multidisciplinar tornaram-se uma alternativa ao longo do tempo, por serem capazes de considerar vários domínios simultaneamente assim como a interação entre eles, satisfazendo diversas restrições de projeto tendo em consideração um ou mais objetivos.

Neste documento analisa-se uma estrutura representativa de uma asa de um avião fornecida pela *Cardiff School of Engineering*. Um algoritmo baseado na evolução, algoritmo genético, é aplicado com o objetivo de maximizar a frequência natural fundamental e a carga crítica de encurvadura da estrutura representativa, sob várias restrições pré-estabelecidas e alterando apenas as orientações e espessuras das camadas de material compósito. Uma rede neuronal artificial é usada para obter os valores de saída necessários à aplicação e desenvolvimento do algoritmo genético, reduzindo o número de simulações de elementos finitos através do *software* Abaqus®. O procedimento baseado na genética é usado quer para otimizar a estrutura da rede neuronal quer para obter o valor maximizado desejado, ω_1 ou P_{crit}, conforme o problema.

Primeiramente, a estrutura é otimizada no que diz respeito à sua frequência natural fundamental, ω_1, através da mudança das orientações das camadas e, de seguida, acrescentando as espessuras como variáveis de projeto. A amplitude de vibração da estrutura pode aumentar consideravelmente se as frequências de excitação forem próximas de frequências importantes no espetro de excitação, particularmente para estruturas de baixo amortecimento, o que pode danificar outras estruturas adjacentes ou até causar falhas humanas. A importância relativa de cada variável de projeto na variância da variável de saída é expressa através dos indíces de *Sobol* de primeira ordem para cada procedimento de otimização realizado. Adicionalmente, um procedimento analítico baseado no método de *Rayleigh-Ritz* foi desenvolvido com o objetivo de obter as frequências naturais do painel compósito com reforços longitudinais de alumínio.

O comportamento de uma certa estrutura pós-encurvadura é completamente imprevisível, sendo acompanhada por mudanças de rigidez, logo a sua otimização em relação à carga crítica de encurvadura é também de extrema importância. Assim, o espetro de cargas admissível para a estrutura pode ser alargado sem comprometer o seu desempenho e segurança. As orientações e espessuras das camadas do painel compósito são convenientemente modificadas. O método da agregação linear é usado a fim de considerar a minimização do peso da estrutura como um objetivo adicional. O método de *Lévy* é aplicado com o objetivo de formular um procedimento analítico capaz de determinar as cargas de encurvadura de um painél compósito, devido à sua facilidade de

implementação.

Keywords: Laminado compósito, Rede neuronal artificial, *Uniform Design Method*, Algoritmo genético, Frequência natural fundamental, Carga crítica de encurvadura.

Acknowledgements

This thesis was written as part of the COST action CA18203, "Optimising Design for Inspection", which has been supported by the Horizon 2020 framework initiative of the European Union. In addition, I want to express my gratitude to everyone who contributed to making the present report feasible:

- To Prof. Carlos Conceição António for sharing his knowledge, availability and motivation to always improve on my work;
- To Prof. Pedro Leal Ribeiro for the theme suggestion and for his prompt support;
- To all COST action members who made a contribution to the development of the current work;
- To my friends at FEUP, particularly André Ramos, Guilherme Tavares, João Pedro Alves and Rúben Araújo, for the companionship over these 5 years, helping me to grow both personally and professionally;
- To my family, especially my parents, for their unconditional support.

Tiago Soares

This article/publication is based upon work from COST Action 18203—Optimized Design for Inspection (ODIN), supported by COST (European Cooperation in Science and Technology). COST (European Cooperation in Science and Technology) is a funding agency for research and innovation networks. Our Actions help connect research initiatives across Europe and enable scientists to grow their ideas by sharing them with their peers. This boosts their research, career and innovation.
www.cost.eu

EUROPEAN COOPERATION IN SCIENCE & TECHNOLOGY

Funded by the European Union

"The only true wisdom
is in knowing you know nothing."

Socrates

Contents

List of Figures

List of Tables

List of symbols

Abbreviations

ACO	**A**nt **C**olony **O**ptimization
AI	**A**rtificial **I**ntelligence
ANN	**A**rtificial **N**eural **N**etwork
AFP	**A**utomated **F**ibre **P**lacement
BSA	**B**acktracking **S**earch **A**lgorithm
BFO	**B**acterial **F**oraging **O**ptimization
BCA	**B**ee **C**olony **A**lgorithm
BRKGA	**B**iassed **R**andom **K**ey **G**enetic **A**lgorithm
BB-BC	**B**ig **B**ang-**B**ig **C**runch
BBD	**B**ox **B**ehnken **D**esign
CFRP	**C**arbon **F**iber **R**einforced **P**olymer
CCD	**C**entral **C**omposite **D**esign
CFO	**C**entral **F**orce **O**ptimizer
CBGA	**C**entre **B**ased **G**enetic **A**lgorithm
CSS	**C**harged **S**ystem **S**earch
CAD	**C**omputer-**A**ided **D**esign
CNN	**C**onvolutional **N**eural **N**etwork
CSA	**C**uckoo **S**earch **A**lgorithm
DM	**D**ata **M**ining
DMT	**D**ata **M**ining **T**echnology
DL	**D**eep **L**earning
EP	**E**nlarged **P**opulation
COST	European Cooperation in Science and Technology
FEM	**F**inite **E**lement **M**ethod
FA	**F**irefly **A**lgorithm
FORM	**F**irst **O**rder **R**eliability **M**ethod
FFD	**F**ull **F**actorial **D**esign
GbSA	**G**alaxy-**b**ased **S**earch **A**lgorithm
GA	**G**enetic **A**lgorithm
GSA	**G**lobal **S**ensitivity **A**nalysis
GSA	**G**ravitational **S**earch **A**lgorithm
HSA	**H**armony **S**earch **A**lgorithm
ICA	**I**ndependent **C**omponent **A**nalysis
LOA	**L**ayerwise **O**ptimization **A**pproach

LSA	**L**ightning **S**earch **A**lgorithm
ML	**M**achine **L**earning
MAC	**M**odal **A**ssurance **C**riterion
MCS	**M**onte **C**arlo **S**imulation
MPP	**M**ost **P**robable Failure **P**oint
MDO	**M**ulti-**D**isciplinary **O**ptimization
MOGA	**M**ulti-**O**bjective **G**enetic **A**lgorithm
MOHGA	**M**ulti-**O**bjective **H**ierarchical **G**enetic **A**lgorithm
NDI	**N**on-**D**estructive **I**nspection
NSGA	**N**on-Dominated **S**orting **G**enetic **A**lgorithm
NTM	**N**umber-**T**heoretic **M**ethod
OAD	**O**rthogonal **A**rray **D**esign
PSO	**P**article **S**warm **O**ptimization
PWAS	**P**iezoelectric **W**afer **A**ctive **S**ensor
PCA	**P**rincipal **C**omponent **A**nalysis
RNN	**R**ecurrent **N**eural **N**etwork
RE	**R**elative **E**rror
RPSOLC	**R**epulsive **P**article **S**warm **O**ptimization with **L**ocal Search and **C**haotic Perturbation
RMSE	**R**oot-**M**ean-**S**quare **E**rror
SORM	**S**econd **O**rder **R**eliability **M**ethod
SA	**S**imulated **A**nnealing
SP	**S**mall **P**opulation
SHM	**S**tructural-**H**ealth **M**onitoring
SVM	**S**upport **V**ector **M**achine
UD	**U**niform **D**esign
UDM	**U**niform **D**esign **M**ethod
VCH	**V**iolation **C**onstraint-**H**andling

General Notation

a, A	Scalar (italic)
$\mathbf{a}$, $\{\bullet\}$	Vector (bold + lowercase)
$\mathbf{A}$, $[\bullet]$	Second-order tensor (bold + uppercase)

Operators

$\dot{(\,)} = \mathrm{d}\,(\bullet)/\mathrm{d}\,(\bullet)$	First total time derivative
$\ddot{(\,)} = \mathrm{d}^2\,(\bullet)/\mathrm{d}\,(\bullet)^2$	Second total time derivative
$\partial\,(\bullet)/\partial\,(\bullet)$	Partial derivative
$\nabla\,(\bullet)$	Gradient operator
$\sum\,(\bullet)$	Summation operator
$\det(\bullet) = \lvert[\bullet]\rvert$	Determinant
$\delta(\bullet)$	First variation/Virtual quantity
$(\bullet)\cdot(\bullet)$	Single contraction / dot product between two tensors
$\int_l (\bullet)\,\mathrm{d}l$	Integral
$\iint_A (\bullet)\,\mathrm{d}A$	Double integral
$\mathrm{var}\langle\,(\bullet)\,\rangle$	Variance
$\mathrm{var}\langle\,\mathrm{E}\,\langle\,(\bullet)\mid(\bullet)\,\rangle\rangle$	Variance of the conditional expectation

Greek Symbols

Γ	Boundary of the plate
Ω_0	Continuum domain
λ_{crit}	Critical load factor
ε	Damping ratio
ρ	Density
μ	Dynamic amplification factor
σ_y	Elastic limit stress
Γ_{error}	Error component associated to the biases
$\boldsymbol{\phi}_X$	Experimentally-measured mode shape
$\boldsymbol{\lambda}_{fix}$	Fixed values vector
β	Frequency ratio
ω_i	i^{th} natural frequency
θ_i	i^{th} ply orientation variable
η	Learning rate of the backpropagation algorithm
ε_i	Limit value assigned to the ith transformed objective
α	Momentum rate of the backpropagation algorithm
ε, η	Natural coordinates
ε	Normal deformation
σ	Normal stress
κ	Parameter of the gaussian function
β_h	Parameter of the hyperbolic tangent function
α, β	Parameters relative to the *Jacobi* polynomials
ϕ_j	Particular constraint
ν	Poisson ratio
λ_i	Roots of the characteristic function
ψ	Shape function
γ	Shear deformation
τ	Shear stress
β_{sig}	Slope of the sigmoidal function curve at its inflection point
$\boldsymbol{\phi}_A$	Theoretically-predicted mode shape
Π	Total energy of the stiffened plate
$\boldsymbol{\varepsilon}_0^b$	Vector of curvatures at the middle surface
$\boldsymbol{\varepsilon}_0^m$	Vector of membrane strains at the middle surface
μ_i	Weight assigned to the ith objective

Latin Symbols

E_{abs}	Absolute error resulted from the training procedure
u	Activation potential
P_{opt}^{ANN}	ANN configuration resulted from the optimization procedure
T_i	Aspiration level assigned to the ith objective
B_{ij}	Bending-extensional stiffness coefficient
M	Bending or twisting moment
D_{ij}	Bending stiffness coefficient
b_i	Bias associated to input node i
$\mathbf{r}^{(L)}$	Bias vector associated to the neurons of layer L

$\mathbf{f}$	Body forces vector
A_i, B_i, C_i	Coefficients which weight each shape function relative to a certain displacement
c	Compressive
P_{crit}	Critical buckling load
d_{crit}	Critical displacement
$\mathbf{d}$	Desired output vector
N_{pop}	Dimension of the population
m, n	Director cosines
u, v, w	Displacement components
$\mathbf{u}$	Displacement vector
q_b	Distributed force per unit area at the bottom of the panel
q	Distributed force per unit area at the panel
q_t	Distributed force per unit area at the top of the panel
E	Error function
A_{ij}	Extensional stiffness coefficient
$\mathrm{FIT}^{(2)}$	Fitness function associated to the physical variable maximisation
$\mathrm{FIT}^{(1)}$	Fitness function for the optimization of the ANN configuration
$\mathscr{P}\mathbf{f}^*$	Front of Pareto
U, V, W	Functions representative of the deformed shape of the plate
i, j, k, l, m, n	General indices
k	Index assigned to each composite lamina
$\mathrm{d}A$	Infinitesimal surface element
$\mathrm{d}V$	Infinitesimal volume element
h_i	i^{th} ply thickness variable
$P_n^{(\alpha,\beta)}(l)$	*Jacobi* polynomial of order n
T	Kinetic energy
L	Length of the composite panel
d_{min}, d_{max}	Limit values of a certain variable
R	Linear aggregator
m	Mass
$\mathbf{M}$	Mass matrix
N_{gen}	Maximum number of generations
t_c	Maximum number of random variables associated to a specific design table
N	Membrane force
$LIMDIF$	Minimum number of equal genes/variables between two different individuals selected from the population capable of taking one out from the population
MAC	Modal Assurance Criterion
I	Moment of inertia
p_n	Natural number which depends upon the number of experiments
$\mathbf{d}_k$	Nodal displacement vector
X, Y, Z	Normal strength
$\overline{S}_i^O$	Normalised Sobol index associated to each variable x_i
$\overline{d}_k$	Normalised value of a certain variable

C_0	Number of central points
N_r	Number of combinations of a fixed and a sample matrix values
n_L	Number of composite layers
n_{exp}	Number of experiments
s	Number of factors
n_e	Number of finite elements
N_f	Number of fixed values
INP	Number of input nodes
INT	Number of intermediate/hidden nodes
n	Number of nodes
n_{nod}	Number of nodes of each particular finite element
OUT	Number of output nodes
N	Number of repetitions of the optimization procedure
N_{stiff}	Number of stiffeners
k_{sub}	Number of subpopulations
B	Offspring group
y_j	Output value associated to node j
c	Parameter of the gaussian function
F_i, F_{ij}, F_{ijk}	Parameters related to the lamina strengths in the principal directions
P_{dist}	Parameter which defines the metric used to quantify the distance between the reference point and the admissible region of the search space
$\mathbf{x}^*$	Pareto optimal
$\mathrm{P}^{(t)}$	Population of solutions for each t-generation of the first genetic algorithm
$\mathrm{X}^{(t)}$	Population of solutions for each t-generation of the second genetic algorithm
p	Pressure acting on the composite panel
d_N^{min}, d_N^{max}	Range of normalisation
d_k	Real value of a certain variable before normalisation
$\overline{Q}_{ij}$	Reduced stiffness coefficient
$\mathbf{z}$	Reference point for multi-objective optimization
$\mathbf{x}^0$	Reference position vector
RE	Relative error
E_{rel}	Relative error resulted from the training procedure
$RMSE$	Root-mean-square error
$\mathbf{J}_\alpha$	Sample matrix
$\mathscr{P}^*$	Set of Pareto's optimals
N_k	Shape function related to node k
G	Shear modulus
S	Shear strength
S_i^O	Sobol index associated to each variable x_i
$\mathbf{S}$	Space of admissible solutions
y_s	Spatial localization of a stiffener along the Oy axis
Q_{ij}	Stiffness coefficient
$\mathbf{K}$	Stiffness matrix
U_s	Strain energy
U_0	Strain energy per unit volume

t	Tensile
t_{ply}	Thickness of each ply of the panel provided by Cardiff School of Engineering
t	Time
$\hat{\mathbf{t}}$	Tractions vector acting on panel's surface
U	Uniform probability distribution function
$c_1, c_2, c_3, k^1, k^2, \alpha_j$	User-defined constants
x_i	Value of the ith input node
$\mathbf{x}$	Vector of design variables
$\mathbf{f}$	Vector of objectives
$\delta\mathbf{u}$	Virtual displacement vector
$\mathbf{W}_{ji}^{(L)}$	Weight matrix whose elements denote the value of the synaptic weight that connects the jth neuron of layer (L) to the ith neuron of layer $(L-1)$
w_{ij}	Weight value between nodes i and j
$\mathbf{y}_j^{(L)}$	Weight vector whose elements denote the output value related to the jth neuron of layer (L)
$\mathbf{i}_j^{(L)}$	Weight vector whose elements denote the weighted input value related to the jth neuron of layer (L)
$A(l)$	Weighting function
b	Width of the composite panel
F	Work done by external forces
E	Young modulus

Chapter 1

Introduction

1.1 Background and motivation

Over time, the need to develop lighter and more mechanically efficient aircraft structures led to an evolution in the structural materials used from the metals, such as steel, aluminium and titanium to composite and hybrid materials. Advanced composites have high-performance reinforcements of a thin diameter embedded in a matrix material such as epoxy or ceramic [1]. Even though the costs of composite materials may be higher, the fact that there are fewer components in an assembly and the cost savings from fuel make them more economical than monolithic metals. Over traditional materials, composites have a number of additional benefits, such as a better specific strength and stiffness, fatigue resistance, impact resistance, thermal conductivity or corrosion resistance, which make them suitable for those demanding applications [1–3].

The main disadvantages of composite materials for aircraft structures are their high cost of fabrication, taking into account the raw material, its processing and certification; their complex mechanical characterization in comparison with the monolithic materials, their relatively low resistance to mechanical impact and through-thickness strength due to low failure strains if the matrix is thermosetting, compared to the metal structures; they do not have neither a high combination of strength and fracture toughness nor a high strength in the out-of-plane direction. Furthermore, the shear stresses produced between the layers, particularly at the edges of the laminate, may cause delamination and the repair procedures are much more complex in comparison with the metals [1–3].

Besides that, in order to make that evolution affordable and amortisable, there is an initial investment to pay for the manufacturing processes change, the automation of the assembling lines and the development of the inspection departments, since the type of defects expected are now different and, sometimes, more difficult to detect. Repair of composites is not a simple task and critical flaws and cracks may go undetected [1, 2].

The majority of polymer matrices used in aerospace applications are epoxy-based due to their high strength, good wetting of fibres during processing and adhesion, low viscosity and low flow rates, low volatility during cure, low shrink rates, and availability in more than 20 grades to meet specific property and processing requirements [2, 3]. Limited operating temperatures, high coefficients of thermal and moisture expansion and low elastic properties in certain directions are the main limitations of polymer matrix composites. Minor epoxies are often added to the main compound in order to surpass some of those obstacles [2, 3].

Regarding the joining of composite structures, they evolved from the mechanical fastening, such as bolts and rivets, welding or soldering to more advanced technology denominated adhesive joints [4]. The adhesives are preferred to avoid the stress concentrations zones resulted from drilling operations. However, these drills are also utilised for interior access or the electronic components implementation. Their design is a very complex task, since these are often the weakest spots and there is the necessity for the connections to be reliable, distribute the load uniformly and, at the same time, be lighter [1, 4, 5]. Although the adhesive joints have better fatigue properties and less stress concentration, there are still some concerns to take into account, such as the inspection difficulties, the need for complex tools and the susceptibility to environmental degradation, due to the inevitable contact with chemical agents [1, 4, 5].

Flaws occur inevitably at composite structures, particularly between the layers and at the adhesive interfaces. They can arise either from the manufacturing process, during the ply collation, curing, adhesive bonding or machining and assembly procedures or throughout their service life. The most common are debonds, porosities, matrix cracks as manufacturing defects, and delaminations, corrosion, impact damage and fatigue during their service life [3, 6, 7] . Delamination, separation of layers resulted from loading conditions, and debond, inadvertent separation between adherends in a adhesively bonded joint during the fabrication process, are the most commonly observed failure modes among the several failure mechanisms [3, 6, 7].

There are several and strict regulations to the types and amount of damage allowed in structured materials without replacement or repair of the damaged component. Furthermore, the inhomogeneity and inherent anisotropy of composite structures make their design even further complicated, particularly for damage tolerance requirements. In order to achieve the large variety of possible defects, the aerospace industry relies on the non-destructive inspection (NDI), which is used to determine the type, size and location of damage. The main procedures range from a simple visual inspection for macroscopic flaws detection to more advanced technologies, such as ultrasonics, radiography, thermography, among others [3, 6, 8].

Nevertheless, these inspection methodologies take a lot of time, which increases substantially the total cost. Therefore, structural health monitoring techniques (SHM) are increasingly used over the time to detect defects and damage. SHM uses in situ sensor networks and intelligent data processing for continuous inspection with little or no human intervention. These sensors ought to be fairly priced, lightweight, and unobtrusive so as not to increase the structure's cost or weight or interfere with its airworthiness [6, 9]. Some examples are the conventional resistance strain gauges, which consists in the conversion between a strain change into a resistance change measured with a

precise instrument; the fiber optic sensors whose functionality is based on their optical properties or the piezoelectric-based sensors coupling the electric and mechanical variables, denominated by PWAS (piezoelectric wafer active sensor) [6, 9].

In today's engineering and, in particular, in the aerospace industry, designers have to challenge themselves in order to comply with the endless requirements, which range from the system's specifications and constrained development time to the need to establish the system's performance accurately in the first design stages.

In the aerospace industry, manufacturers create a wide range of composite structures exhibiting complex and different material behaviours as well as several designs, leading to the need of testing each one of them for validation, which is time consuming and expensive. Optimization procedures could constitute a solution, because they consider several domains and their own goals, as well as the interaction between them, that is, the goal is to find practical optimal solutions satisfying a given set of design constraints and requirements [10]. The design of aerospace systems is a multidisciplinary and complex process, which makes those procedures even more fundamental. Furthermore, composite materials offer more design variables than do metals, therefore they allow for more refined tailoring and more extensive optimization [10].

Regarding the aircraft structures, they are usually thin shell structures, whose outer surface or skin may be reinforced with longitudinal stiffening members and transverse frames to resist from bending, compressive and torsional loads without buckling. These ones are known as semi-monocoque structures. Otherwise, the monocoque structures rely exclusively in the load carrying capacity of their skin. Therefore and regardless of their construction or complexity, an aircraft structure is used to transmit and resist external loads, to provide an aerodynamic shape and to protect passengers and so forth from the environmental conditions encountered during a flight [11].

Wing structures are composed of thin skins and stiffening elements, such as stringers, spar webs and caps, and ribs. The overall structure is comprised by many cells closely spaced, which enables to assume a constant shear flow in the skin between adjacent stringers. Bending moments at any section of a wing typically result in shear loads at other sections of the wing. The ribs are transverse components which increase the column buckling stress of the longitudinal stiffeners (stringers), due to an end constraint on their column length, and the plate buckling stress of the skin panels. Ribs act as formers for the aerofoil shape at the outer zones of the wing, owing to low load levels. On the other hand, they have a robust construction closer to the wing root due to the necessity to absorb and transmit high concentrated loads derived from the undercarriage, engine thrust or fuselage attachment points reactions. In turn, the impermeable wing skin supports the aerodynamic pressure distribution capable of generating the lift necessary during a flight. Those forces are then absorbed by the ribs and stringers. Despite its high performance in resisting shear and tensile loads, wing skin generally buckles under low compressive loads, being the stiffening elements fundamental in avoiding or delaying that issue, as referred above. Regarding the spar webs, their main function is to develop shear stresses capable of resisting shear and torsional loads, performing a stabilizing function in the overall structure [11, 12].

Due to their flexibility, aircraft structures are extremely susceptible to distortion under load, which influences the aerodynamic forces and, consequently, further structural distortion is developed. Aircraft vibration may be generated by aerodynamics, mechanical issues or outside sources such as atmospheric turbulence. Every airplane has a characteristic normal vibration signature. This is a result of vibration modes at particular frequencies triggered by mass distribution and structural stiffness. Very low-level vibrations occur when the airplane is subjected to typical airflow over its surfaces. However, the airplane's response to turbulent air is more evident and the vibration's magnitude may be greater and audibly detectable [13, 14].

Therefore, the main objectives of this work are to implement and develop an optimization framework, particularly embedded in a genetic algorithm, in an airplane wing representative structure composed of aluminium and composite materials assembled with hybrid joints, in order to achieve optimal configurations regarding the fundamental natural frequency of the structure, with the aim of avoiding an undesirable amplitude of vibration, and the maximum critical buckling load, aiming to assure the structure's safety, varying the stacking sequence, fibres' orientations and layers' thicknesses.

1.2 Optimising design for inspection

The European Cooperation in Science and Technology (COST) develops several actions, named COST actions, whose main goal is to create research networks between european scientists and, therefore, to contribute to research development and advancement. The present thesis is developed within the EU COST action CA18203, "Optimising Design for Inspection". The goal is to support the development of an integrated framework for optimised self-sensing structures capable of diagnosis and prognosis, together with demonstrators and educational activities, including training programs, which ultimately lead to cleaner and safer skies [15].

This work integrates the group responsible for establishing the design criteria based on industry needs and to analyse the requirements for integrating structural health monitoring systems (SHM) at the beginning of the design. The structure that represents the airplane wing was made available by the Cardiff School of Engineering in cooperation with the company Airbus and it is represented below, Figure 1.1.

The airplane wing representative structure is composed by two composite plates reinforced by aluminium longitudinal and transverse stiffeners. For assembling the several components, mechanical fasteners and adhesive joints are used.

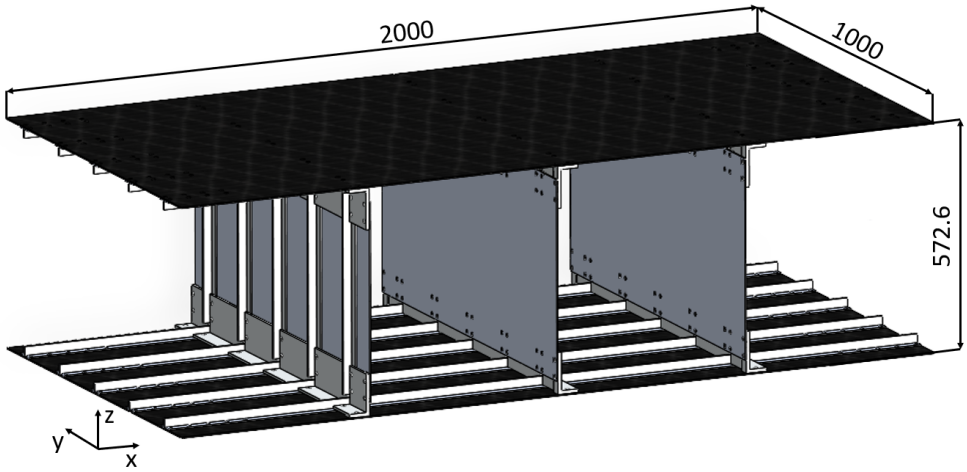

Figure 1.1 – Airplane wing representative structure. Adapted from [15].

1.3 Objectives

The main objective of this work is to implement and develop an optimization framework based on a genetic algorithm capable of predicting fibres' orientations and layers' thicknesses that maximise the fundamental natural frequency of vibration, as well as the critical buckling load due to in-plane loads. The mechanical responses are obtained using an artificial neural network (ANN) arrangement in order to reduce the computational time. Abaqus® software is used to provide the necessary data to train and validate the ANN.

The work plan is constituted by the following tasks:

- Understand the finite element model already implemented for the wing representative structure;
- Decompose the original optimization problem into smaller problems (substructures);
- Carry out analysis in order to maximise the first natural frequency of vibration;
- Carry out analyses in order to maximise the critical buckling load due to in-plane loads;
- Carry out a multi-objective optimization regarding the critical buckling load and weight of the structure due to in-plane loads;
- Development of an analytical first approach to validate the FEM model used to obtain the fundamental natural frequency of a stiffened composite panel;
- Compare the diverse optimum designs.

1.4 Thesis layout

The work developed is divided into the following chapters:

- Chapter 1: "Introduction", in which the main motivations for the realization of this dissertation are presented coupled with its applicability on the aerospace industry nowadays;
- Chapter 2: "State of the art", wherein the principal optimization procedures are reviewed and assessed upon their possible application in this concrete problem. The genetic algorithm capable of optimising the ANN arrangement and the mechanical variables under consideration is deeply analysed;
- Chapter 3: "Mathematical model". In this section, the main equations regarding the composite laminates behaviour are formulated, particularly their performance under free conditions and in-plane loads;
- Chapter 4: "Wing representative structure's description", in which the complete description of the structure under analysis is performed, including its main parts and the respective mechanical properties. Besides that, the peculiarities of the implemented FEM models are discussed (e.g. type of elements);
- Chapter 5: "Optimization of the airplane wing representative structure for vibration". In this chapter, the simplified structure is optimised regarding its fundamental natural frequency, under certain prescribed constraints and altering only the layers' orientations and/or thicknesses. The thorough description of the optimization algorithm is provided;
- Chapter 6: "Optimization of the airplane wing representative structure for buckling". The same procedure described in the previous chapter is implemented to maximise the structure's critical buckling load due to in-plane loads, considering the plies' orientations and layers' thicknesses as design variables. The aggregation method is used to take into account the minimisation of the structure's weight as an additional goal;
- Chapter 7: "Conclusions and future work", wherein the main conclusions about the developed work are synthesised and a perspective of future work regarding possible improvements on the optimization procedure are drawn.

Chapter 2

State of the art

2.1 Introduction

In this chapter, an overview of the optimization algorithms applied to the aerospace industry is performed, particularly the genetic algorithms embedded in an artificial neural network arrangement. The goal is to list and differentiate the already implemented ones, mainly those related with the fundamental natural frequency and critical buckling load optimization, highlighting their advantages and drawbacks and, at the same time, to do a study upon the possibility of implementation in this concrete problem. It is intended to give a future perspective of their evolution in order to understand how optimization can help engineering work and growth even more, reducing testing and development time drastically, therefore allowing costs reduction. Moreover, the main types of optimization algorithms will be distinguished regarding their nature, namely the gradient-based and the evolutionary-based methods.

2.2 Optimization algorithms and machine learning

ML (Machine learning) is described as a computer science branch, wherein a certain machine is trained in order to perform a specific task with minimal human intervention [16]. It belongs to the area of AI (artificial intelligence) and its scope is based on computational learning and pattern recognition [16–18]. The algorithm is obtained by a learning process, in which the machine is trained on some data sets. Then, the model is capable of doing predictions according to the model itself and a given input [16–18].

Machine learning can be categorised in the following classes which differ upon the necessity of labelled data [16, 18–21]:

- supervised learning, in which a certain machine is trained by using labelled datasets and the label itself is the outcome that we are focused in predicting by using a suitable model. There are two main types of supervised learning models, such as the Regression ones which are capable of predicting characteristics represented by numbers, and the Classification ones

that are suitable to forecast states. Examples: Simple linear regression algorithm, Multivariate regression algorithm, Decision tree algorithm (Regression); Support Vector Machine (SVM), Naive Bayes, Logistic regression algorithm, Decision tree algorithm (Classification);

- unsupervised learning, in which the model is created based on raw data, without a label assigned to each feature, being particularly interesting to understand patterns and trends within unlabelled data through some techniques such as clustering, wherein the data is grouped based on similarity and according to several classes, or dimensionality reduction, which consists in reducing the number of features necessary to describe the data without losing generality. The two strategies above are combined in a procedure known as matrix factorization. Examples: K-Means Clustering, Principal Component Analysis (PCA), Independent Component Analysis (ICA);

- semi-supervised learning, which gathers some characteristics of the two mentioned above, attempting to overcome their individual drawbacks;

- reinforcement learning, reward or punishment-based learning, in which the network variables are continuously updated through qualitative and quantitative information acquired through the contact with the environment with no input data associated.

Deep learning (DL) is a component of the main machine learning architectures that attempt to incrementally extract higher-level properties from data while implicitly extracting features [16, 22, 23]. However, there are many more definitions and perspectives of what really means this complex subject, such as the transformation of lower-level information into higher level-information, using multiple layers of representation and abstraction or regarding the high number of hidden layers belonging to the artificial neural networks that the input data has to overpass in order to acquire implicit information [16, 22, 23]. The increase on the number of layers outperform this complex procedure by increasing the level of abstraction. In comparison with the conventional machine learning techniques, both use optimization methods and the main difference is that the last one does not need the selection of data features beforehand, this procedure is accomplished during the training phase [23].

The machine learning applications are extensive, ranging from particular and simple tasks such as image or handwriting recognition to more demanding and responsible ones, like self driving cars or aerospace structures design [16, 18]. Therefore, machine learning is fundamental to make daily life easier for people by enabling them to comply with several tasks simultaneously and to reduce development, testing and production timelines drastically when applied to the several businesses.

DMTs (data mining technologies) have, recently, been employed in SHM area due to their powerful computational ability to detect damage in structural systems, where the main components of any structural damage detection approach consist of a set of accelerometers or others types of sensors and a DM (data mining) procedure [24]. In the monitoring process, the network of accelerometers is utilised to create a database using response data collection. The DM approach is

used to extract information on the structural health condition from the database and to obtain the relationship between data in the form of patterns [24]. This ability is particularly useful for the aerospace industry.

Optimization algorithms are essential for selecting the best solution out of a set of all possible solutions for analysing and improving a certain system or data. They involve at least one objective function which must be maximised or minimised under certain constraints. Therefore, they are a tool with a widespread application in many areas, such as engineering, medicine, business, among others [17]. The ability to quickly obtain a problem's global minimum value with a minimal number of control parameters and low computational cost, as well as robustness and flexibility of application to diverse problem models, are desirable properties for optimization algorithms [17, 25–27].

Optimization problems can be classified into the following categories and according to several criteria [17, 26, 28, 29]:

- deterministic optimization, wherein the algorithms pass through the same states repeatedly, producing the same outputs for a given input, exhibiting no randomness; or stochastic-based optimization based on probabilistic rules, which make it suitable to deal with noisy, unknown and nonlinear systems;
- classification based on the nature of the design variables: parametric problems (static optimization) or path/trajectory problems (dynamic optimization);
- according to the physical structure of the problem: optimal or non-optimal control problems;
- linear, non-linear, geometric or quadratic programming problems;
- classification based on the separability of the functions, describing the objectives or constraints functions, into several ones of only one dependent variable;
- according to the nature of the optimal project: topology optimization or internal optimization of the material's parameters;
- continuous, integer, mixed-integer or discrete optimization;
- constrained or unconstrained optimization problem;
- unimodal or multimodal optimization problem;
- one-objective or multi-objective optimization problem.

Stochastic and deterministic algorithms are the two main categories of optimization algorithms. Deterministic algorithms, such as linear programming, integer programming, nonlinear programming, convex optimization or gradient-based, carry out specific steps in a predefined sequence. The objective function and design variables consistently have the same values. On the

other hand, stochastic-based algorithms, such as the heuristic or meta-heuristic ones, usually incorporate unpredictability. Metaheuristic algorithms are higher-level heuristics that use memory, solution history, and other forms of learning strategies instead of the trial-and-error method used by heuristic algorithms to generate new solutions [26, 30]. Nowadays, the majority of metaheuristic algorithms are nature-inspired [26].

The optimization techniques can also be classified according to the underlying principle of a biological or physical-based algorithm. In the first category are included, for example, the genetic algorithm (GA), wherein a sequence of genetic operators is used to generate better solutions; the harmony search algorithm (HSA), which is driven by the understanding that harmony perfection is what music aims for, establishing an analogy to the optimality in a process of optimization; modelling equations of the swarming behaviour of fish and birds are used in the particle swarm optimization (PSO); the bacterial foraging optimization (BFO) inspired by the social foraging behaviour of *Escherichia coli*, in which bacterias look for nutrients in a way that corresponds to the maximization of the amount of energy per unit time, communicating between each other by sending signals; the cuckoo search algorithm (CSA) based on the remarkable brood parasitism of some species of cuckoos and their co-evolution with host bird species like warblers; the bee colony algorithm (BCA) mimicking the honey bee swarm's foraging behavior; the ant colony optimization (ACO) which tries to replicate how social ants forage in a colony; the firefly algorithm (FA) derived from the swarming and light-flashing behaviour of tropical fireflies; the backtracking search algorithm (BSA) which is an iterative population-based evolutionary algorithm meant to be a global minimizer divided into five sequential processes: initialization, selection-I, mutation, crossover, and selection-II; the lightning search algorithm (LSA) based on the concept of quick particles known as projectiles and the step leader propagation mechanism used in the natural phenomena of lightning; among others [17, 26, 27, 31–36]. On the other hand, the simulated annealing (SA) based on the annealing process of metals, tending to settle at local minima as its agents loose energy; the gravitational search algorithm (GSA) which is based on the law of gravity and mass interactions, in which objects attract each other by the gravity force, resulting in a global movement of all agents towards the objects with heavier masses correspondent to the better solutions and slow movement ensuring the exploitation ability of the algorithm; the Big Bang-Big Crunch (BB-BC) algorithm inspired by the expansion phenomenon of Big Bang and shrinking phenomenon of Big Crunch; the Galaxy-based search algorithm (GbSA) encouraged to explore its surroundings by the spiral arm of galaxies in order to effectively search the domain; the Central Force Optimizer (CFO) based on the theory of particle kinematics in gravitational field; or the Charged System Search (CSS) which is based on Coulomb and Gauss's laws relative to electrostatics are some examples of physics-inspired algorithms [17, 26, 27, 31–36]. Moreover, there are the conventional ones which are gradient-based, that is, their operation involves the calculation of the objective function derivatives of first order or even a higher order [17, 26]. This procedure is extremely time-consuming, which leads to the development of distinct techniques like the ones referred above, whose foundation is completely opposite.

2.3 Optimization algorithms: ANN's

The neural networks are included in the deep learning and machine learning techniques, being the ANNs the most recognized due to their peculiar architecture with several interconnected layers [17]. Their main characteristics which make them the most suitable method to model and interpret complex data is their ability to scale through optimization and parallelization and the capability to learn from their own environment [17, 37].

The most well-known neural networks are ANN, CNN (convolutional neural network) and RNN (recurrent neural network) which differ mainly in their architecture [17]. The convolutional neural networks have convolutional layers, pooling ones aiming to reduce the number of parameters and complexity of the model and fully-connected ones behaving like a simple connection to produce an output. These ones integrate the hidden layers, in which each one of them defines the number of filters used to identify the patterns of shapes in specific object shapes, being then extremely useful for image analysis. Their neurons are organised into three dimensions, the spatial dimensionality of the input (height and the width) and the depth. On the other hand, the recurrent neural networks are the ones whose neurons send signals between each other. They have looping constraints at each hidden layer, which are back-propagated to guarantee that the subsequent data is looped into the input data from the last step in each neuron's first step [17, 38–41].

2.3.1 Description

ANNs are self-organising computational techniques that can solve many functions through pattern recognition. They were first proposed in the 1980s and can be used to reconstruct nonlinear relationship learning from training [20, 24, 42, 43].

The artificial neural networks structures are based on the biological nervous systems and the human brain. The computational processing units are simplified models of the biological neurons and are denominated by artificial neurons/perceptrons [19, 20, 43, 44].

The feedforward neural network is used when the input data is sorted in the forward direction. The basic structure of an ANN consists of three layers: the input layer, hidden layer and output one (see Figure 2.1). The input layer receives the input data, whereas the hidden one computes it and the output layer provides outcomes. The number of required hidden layers rises when the complexity increases. The activation functions provide nonlinear properties to the ANN, which can suit the mapping of complex relationships, known as an universal approximation [17, 20, 42, 43] .

2.3.2 How ANN's work

Backpropagation is the learning algorithm used most frequently in artificial neural networks.

Backpropagation attempts to minimise the least mean square difference over the entire training set. The training set is made up of a large number of cases for which the outcome is already known. When the network is set up, the connections between the neurons in the input and hidden layers

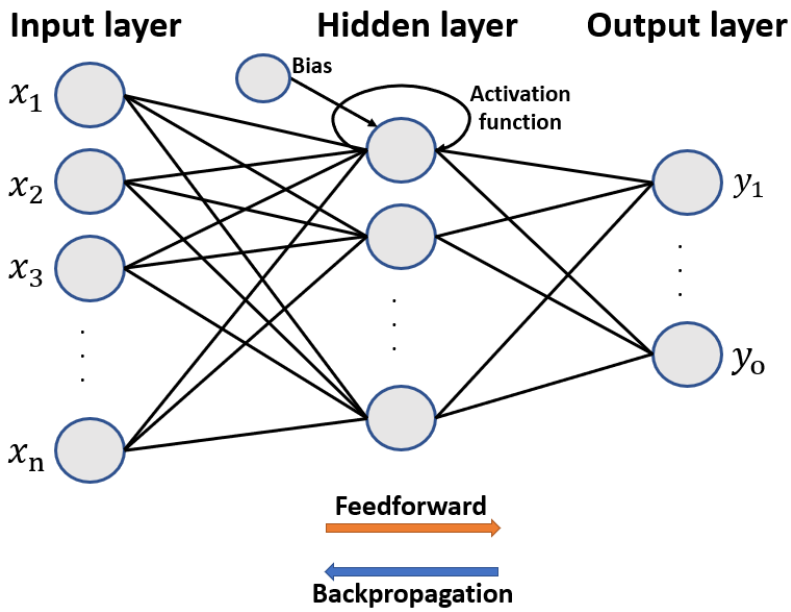

Figure 2.1 – Simple ANN's configuration.

are assigned with random weights and the network then produces an output. The ANN output is compared with the true one, and the error is back-propagated through the network, altering the weights of the connections to reduce the least mean square error. This is repeated until the error is minimised, that is, a certain prescribed convergence criteria is attained. Then, the ANN must be validated through some design points apart from those which were used to construct the network. Regarding the number of hidden layers and the number of nodes in each one of them, they are set through experimentation. Genetic algorithms are recently used to achieve the optimal ANN's architecture. The sequence of training, replication, crossover and mutation is repeated until the optimum net architecture is produced [24, 43, 45] .

2.3.3 Composition

The main elements of these networks are the synaptic weights and biases, and the activation functions between the several layers, as represented in Figure 2.2 and mathematically expressed in equation 2.1,

$$y_i = g_i \left(\sum_{j=1}^{n} w_{ij} \cdot x_i + b_i \right), \tag{2.1}$$

where x_i indicates the input values, w_{ij} the value of the weight between input, hidden or output layers, b_i is the bias, n represents the number of nodes, g_i shows the transfer/activation function and y_i the value of the output node [20, 24, 43].

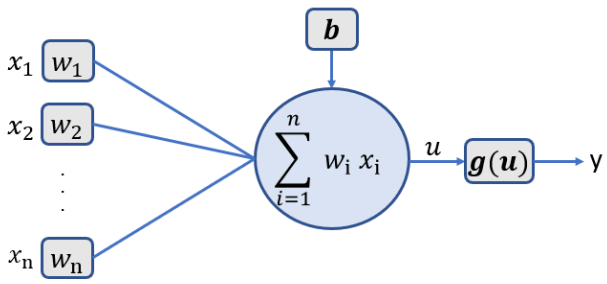

Figure 2.2 – ANN's main architecture.

The ANN is composed by the following elements [19, 20]:

(a) Input signals (x_1, x_2, (...), x_n): represent the values assumed by the variables of a particular application. The input signals are usually normalised in order to enhance the computational efficiency of the learning algorithms;

(b) Synaptic weights (w_1, w_2, (...), w_n): are the values used to weight each one of the input variables, representing their importance in relation to a certain neuron;

(c) Linear aggregator (R): gathers all input signals weighted by the synaptic weights for each neuron belonging to a certain layer;

(d) Activation threshold or bias: corresponds to the threshold characteristic of each individual neuron that the linear aggregator value must, at least, equalize in order to generate a trigger in the neuron output;

(e) Activation potential (u): result produced by the difference between the linear aggregator and the activation threshold;

(f) Activation function (g): limits the neuron output within a reasonable range of values. They could be: partially differentiable, such as the step function (*Heaviside*), the bipolar step function and the symmetric ramp function or fully differentiable, that is, with non-zero first derivative for all points of the domain, such as:

- logistic/sigmoidal function, in which the outputs assume a value between 0 and 1 and the parameter β_{sig} represents the slope of the curve at its inflection point;

$$g(u) = \frac{1}{1 + e^{-\beta_{sig} \cdot u}} \tag{2.2}$$

- hyperbolic tangent function, in which the outputs assume a value between -1 and 1;

$$g(u) = \frac{1 - e^{-\beta_h \cdot u}}{1 + e^{-\beta_h \cdot u}} \tag{2.3}$$

- gaussian function;

$$g(u) = e^{-\frac{(u-c)^2}{2 \cdot \kappa^2}} \tag{2.4}$$

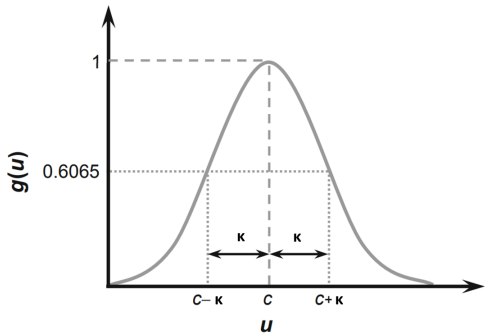

Figure 2.3 – Gaussian function. Adapted from [19].

- linear function;
- rectified linear activation function or ReLU.

(g) Output signal (y): results from the activation function computation on their input vector.

2.3.4 Applications

Due to their ability to model complex nonlinear functions, ANNs are suitable for a wide range of applications, such as constraint satisfaction and optimization; data compression; forecasting and risk assessment (stock selection, foreign exchange trading and portfolio management); precise control (parameters optimization); pattern recognition; diagnosis in almost all fields of engineering and medicine, including anomaly identification on medical images; analysis of images acquired from artificial satellites; speech and writing pattern classification; face recognition with computer vision; control of high-speed trains; control of electronic devices and appliances, such as washing machines, microwave ovens, freezers, coffee machines, frying machines, video cameras, and so on [19, 24].

2.3.5 Advantages and disadvantages

Artificial neural networks are heavily used and studied due to the following main reasons: the number of inputs and outputs are not constrained, which makes them suitable for all the datasets' dimensions; the ability to learn and to model complex relationships, even nonlinear ones; the possibility to operate with incomplete information, however with an eventual performance compromise; they do not need enforcement constraints on the input data, that is, a required pre-distribution of the input data; the high numerical efficiency inherent to their multi-processing capability; the ability to tolerate faults and to generalise, being therefore able to predict unknown data; they can be developed using several training algorithms [17, 46, 47].

Although those benefits, ANNs are a very stochastic problem, remaining several challenges that the user may face and improve with his experience, such as the difficulty to tune them and to achieve their best configuration; the best network design must be achieved by a trial and error procedure which is extremely time consuming; they are equipment-dependent to achieve the best results in the lowest time possible; the possibility to occur gradual corruption which slows down the process over time and promotes degradation; and the troubles associated to the identification of their problems due to their numerical-essence [17, 46, 47] .

The ANN's network configuration can be improved by the application of an optimization algorithm in order to fine tune their parameters, including the best number of neurons, hidden layers, weights, bias, self-shaping architecture and multi-stage objective functions. This problem is known as an hyper-optimization procedure.

2.3.6 Training process

The training process of a given network aims to tune the synaptic weights and thresholds of its neurons in order to minimise the mean square error between the network's outputs and the ones provided by training data. The learning algorithm is divided into two different steps: training subset and test subset. In the last one, the network arrangement is validated by a set of input data apart from those associated with the training phase [17, 20].

It is important to ensure, particularly in the backpropagation algorithms, that the training patterns cover the entire design space, that is, they have a high representativeness in the domain under analysis [42, 45].

There are several statistical-based approaches whose main goal is to appropriately select the design samples, such as [28, 42, 48–50]:

- Full Factorial design (FFD), wherein combinations of the design variables are established, taking into account the number of levels that each one may assume. For two-level experiments, the dimension of the dataset must be equal to 2^s, where s corresponds to the number of factors;

- Box-Behnken design (BBD): class of rotatable or nearly rotatable second-order designs based on three-level incomplete factorial design. The number of experiments (n_{exp}) required for the development of BBD is defined as $n_{exp} = 2s \cdot (s - 1) + C_o$, where C_o is the number of central points. Compared to the three-level full factorial design, it is more effective and does not contain combinations for which all factors are simultaneously at their maximum or lowest values. Therefore, these designs are helpful in avoiding experiments undertaken in extreme conditions, which could lead to unpleasant results;

- Plackett-Burman design, in which the designers aimed to create a set of experimental points for investigating the dependence of some measured quantity upon the independent variables

(factors), each taking q levels, in order to minimize the values of those dependencies using a limited number of experiments;

- Fractional factorial design: the number of experiments turns to 2^{s-p_n}, where p_n is a natural number which takes into account the constrained number of experiments that are performable;

- Orthogonal array design (OAD): imposes representative samples and orthogonal relationships between sub-columns of the table of the experimental points;

- Central composite design (CCD): appropriate for fitting second-order models with neither representative nor uniformly scattered samples. The number of experiments for a central composite design is $n_{exp} = 2^s + 2s + C_o$. This method allows an initial study with a 2^{s-p_n} design to be extended to a second order model exploration with only star points ($2s$) and more center points added (C_o);

The main drawback of those methods is that the majority of them are based on a specific statistical distribution, which requires pre-assumptions about the model. The nature of the ANN is to always assume the model to design as unknown. In addition, if the number of factors (random/design variables) rises, a significant number of experiments are needed, which takes a lot of time. OAD can reduce it to q^2 instead of q^s, however that procedure is restricted to 2-level experiments, being expensive for a higher number of levels [42].

An alternative was proposed by *Wang* and *Fang*, denominated by Uniform Design Method (UDM), according to theoretic achievements in the number-theoretic method (NTM). The kernel problem of NTM is to find a set of points called the number-theoretic net (NT-net), which are uniformly scattered in the s-dimensional unit cube C^s. The main application of NTM is numerical integration, being extrapolated to the numerical resolution of integral and differential equations. The discrepancy is used as a measure of uniformity of points scattered [42, 51].

Notation: $\mathrm{U}_{n_{exp}}(q^{t_c})$, in which U is the abbreviation for Uniform Design, n_{exp} represents the number of experiments (experimental points), q the number of levels of each factor and t_c the maximum number of columns of the table. There are tables which allow the selection/creation of the datasets according to the established number of experiments and the number of design variables. It is important to highlight that just one experiment is needed for each level of each factor and there is an accessory table associated with the main one, describing the columns to consider taking into account the number of design variables. That correct selection results in the lowest discrepancy value. The points in UD are more uniform than those in OAD. For the same number of experiments and factors, the discrepancy of OAD is much larger than that of UD [42].

The *Taguchi* method uses an engineering approach to plan and design optimum neural networks systematically. It makes use of the orthogonal arrays and signal-to-noise ratios to design high quality and robust neural networks. Neural network's robustness is defined as its sensitivity measure of the performance quality to noise. Some guidelines [51]:

- creating a neural network which is robust against initial weights condition during learning phase, thereby reducing the chance of settling at a local minima;
- ensuring that the performance of neural network is insensitive to the architectural variation, thus allowing for the selection of the right number of hidden layers and neurons;
- making the neural network design insensitive to input data variation by using a suitable method to select the training dataset which covers the maximum portion of the design space, thereby improving the reliability and accuracy of the network.

The trial and error method is the most common method to achieve the micro and macro parameters of an artificial neural network. However, that method is expensive and may lead to a premature convergence and, consequently, to a non-optimal solution [51].

The main architectures of the artificial neural networks differ from the neuron disposition and interconnections to the layers composition [17, 19, 47]:

- single-layer feedforward network, which is composed by one input layer and a single neural layer that corresponds to the output one;
- multilayer feedforward network, composed by one or more hidden layers, being suitable for a wide range of applications due to their universality;
- mesh networks, in which the spatial localization of the neurons is directly related to the process of adjusting their synaptic weights and thresholds, influencing pattern extraction processes. They must have continuous connections and reconfigure itself if a path is broken, using self-healing algorithms.

There are some concerns to take into account when a certain system is modelled by a multilayer perceptron network. Increasing indiscriminately the number of nodes and hidden layers does not guarantee the best generalisation of the data under analysis. The method to achieve the best artificial neural network configuration is a balance between overcoming underfitting and avoiding overfitting. Overfitting often occurs when the model performs well on the training dataset but fails on the testing dataset. This could arise either from an unbalanced model or due to a low number of samples. On the other hand, the model is underfitted whether it performs badly on both datasets. The model itself or an insufficient characterization of the algorithm per si may be some of the starting problems [17, 23].

A network with a small number of hidden nodes is unable to distinguish between complicated patterns, providing only a linear estimation of the true tendency. On the other hand, if the network has too many hidden nodes, the trend will become noisy due to overparameterization, which leads to a poor generalisation for the testing dataset. According to Papadrakakis et al. (1998), the number of nodes in the hidden layer(s) may be selected as the mean value of the number of input and output nodes plus the input nodes. It is certainly a good rule to begin the best network's configuration achievement through an iterative procedure. On the other hand, Kolmogorov and Lipmann (1995) say that the lower bound of neurons in the first hidden layer is equal to $2 \cdot INP + 1$,

whereas the upper bound is $OUT \cdot (INP+1)$, in which INP represents the number of input neurons and OUT the number of output nodes. Moreover, they say that if more than one hidden layer is required, the number of neurons in the second hidden layer has a ratio of 1:3 to that of the first layer. There are several others empirical relationships to obtain the optimal starting number for the hidden nodes, such as the ones supplied by Jadid and Fairbairn (1996), Lachtermacher and Fuller (1995) or Widrow and Lehr (1990) [45, 47, 51–54].

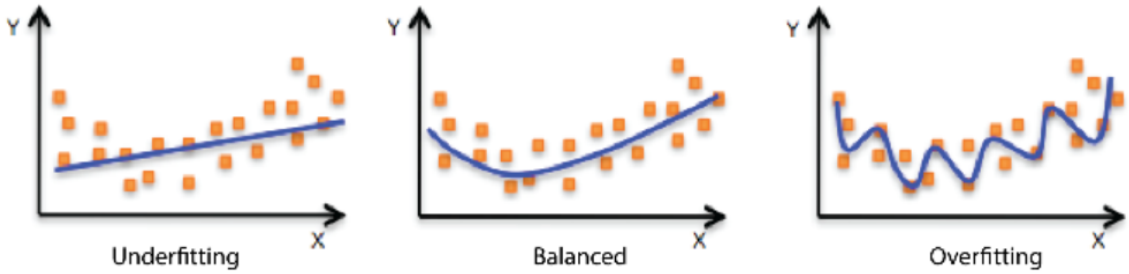

Figure 2.4 – Different ways of data generalisation [55].

In composite laminate design, the precise calculation or even approximation of objective function derivatives (gradient-based algorithms) is often computationally costly or, in some cases, even impossible due to discontinuities. One of the advantages of direct search algorithms (or zero-order optimization algorithms, e.g. GAs) is that they require only objective function values. However, these algorithms request that calculation to be repeated thousands of times. ANNs are applied to reduce that demand [56, 57].

2.4 Gradient-based optimization algorithms

In the gradient-based optimization algorithms, the synapses weights and biases of the backpropagation algorithm are updated by the calculation of the error function gradient. In order to minimise the error, the adjustment must be made in the opposite direction of the gradient [19, 28].

There are two main categories which differ in the dimension of the dataset required for computing the error measure. Batch or offline training methods compute the error measure and gradient taking into account the whole dataset, whereas the incremental or online training methods only consider a small set out of the entire dataset. The last ones can be unstable and do not provide a criteria for the ending of training [45].

In these procedures, the synapses weights are initialised randomly several times in order to prevent entrapment at local minima [19, 20].

2.4.1 Mathematical model

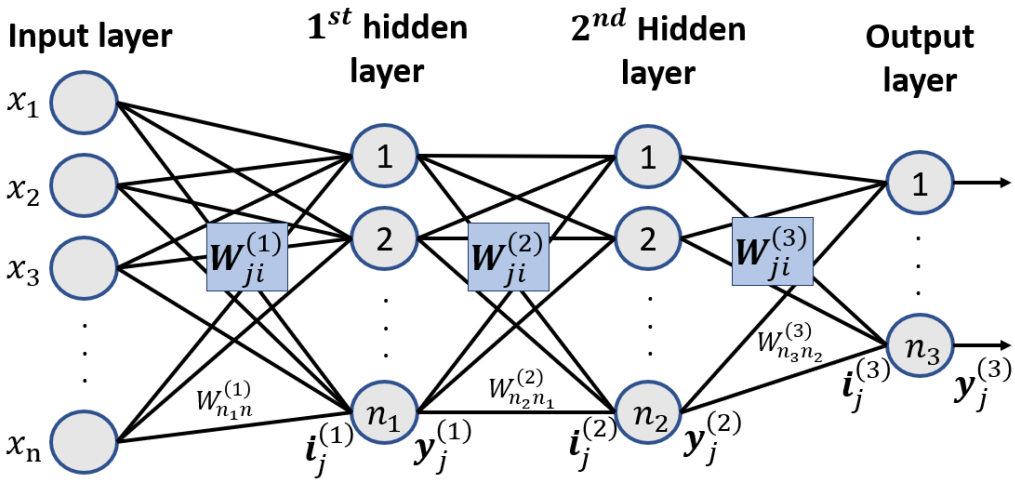

Figure 2.5 – Multilayer perceptron network. Adapted from [19].

Notation:

- $\mathbf{W}_{ji}^{(L)}$: weight matrices whose elements denote the value of the synaptic weight that connects the jth neuron of layer (L) to the ith neuron of layer $(L$ - $1)$;
- $\mathbf{i}_j^{(L)}$: vectors whose elements denote the weighted inputs related to the jth neuron of layer (L), being defined by:

$$\mathbf{i}_j^{(L)} = \sum_{i=0}^{n_i} \mathbf{W}_{ji}^{(L)} \cdot \mathbf{x}_i \tag{2.5}$$

- $\boldsymbol{y}_j^{(L)}$: vectors whose elements denote the output of the jth neuron of layer (L), being defined by:

$$\boldsymbol{y}_j^{(L)} = g\left(\boldsymbol{i}_j^{(L)}\right) \tag{2.6}$$

- $\mathbf{d}$: desired output vector

The backpropagation algorithm consists in the following steps [19, 20]:
Initial steps:

- randomise the synapses weights and biases according to a pre-defined statistical distribution or any other method;
- calculation of the output vector through the network propagation;
- defining a function that represents the error measure between the obtained values and the target ones, for example the squared error function

$$E(k) = \frac{1}{2} \sum_{j=1}^{n_3} \left(d_j(k) - y_j^{(3)}(k)\right)^2, \tag{2.7}$$

in which n_3 represents the number of output nodes.

Backpropagation steps:

- adjusting the synaptic weights of the output layer by the direct application of the gradient definition and the chain rule:

$$\nabla E^{(3)} = \frac{\partial E}{\partial W_{ji}^{(3)}} = \frac{\partial E}{\partial y_j^{(3)}} \cdot \frac{\partial y_j^{(3)}}{\partial i_j^{(3)}} \cdot \frac{\partial i_j^{(3)}}{\partial W_{ji}^{(3)}} \tag{2.8}$$

$$\frac{\partial E}{\partial W_{ji}^{(3)}} = -\left(d_j - y_j^{(3)}\right) \cdot g'\left(i_j^{(3)}\right) \cdot y_i^{(2)} \tag{2.9}$$

The adjustment is performed in the opposite direction of the gradient,

$$\Delta W_{ji}^{(3)} = -\eta \cdot \frac{\partial E}{\partial W_{ji}^{(3)}}, \tag{2.10}$$

wherein η represents the learning rate of the backpropagation algorithm.

- adjusting the synaptic weights of the intermediate layers, until the first one. The neurons of the intermediate layers do not have direct access to the outputs, therefore, the synaptic weights update is performed through estimations of the output errors produced by those neurons, that is, their adjustment is based on the output layers' synaptic weights already adjusted. Thus, the error is back-propagated. The main equations regarding the updating of the synaptic weights between the second and first hidden layers are presented below, as an example:

$$\nabla E^{(2)} = \frac{\partial E}{\partial W_{ji}^{(2)}} = \frac{\partial E}{\partial y_j^{(2)}} \cdot \frac{\partial y_j^{(2)}}{\partial i_j^{(2)}} \cdot \frac{\partial i_j^{(2)}}{\partial W_{ji}^{(2)}}, \tag{2.11}$$

$$\frac{\partial E}{\partial y_j^{(2)}} = \sum_{k=1}^{n_3} \frac{\partial E}{\partial i_k^{(3)}} \cdot \frac{\partial i_k^{(3)}}{\partial y_j^{(2)}} = \sum_{k=1}^{n_3} \frac{\partial E}{\partial i_k^{(3)}} \cdot \frac{\partial \left(\sum_{k=1}^{n_3} W_{kj}^{(3)} \cdot y_j^{(2)}\right)}{\partial y_j^{(2)}} \tag{2.12}$$

$$\frac{\partial E}{\partial y_j^{(2)}} = \sum_{k=1}^{n_3} \frac{\partial E}{\partial i_k^{(3)}} \cdot W_{kj}^{(3)} = \sum_{k=1}^{n_3} -\left(d_k - y_k^{(3)}\right) \cdot g'\left(i_k^{(3)}\right) \cdot W_{kj}^{(3)} \tag{2.13}$$

Thus:

$$\nabla E^{(2)} = \frac{\partial E}{\partial W_{ji}^{(2)}} = \sum_{k=1}^{n_3} \left(-\left(d_k - y_k^{(3)}\right) \cdot g'\left(i_k^{(3)}\right) \cdot W_{kj}^{(3)}\right) \cdot g'(i_j^{(2)}) \cdot y_i^{(1)}, \tag{2.14}$$

$$\Delta W_{ji}^{(2)} = -\eta \cdot \frac{\partial E}{\partial W_{ji}^{(2)}} \tag{2.15}$$

2.4.2 Optimised versions of the backpropagation algorithm

The backpropagation algorithm is continuously improved, aiming to boost its convergence rate. Therefore, some variations have been introduced over time [19, 20, 25]:

- **Momentum parameter**: α is defined as momentum rate and it performs a weighting upon how much the synaptic matrices are changed between two successive iterations. When the current solution is far from the real one, the contribution of the momentum term is bigger than the learning term and the opposite occurs near the real solution. Values between the range of ($0.05 \leq \eta \leq 0.75$) and ($0 \leq \alpha \leq 0.9$) are usually recommended for the training of MLP networks;

$$W_{ji}^{(L)}(t+1) = W_{ji}^{(L)}(t) + \alpha \cdot \left(W_{ji}^{(L)}(t) - W_{ji}^{(L)}(t-1)\right) + \eta \cdot \frac{\partial E}{\partial W_{ji}^{(L)}} \tag{2.16}$$

- **Resilient-propagation method**: it is observed that small variations in the gradient of the error function combined with the saturation intervals of the activation functions makes the convergence process slower. Thus, the objective of the resilient-propagation method is to consider only the signal variations of the gradient of the error function, instead of considering the variations in its magnitude. When the signals of the gradient are the same between two successive iterations, the learning rate increases, since the convergence is distant from a minimum point (null gradient) of the error function. On the other hand, if the gradient signals are different, it means that the process passed through a point in which the gradient is null (minimum point), therefore, the convergence must be smooth in order to acquire precise results;

- ***Levenberg-Marquardt* Method**: it was introduced in order to reduce the convergence time. This method is a second-order gradient method, based on the least squares method for non-linear models. It involves the calculation of the *Jacobian* and *Hessian* matrices, being similar to *Newton*'s method. If the eigenvalues of the function's *Hessian* matrix at the zero-gradient position are all positive, there is a local minimum for the function; whereas if they are all negative there is a local maximum for the function and a saddle point is positioned at that particular point whether they are both positive and negative.

  The effect of each specific parameter on the performance of the gradient-based backpropagation method is summarized in the following table, Table 2.1.

2.4.3 Optimization of composite structures using gradient-based methods

Several investigators have performed optimization procedures using the gradient-based methods. Honda et al. (2008) maximised both the fundamental natural frequency and the difference between two selected adjacent frequencies. A new method was introduced by them to convert four lamination parameters optimised at the first stage using a gradient method into the optimal stacking

Table 2.1 – Performance of the gradient-based backpropagation algorithm. Adapted from [19, 20, 25].

Design parameter	Too high	Too low
No. training cycles	• good memorization of data	• incapability of representing the data
Training dataset	• ANN with good recalling and generalisation	• limited or bad generalisation
Testing dataset	• confirmation of ANN's generalization capabilities	• inability to confirm ANN's generalisation capabilities
No. hidden nodes	• overfitting	• underfitting
η	• oscillation about the optimal solution (instability)	• slow training
α	• reduces the risk of local minima • speeds up training • risk of overshooting the iterative solutions	• potential entrapment on local minima • slow training

sequence. The corresponding layup is obtained by minimising the errors between the optimum parameters and the parameters for all possible discrete stacking sequence designs. The optimization procedure was done sequentially from outer domains, because the bending stiffness is more controlled by outer layers than by the inner ones according to the laminate theory and physical evidences [58].

The optimization regarding the lamination parameters is, without any simplifications, a convex problem whose search space is a 16th dimension hypercube and they are limited by the interval [-1,1], 4 for extensional stiffness, 4 for extensional-bending (coupling) stiffness, 4 for bending stiffness and another 4 for transverse shear stiffness [28].

Moreover, Herencia et al. (2007) applied a two-level optimization procedure of a composite stiffened panel. In the first step, a gradient-based method was applied to achieve the optimal six lamination parameters, membrane and bending ones, in order to minimise the mass of the structure. The design was restricted concerning the lamination parameters bounds, strength, buckling and practical design constraints. On the other hand, several stiffener designs were considered. In the second step, an evolutionary-based algorithm was applied to reach the optimal stacking sequence, in which the constraints were approximated by the development of a *Taylor* series about the step-1 optimal design [59].

Liu et al. (2007) also applied a bi-level optimization procedure to a composite stiffened panel under compressive loads and lateral pressure. Their goal was to minimise the panel weight, satisfying strength, buckling and design constraints. VICONOPT gradient-based optimization technique was implemented to achieve the optimal panel and stiffeners dimensions aiming to minimise the overall weight. This particular gradient-based technique allowed lateral pressure consideration.

Besides that, it considers the coupling between the skin and stiffeners and the interaction between local and overall buckling [60].

On the other hand, the optimal stacking sequence correspondent to the maximum values for the first natural frequency and critical buckling load was achieved by Abouhamze and Shakeri (2007), using the weighted summation method. The optimization process speed was improved through the implementation of an artificial neural network to reproduce the behaviour of the structure both in free vibration and buckling conditions. The neural network was a multilayer perceptron and the learning was performed by the *Levenberg-Marquardt* backpropagation method in order to reduce the computational time [61].

Reddy et al. (2012) applied an artificial neural network arrangement (multilayer perceptron) to predict the fundamental natural frequency of laminated composite plates under clamped boundary conditions. The experiments to train and test the network were chosen according to D-optimal design. The gradient descent method was chosen by them to achieve the best ANN's configuration regarding the weights of the synapses and the biases [62].

The same strategy, in terms of the ANN's optimization technique, was used by Mallela and Upadhyay (2016) to forecast the critical buckling load of laminated composite stiffened plates under in-plane shear [63].

Bacarreza et al. (2015) studied the post-buckling phenomena of a composite plate because they considered that the post buckling strength capacity has an important role for weight savings, which is undoubtedly prevalent in the aerospace industry. A genetic algorithm was applied to the described multi-objective problem in order to obtain the front of Pareto. A more robust solution was obtained by a gradient-based optimization procedure together with the Monte Carlo Simulation (MCS), which provides a statistical viewpoint to the problem under analysis [64].

Automated Fibre Placement (AFP) developments led to an increase in the use of grid-stiffened composite structures which are high damage tolerance and lightweight structures. Moreover, the manufacturing cost has been reduced by the use of less mechanical fasteners and it is easier to tailor the required stiffness and strength to a desired direction. For this type of structures, ply angles and stiffeners sizing and spacing are, normally, the design variables. A gradient-based optimization procedure was implemented by Wang et al. (2017) in the unstiffened structure with similar spatial properties compared with the stiffened one, in order to reduce the computational cost and to make the implementation of a finite element model easier. Then, the sensitivities related to the structural responses were calculated by the finite difference method [65].

Ma et al. (2021) performed the same equivalence method, denominated by homogenization, regarding the grid-stiffened plate stiffness. They maximised the stiffness of a rectangle stiffener plate and they tried to optimise the buckling load of a square stiffened panel. The results demonstrated that there is an increase in those variables in relation to the unstiffened plate. Firstly, a genetic algorithm was implemented and then a gradient-based sequential quadratic programming method was used to find the global optimal solution, in which the result obtained from the first phase was set as the initial solution. The evolutionary algorithm's early convergence led to the employment of the gradient-based approach [66].

Nowadays, multidisciplinary optimization (MDO) is crucial for the development of composite structures. Particularly in the aerospace industry, the structure and aerodynamic departments must be always in touch because their works are highly interconnected. The aerodynamic loads are used for structural design, whereas the deformed shape of the structure is fundamental to accurately assess the aerodynamic performance. D*ä*hne and Werthen (2018) selected the gradient-based techniques to perform optimization procedures due to their capacity to deal with a large number of variables which are assigned to the composite materials. Moreover, the concept of lamination parameter is used to simplify the algorithm and the optimization is based on the stiffness matrix terms of the individual substructures [67].

2.5 Evolutionary-based optimization algorithms

The evolutionary-based optimization algorithms are, as the name suggests, biology-based procedures whose utilisation has increased over time particularly because they are zero-order algorithms which allows to considerably reduce the computational time and, at the same time, to obtain precise results. Besides this, they are, in general, easier to implement and they are capable of dealing with complex problems. Some of them were already explained in Section 2.2. The genetic algorithm will be presented and deeply discussed later on. Some characteristics about several nature-inspired algorithms are summarised in Table 2.2 and Table 2.3 [17, 68].

A combination of PSO and neural networks is the most common one among the optimization algorithms and AI (artificial intelligence) and is widely used in many application software and controllers [17, 56]. Many researchers consider BCA for boosting neural network performance either by optimising the hyperparameters or somehow merging with some other method to enhance the neural network configuration or the correspondent applications [69]. The genetic algorithms were firstly introduced by *Holland* in his book “Adaptation in Natural and Artificial Systems” (1975) and they are a stochastic search and optimization method inspired by the evolutionary process that occurs in nature. The idea of a GA is based on the theory of natural selection, where a group of possible solutions, each possible solution is called a chromosome, a whole group of them is called a population, of an optimization problem competes to transfer their features to the population in the next iteration step, which is called a generation [29].

Table 2.2 – Biology-inspired algorithms: advantages and disadvantages. Adapted from [17, 26, 27, 31–35].

Biology-inspired algorithms		
Technique	**Advantages**	**Disadvantages**
GA	• zero-order algorithm • suitable for a large number of variables • no explicit equations to generate new solutions • high search space exploration	• could get trapped in local minima • hard to fine-tune all parameters • long time for convergence
PSO	• fast convergence • ability to handle complex problems	• easily get trapped in local minima • strict selection of control parameters • too high velocities could lead to a slower convergence
BCA	• strong robustness • no explicit crossover • fewer control parameters • good for exploration phase due to mutation and fitness-related selection	• accuracy problems • easily get trapped in local minima when solving multimodal problems • poor at exploitation phase due to lack of crossover
ACO	• no explicit crossover operator • fewer control parameters • good for exploration phase	• complex mutation depending on the pheromone concentration (indicator of quality) and route distance • poor at exploitation phase
FA	• suitable for multimodal optimization problems due to swarm division • scaling control • easy to implement	• easily get trapped in local minima • only local searches
BSA	• single control parameter • ability to handle multimodality • suitable for exploration phase due to their memory capability • low computational cost	• time-consuming
BFO	• high stability about the optimal solution • associations with GA and PSO to enhance local and global search capabilities	• potential premature convergence in local minima
CSA	• introduce nonlinearity • combination of both local and global search capabilities, controlled by a switching probability	• slower convergence

Table 2.3 – Physics-inspired algorithms: advantages and disadvantages. Adapted from [17, 26, 70, 71].

Physics-inspired algorithms		
Technique	**Advantages**	**Disadvantages**
CFO	• effective search of the search space due to probes interactions	• no explicit mechanism to enhance exploitation capability • highly dependent on initial probes distribution
GSA	• variable gravitational constant controls the convergence speed • fast convergence	• easily get trapped in local minima • exploration and exploitation capabilities highly dependent on random parameters correctly tuned
BB-BC	• Big Bang phase ensures exploration of solution space • exploitation and convergence assured by Big Crunch phenomena	• potential early entrapment at local minima if the initial population is not well distributed
GbSA	• Local Search ensures exploitation of the search space • Spiral Chaotic Move provides powerful exploration mechanism	• the global optima achievement is strongly dependent on Spiral Chaotic Move performance
CSS	• good exploration and exploitation capabilities resulting from handling attractiveness and repulsiveness of resulting electric force	• easily get trapped in local minima whether the initial charge particles are not well distributed
SA	• high search space capabilities due to the use of multiple bouncing balls • diversification via randomization	• regularity control • time-consuming
HSA	• usage of harmony memory, pitch adjusting and randomization as selection, mutation and diversity mechanisms, respectively	• poor search capabilities • possible performance disturbance in final iterations

2.6 Genetic algorithms

The genetic algorithms are based on this fundamental principle: "the variability between individuals in a population of individuals which reproduces sexually is produced by mutation and genetic recombination" [29].

Holland's genetic algorithm consists in the transformation of a population of chromosomes, which serve to encode possible solutions, into a new population through a natural selection process and using several genetic-inspired operators such as selection, crossover and mutation until predefined criteria is met regarding a certain fitness value or a maximum pre-established number of generations. Each chromosome, representing a possible solution, is composed of genes and the latter ones assume a particular value known as allele [17, 29, 56, 69, 72].

The selection operator chooses the chromosomes that are able to reproduce, based on a fitness function representative of the problem under analysis. The crossover operator mimics the genetic recombination between two different individuals, in which they share a part of their chromosomes in order to create another individual. The mutation operator changes randomly an allele(s) of the chromosome and the inversion operator, an additional one only possible for certain applications, reverses the order of a small part of the chromosome, rearranging the position of its genes. In the genetic algorithms, each chromosome/possible solution is coded by a sequence of bits, representing each of them an allele and assuming a binary value (0/1). The majority of the genetic algorithms use haploid individuals (one chromosome individuals). The genotype of an individual is merely the configuration of bits and the phenotype is the representation of the individual's characteristics in its own environment. In general, the genetic algorithms do not work directly with the real representation of the solutions in the search space, instead they work with a suitable codification, such as binary coding, real coding, e.g, which makes the genetic operations much easier. That codification is frequently denominated by representation. The reverse process, known as decoding, occurs at the end of the process [29, 56, 69].

The complete description of the used genetic algorithm is performed later on, in Section 5.2.

The main goal of these kinds of evolutionary algorithms is to use simple representations to encode complex structures and simple operations to improve them during the evolution process. They are able to handle problems with very difficult objective functions, such as discontinuous or non-differentiable, nonconvex, multimodal or noisy. Their main characteristic which makes them suitable for a wide range of applications is that they work with a population of solutions instead of a single point in the search space, therefore the probability of finding local minima is lower since they climb many peaks in parallel. Apart from that unequivocal advantage, they are clearly easy to implement, are capable of solving multimodal minimization problems and, as referred in others subsections in order to compare them with the gradient-based optimization algorithms, they do not need any objective function derivatives to be calculated. Due to their probabilistic nature, new points in the design space are explored, improving and preventing convergence in sub-optimal designs, which is prone to occur in the gradient-based procedures, owing to their deterministic rules [17, 56, 73].

Their main disadvantages are the long time to achieve a certain level of convergence, the difficulty to apply to decision-making problems, scalability troubles and the difficulty to tune all parameters (mutation rate, crossover rate, crossover parameters, population's dimension, information coding mechanism, among others) in order for the algorithm to represent the system under analysis with more faithfulness/ fidelity. That process is usually a trial and error procedure, unless a mechanism is established that updates their values throughout the evolutive process. The population's dimension is chosen according to a balance between efficiency and computational cost. A small population can lead to an insufficient exploration of the search domain, whereas a large population increases substantially the computational time [17, 56, 73].

The application of genetic algorithms in the optimization of laminated structures started in the 1990's. Optimization procedures for laminated composite structures, anisotropic materials,

are much more complex than those associated with isotropic material structures, due to the large number of variables involved and the independent behaviour of an individual layer [56, 74]. The two main design variables in laminate design of the prepreg layup are the fibre's angles and layer stacking sequence. The fibre's angles are normally constrained to some orientations due to manufacturing issues, which results in an integer programming problem regarding the stacking sequence. Other variables can be considered like the layer's thickness, fibre volume fraction or some variables related to the manufacturing process, such as the mold filling time or the mold clamping force. The fibre volume fraction is one of the most important parameters in the design of laminated composites, because it increases the specific stiffness and strength and, at the same time, the laminate's density ρ. On the other hand, it has usually a limited value owing to manufacturing troubles and assumes a constant value in prepreg techniques [74].

Table 2.4 – Properties of prepreg composite materials. Adapted from [74].

Layer combination dependent criteria	**Layer sequence dependent criteria**
• in-plane properties (e.g., planar stiffness)	• out-of-plane (flexural) stiffness/strength
• mold filling time	• interlaminar shear strength
• mold clamping force	• buckling
	• vibration (natural frequencies)
	• aeroelastic efficiencies

The layer combination is related to the number of layers of each angle, whereas the layer sequence dependent criteria is associated to the stacking sequence. The planar stiffness depends on the extensional stiffness coefficients which are not a function of the position of a certain layer along the laminate. Moreover, the average composite's permeability is practically the same for two different laminates consisting of the same number of similar layers positioned differently. Therefore, the mold filling time and clamping force are integrated in the layer combination dependent criteria. Otherwise, all parameters included in the layer sequence dependent criteria depend upon the bending-extensional stiffness coefficients and these ones change whenever a certain layer is placed at another position in the same laminate [74].

2.6.1 Fitness function definition

In order to have a good performance, the fitness functions cannot have many local optima or an isolated global optima, because the search process may concentrate at some sub-regions of the search space, hindering the achievement of the global optima whether some randomness mechanisms are not properly introduced. It is necessary to create a fitness function where the fitness of an invalid chromosome, corresponding to a non-admissible solution, is seen as a measure of the capacity to guide us in the direction of the admissible solutions space. They are created based on the objective

function and on the constraints used for the mathematical formulation of the problem. Normalisation procedures are also applied with the aim of keeping the amplitude of the fitness function values within a desired gap in order to do not have premature convergence or slow ending of the evolutionary mechanism resulted from the successive proximity between well-fitness individuals as long as the evolutionary process occurs [29, 74].

2.6.2 Methods to include the problem constraints based on genetic algorithms

There are several distinct techniques to include and enforce the constraints amongst the evolutionary-based algorithms [29, 75, 76]:

- methods based on the preservation of the admissibility of the constraints: creation of a set of operators which transform inadmissible solutions into admissible ones. They are only applicable to linear restrictions;
- penalty functions-based methods: this method is widely used within the evolutionary algorithms. They are basically based on the penalization of the fitness function when any constraint is violated. The more the violation, the larger the penalization. The penalty factors are tuned in order to be relevant for the fitness function penalization and, at the same time, not locking the algorithm. The violation parameters could be adaptive and dynamic, which means that they may change with the evolutionary process:

  Static penalty: the penalty factors remain constant during the evolution process and throughout the generations. Despite that uniformity, they increase with the level of violation.

  Dynamic penalty: the penalty parameters increase with the generation and level of violation. These parameters must be called adaptive penalty functions when they are updated whenever the solution is locked near a local optimal, since they learn from the search process.
- methods based on the search for admissible solutions: use several search operators in order to handle feasible and infeasible solutions;
- methods based on decoders: use decoding schemes to construct a feasible solution;
- hybrid methods: some hybrid methods use the objective function and penalty function values as vector components and apply multi-objective optimization techniques in order to minimise all of the vector components. In the algorithm, the population is splitted into several subpopulations and each one of them optimises a different part of the vector.

2.6.3 Selection operator

There are several mechanisms whose main goal is to carefully select the individuals for mating.

Proportional selection: the individuals are selected based on their fitness values, having the best ones a bigger probability of reproduction and surviving. This process suffers from scaling problems [29, 77, 78]:

- roulette wheel method: the individuals with higher fitness values are selected more frequently because they take a bigger roulette wheel's space. It has the inconvenient of making the loss of diversity premature;
- stochastic universal sampling: only one shot selects all individuals for reproduction through several pointers, reducing the bias of the method.

Ordination-based selection: the individuals are selected based on their classification in the ordered population [29, 77, 78]:

- tournament selection, in which it is done a copy of the best element present in a two element-tournament;
- the population is sorted by fitness and the individuals with the lower value according to a certain truncation probability are disregarded in the truncation selection;
- linear ranking method, in which the individuals are sorted according to their fitness value and a certain probability of selection is assigned to each one of them as a function of their classification in the ordered population;
- those referred probabilities are weighted exponentially in the exponential ranking selection;
- the elitist method, the one that is used here, consists in the automatic transfer of the best individuals to the next generation without being modified by the genetic operators. It is used to assure a faster convergence, however, it could lead to a premature convergence whether the algorithm is not properly accomplished by a population diversity control.

2.6.4 Crossover operator

The crossover operator is the most important one regarding evolutionary algorithms, being responsible for the genetic information interchanging between chromosomes. It generates new individuals through a combination of genetic material of two parents previously selected. It must produce valid solutions, which is not always possible for constrained problems. The crossover probability is chosen taking into account a balance between the hypothesis of losing high-fitness individuals and the convergence rate [29, 77].

Some of the main operators are described in the table below, Table 2.5, both for real and binary coding mechanisms.

2.6.5 Mutation operator

The mutation operators are unary operators which act in one individual. They affect the chromosome's genes, being defined by a happening probability. The mutation probability is their main parameter and must be controllable in order to achieve the optimal diversity level without compromising the loss of high-fitness individuals. For binary representation, the flip-bit mutation is the

Table 2.5 – Crossover operators. Adapted from [29].

Crossover operators (binary coding)	Crossover operators (real coding)
• single-point crossover (single cut point on the chromosome	• mena-centric recombination
• multipoint crossover (several cut points)	• parent-centric recombination
• uniform crossover (each position can be a cut point)	• single-point or multi-point crossover
• segmented crossover (multipoint crossover variation)	• uniform crossover

main one. It consists in changing one or more chromosome's genes. Uniform and creep mutation are some methods which are applied to real-coded individuals, consisting in the replacement of one or more bits values by a random value between an upper and lower level [29, 77, 79].

2.6.6 Convergence and stopping criteria

There are genotype and phenotype-based stopping criteria. In the genotype ones, the search stops when the population reaches a certain level of convergence regarding the decoded value of its chromosomes. On the other hand, in the phenotype-based criteria the achieved progress in the last pre-defined number of generations regarding the fitness function value, parameter defined by the designer, is measured and assessed. For complex optimization problems, the designer may define a maximum number of generations for the evolution process [29, 80].

2.6.7 Guidelines to achieve a good performance

The diversity of a population is a measure of the different solutions that are presented in a population. The bigger the chromosome's variability, the larger is its entropy and the better its quality. The elitism is frequently used with stochastic schemes of reposition based on fitness, in order to avoid the loss of the better-fitness individuals. The limiting factor in the genetic algorithm's search is, in the majority of cases, the number of assessments of the fitness function. The key for an efficient search is the balance between exploration and exploitation. Exploration is more prevalent in the beginning of the search with its participation grade decreasing with the number of generations, whereas the opposite happens with the exploitation. The exploration process allows to efficiently explore the search domain and generates diverse solutions, making the global optimization more plausible. Randomization in terms of some predefined probability distributions are frequently used for exploration. Although that, the convergence is slower. The exploitation process uses any information which allows itself to generate better solutions and, therefore, substantially increases the convergence rate. However, that information is, in general, local, which could lead to a local optimum. Achieving that balance trivially remains unknown, because essentially it is the optimization of the optimization process, that is, an hyper-optimization problem [29, 33].

2.6.8 Optimization of composite structures using evolutionary-based algorithms

Genetic algorithms are usually used for the ANN's architecture optimization (e.g synaptic weights, biases) due to their inherent specifications and particularly their advantages. There are several works regarding this theme, the optimization of composite structures for vibration and buckling, using an evolutionary-based algorithm, particularly the genetic one, associated with an ANN arrangement to compute efficiently the required mechanical or geometrical parameters.

Due to manufacturing constraints and design verification and assessment, the angles of the composite plies were normally restricted to 0, 45 and 90°. Liu et al. (1998) applied a two level optimization for wing design under strength and buckling constraints. At the first level, the design variables were the number of plies of those prescribed angles and the main goal was the weight minimisation. Then, knowing the number of plies of each orientation and the in-plane loads as well, a genetic algorithm was applied to optimise the stacking sequence so as to maximise the buckling load. Because the thickness of the skin is small compared to the wing depth, stresses and strains are calculated by neglecting the bending stiffness of the skin. Therefore they depend only on the number of plies and not on the stacking sequence [81].

The LOA (layerwise optimization approach) consists in N repetitions of the optimization procedure in an one-dimensional space instead of the search for the optimum solution in a N-dimensional space. This idea is based on the physical consideration of bending plates, during which the outer layer has a greater influence on the structure stiffness than the inner one and it is more important in the determination of the natural frequency [57].

Thus, Narita and Robinson (2006) optimised sequentially the layer's orientation from the outermost to the innermost layer, using the layerwise optimization approach in laminated cylindrical panels with small curvature in one direction [82].

Despite the success of GA's in a wide range of applications, solving constrained optimization problems is not an easy task. The most common technique is to apply penalty functions, converting the problem into an unconstrained optimization one. The major drawback of these penalty functions is the tuning of their parameters, in order to obtain the required final values. Chehouri et al. (2016) implemented a constraint-handling technique which does not use penalty functions and is free of additional parameters. That technique, denominated as VCH (violation constraint-handling), uses a violation factor and is based on the genetic algorithms, since the objective function is preserved during the evolution process and not affected by a modification in the penalty parameters [75].

On the other hand, Todoroki and Haftka (1998) introduced a new repair strategy similar to the way recessive genes operate in biology in order to handle the difficulty to enforce constraints in genetic algorithms. That new strategy changes the decoding rules used to transform the gene's information into the stacking sequence, not altering the genes per si. The genetic algorithm was applied to obtain the stacking sequence corresponding to a set of lamination parameters closer to the target ones. An elitist strategy is used in order to ensure that the best individual is transferred to the next generation, whereas a roulette wheel method is applied for the selection of two par-

ents for crossover. They clamied that the angles of the plies must be balanced in order to avoid stiffness coupling effects. Besides that, the number of successive plies with the same orientation are limited to four due to the risk of delamination resulting from large-scale matrix cracking. The new repair strategy is used to enforce those constraints. In this article, a permutation operator was implemented and it improved the performance of the genetic search [72].

Nagendra et al. (1994) studied the effect of the introduction of several genetic operators on the genetic algorithm whose target was the design of a stiffened panel for minimum weight under stability and strain constraints. His main goals were to improve the algorithm's reliability and reduce its computational cost [83].

Chung et al. (2008) presented some new approaches whose main goal was to reduce the number of fitness function assessments in genetic algorithms applied to the multidisciplinary optimization of composite structures. That improvement results from the needlessness of assessing some individuals already evaluated in previous generations. They validated their procedures by a weight minimization problem of a composite laminated plate under several design constraints. In order to decrease the computational cost, a combination of local improvement with global combinatorial search is performed, which results in an hybrid genetic algorithm. In the design of composite wings, if the standard crossover operator leads to inadmissible solutions regarding some constraints, "gene repair" or "fixing-up" operations are intensively utilised, particularly to handle the number-of-ply constraints, which limit the number of layers of each angle. Besides that, a new permutation crossover was developed designated by gene-rank GA [74].

In order to overcome the premature convergence, Jia-qing Zhao and Wang (2011) developed a kind of centre based genetic algorithm (CBGA). Central chaotic mutation and space shrinking strategies were designed with the information of the population centre, aiming to guide the evolutionary search. The rank value based roulette selection and a new *Cauchy* preferential crossover operator are used with the mutation operators in the CBGA. The elitist strategy is employed to avoid the loss of the best solution. The premature convergence of the genetic algorithms can be regarded as that the population stops evolving towards better solutions, thus the algorithm cannot obtain the global optimum. Population size, selection pressure, mutation rate, fitness function property and population initialization are the main factors to affect premature convergence. To enhance the ability of escaping from local minima, two mutation operators are designed in the CBGA based on the information of the centre, that is, central chaotic mutation and population recombination strategy [84].

Miller et al. (2020) upgraded the standard genetic algorithm, combining it with a deep neural network along with Curriculum learning loop for the optimization of either the fundamental natural frequency or the gap between two successive frequencies of a laminated cylinder through stacking sequence optimization, aiming to avoid the structure's resonance taking into account the excitation frequencies and their approximation to the natural ones. The Curriculum learning Loop is applied after a first stage optimization procedure, being accomplished by a narrowing in the bounds of the variables resulting from the first stage [56].

The optimization with regard to the lowest natural frequency is also largely applied to rotating

machines, whose dynamic forces generated by their moving parts induce large vibration amplitudes. The development of fault diagnosis systems for the vibration detection and isolation of these equipments can be based on artificial intelligence using artificial neural networks [85].

Cicek and Ozturk (2021) developed a hybrid algorithm for time series forecasting based on a biassed random key genetic algorithm in order to optimise an artificial neural network, which is a very time-consuming procedure, since it involves the correct tuning of several parameters together. That algorithm, denominated BRKGA-NN, assists the determination of the number of hidden neurons, their biases and the synaptic weights. They concluded that the BRKGA-NN-based genetic algorithm predicts better results compared to the standard one. However, the main drawback is the running time, which extremely increases with the enlargement of the training set. The motivation for this development is the difficulty inherent to the definition of the ANN's architecture by some method besides trial and error. Moreover, that procedure depends strongly on the type of problem and dataset and, on the other hand, gradient-based algorithms frequently stay trapped to local minima [69].

As referred above, to be able to obtain reliable results regarding the obtained artificial neural network, the train and test data must be representative of the search space. Dey et al. (2016) trained the artificial neural network using Latin hypercube sampling. The multilayer perceptron network that was used had gradient descent as its feedback mechanism. Latin hypercube sampling is employed for generating sample points to ensure the representation of all portions of the vector space [86].

For multiconstraint problems (e.g. fundamental natural frequency together with the critical buckling load), the best objective usually does not imply that the other(s) objective(s) is (are) simultaneously optimised. Thus, the concept of Pareto optimality is often used in multiconstraint problems to help to determine the best way to simultaneously satisfy all objectives to the greatest extent possible [87].

The developed algorithms must be verified regarding their reliability in order for the user to believe in their results. "A measure is said to have a high reliability if it produces similar results under consistent conditions". António and Hoffbauer (2013) performed a design optimization of a composite structure in order to achieve a target reliability level. An artificial neural network was developed and a MCS procedure was implemented to assess the variability of the structural response based on global sensitivity analysis (GSA). The variables under control were the mechanical properties of the composite materials, because they are a considerable source of uncertainties. The uncertainty propagation was performed using the first order *Sobol* indices and relative sensitivities. The composite's stacking sequence was optimised, taking into account the less sensitive performance properties regarding the uncertainties in the input parameters [88].

Moreover, António et al. (2010) studied the propagation of uncertainties of the composite's mechanical properties on the composite laminate structure response in order to achieve a desired reliability level. First order (FORM) and second order (SORM) reliability methods use the most probable failure point (MPP) to estimate the failure probability. The limit state function and its derivatives, if necessary, are approximated by the implementation of an artificial neural network

(ANN). Cheng (2007) proposed a hybrid technique which consists of its combination with genetic algorithms for structural reliability analysis. The ANN-GA arrangement searches for the most probable failure point and its corresponding reliability index [89].

2.7 Multi-objective optimization

The first studies regarding the multi-objective optimization came out in the XIX century by *Edgeworth* and *Pareto* and were based on successive one-objective problems, using the lexicographic ordination (ordination of the objectives by their importance) and linear aggregation functions, assigning to each one of them a certain weight representative of their individual importance. For multi-objective problems, the optimal solution is a set of solutions designated by Pareto's optimal solutions. A certain solution is one of those if it is not possible to improve an objective without deteriorating at least one of the others. The number of Pareto's optimal solutions increases with the size of the problem and, mainly, with the number of considered goals [29, 90, 91].

A multi-objective optimization problem for a minimisation problem can be defined as

$$\text{Min}\,\mathbf{f}(\mathbf{x}) = (f_1(\mathbf{x}), f_2(\mathbf{x}), \ldots, f_n(\mathbf{x})) \tag{2.17}$$

under the constraint $\mathbf{x} \in \mathbf{S}$ and where $n \geq 2$ corresponds to the number of objectives, $\mathbf{x}= (x_1, \ldots, x_k)$ is the vector of the design variables and $\mathbf{S}$ represents the space of admissible solutions associated with the considered constraints and the bounds of the input variables [29, 90, 91].

Pareto dominance: An objective vector $\mathbf{u}$ dominates $\mathbf{v}$ ($\mathbf{u}<\mathbf{v}$) if and only if there is not a $\mathbf{v}$ component lower than the $\mathbf{u}$'s correspondent and at least one component of $\mathbf{u}$ is strictly lower, that is [29, 90, 91]:

$$\forall i \in \{1, \ldots, n\}: \quad u_i \leq v_i \wedge \exists i \in \{1, \ldots, n\} : u_i < v_i \tag{2.18}$$

Pareto optimality: A certain solution $\mathbf{x}^* \in \mathbf{S}$ is a Pareto optimal if for each $\mathbf{x} \in \mathbf{S}$, $\mathbf{f}(\mathbf{x})$ does not dominate $\mathbf{f}(\mathbf{x}^*)$, that is, $\mathbf{f}(\mathbf{x}) \not< \mathbf{f}(\mathbf{x}^*)$.

Set of Pareto's optimals: The set of Pareto's optimals is given by:

$$\mathscr{P}^* = \left\{\mathbf{x} \in \mathbf{S} \mid \nexists \mathbf{x}' \in \mathbf{S}, \mathbf{f}\left(\mathbf{x}'\right) < \mathbf{f}(\mathbf{x})\right\} \tag{2.19}$$

Pareto's front: The front of Pareto is defined as:

$$\mathscr{P}\mathbf{f}^* = \{\mathbf{f}(\mathbf{x}), \mathbf{x} \in \mathscr{P}^*\} \tag{2.20}$$

The number of Pareto's optimal solutions can be different depending on the considered space, the decision or the objective spaces. In the objective space, the solutions with the same objective vector are considered the same, whereas that does not happen in the decision space [29].

Some Pareto's optimal solutions can be obtained by the resolution of the following mathematical programming problem,

$$MOP_{\mu} = \text{Min}\,\mathbf{f}(\mathbf{x}) = \sum_{i=1}^{n} \mu_i f_i(\mathbf{x}), \tag{2.21}$$

subjected to $\mathbf{x} \in \mathbf{S}$ and in which those solutions are designated by supported solutions. The supported solutions are obtained by the multi-objective problem resolution for several values of the weights. On the other hand, some problems cannot be solved by that method, because their solutions are dominated by convex combinations of supported solutions, being denominated by unsupported solutions [29, 90, 91].

2.7.1 Multi-objective optimization methods

The procedures for solving multi-objective optimization problems can be splitted into exact methods, involving certain algorithms, or approximate solutions which take into account the definition of front of Pareto. The branch and bound, dynamic programming and constrained programming are some examples of exact algorithms. The main approaches to deal with these kind of problems are described in subsection 2.7.2.

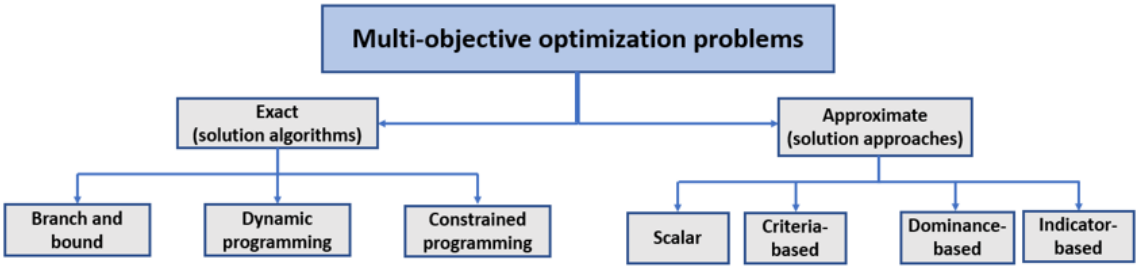

Figure 2.6 – Multi-objective optimization methods. Adapted from [29, 90, 92].

2.7.2 Multi-objective optimization classification

The multi-objective optimization problems can be categorised according to the fitness function definition:

- **Scalar approaches**: They are based on the transformation of the multi-objective problem into an one-objective one. These approximations require the user to have a good knowledge about the problem under analysis. They have a strong sensibility in relation to the selected weights, constraints or reference points, which leads to a high computational effort resulting from the repetitive procedures aiming to obtain different Pareto's optimal solutions [28, 29, 90].

Aggregation method: it uses a linear aggregation function combining all objective functions. The aggregation method is one of the most used to generate Pareto's optimal solutions:

$$F(\mathbf{x}) = \sum_{i=1}^{n} \mu_i \cdot f_i(\mathbf{x}), \mathbf{x} \in \mathbf{S} \tag{2.22}$$

For multi-objective problems with a concave Pareto's front, the decider will have an erroneous idea of the Pareto's front came from the sequential weight vector's changing. If the objectives are not at the same scale, they must be normalised in the aggregation function. The obtained results depend strongly on the considered weight vector. It can be an unique weight vector previously defined according to the designer preferences, a simple hypothesis only possible for linear utility functions; multiple weight vectors previously defined, being the problem solved for each one of them in parallel; dynamic definition of multiple weights, in which the weights are changed in order to approximate the Pareto's front; adaptive definition of multiple weights, in which are accordingly defined sub-regions of the Pareto's front to refine the search space [28, 29, 90].

Ponderate metrics: the designer must define the reference point $\mathbf{z}$ to be achieved and the parameter used to quantify the distance between $\mathbf{z}$ and the admissible region of the search space, p_{dist}. Therefore, that referred distance is minimised [29]:

$$MOP(\mu, \mathbf{z}) = Min \left(\sum_{j=1}^{n} \mu_j \mid f_j(\mathbf{x}) - \mathbf{z}_j \mid^{p_{dist}} \right)^{\frac{1}{p_{dist}}} \tag{2.23}$$

Goal programming: the designer defines aspiration levels, T_i, for each objective which establishes goals to achieve:

$$\min \sum_{i=1}^{n} |f_i(\mathbf{x}^*) - T_i|, \quad \text{subject to } \mathbf{x}^* \in \mathscr{P}\mathbf{f}^* \tag{2.24}$$

This method is computationally effective as long as the solution $\mathbf{x}^*$ is chosen within the feasible domain. However, it is strongly dependent on the correct selection of the target vector [29, 90].

Achievement functions: an arbitrary reference point can be defined, because this method uses normalisation factors [29].

Goal Attainment method: this method is again based on the designer preferences. The weight and goal vectors must be defined by the designer for all objectives. Relatively to the ponderate metrics method, the function is now differentiable, which makes plausible the use of gradient-based optimization algorithms. The main disadvantage is the absence of pressure selection for the generated solutions, that is, if there are two candidate solutions which are the same in one objective function value but different in the other, they will still

have the same goal-attainment value for their two objectives. Despite that, this method is simple and easy to implement [29, 90].

ε-constrained method: the objectives, apart from only one, are transformed into additional constraints and a limit value is assigned for each one of them. The variation of those limit values enables to reach the front of Pareto. Although its simplicity, this method is time-consuming and may originate unsupported solutions, that is, solutions at a concave region of the search space [29, 90] .

- **Criteria-based approaches**: They separate the objectives according to a certain criteria and then treat each set separately. The lexicographic optimization and the evolutionary-based algorithms are examples of them.

  Parallel approach: the generation of new solutions is performed independently according to the objective's nature. The population of individuals is splitted into k_{sub} subpopulations, in which k_{sub} represents the number of objectives. The individuals with the better fitness value regarding each one of the objective functions individually are integrated in those subpopulations, then they are mixed and the conventional crossover and mutation operators are implemented. The main disadvantage of this approach is the inability to produce Pareto-optimal solutions for non-convex search spaces due to the linear combination of the objectives [29, 90].

  Lexicographic or sequential approach: the objectives are ordered according to the respective importance assigned by the designer. The optimal solution is achieved by the sequential optimization procedure, in which the number of constraints is incremented as a result of a search space narrowing. Despite its simplicity, it may favour a particular set of similar objectives, driving the evolution process to a specific part of the front of Pareto instead of precisely defining it [29, 90].

- **Dominance-based approaches**: These methods use the dominance concept in the fitness function definition. The main idea is to find a set of individuals in the population which are Pareto solutions and are not dominated by the remaining population. This concept was introduced by *Goldberg*, particularly in the genetic algorithms. A niching technique was, posteriorly, suggested, aiming to avoid the convergence for only one point in the Front of Pareto, allowing to keep individuals along the non-dominated border. The main advantage is that these methods do not need the problem to be transformed into a mono-objective one. With only one execution, they are capable of generating a diverse set of Pareto's optimal solutions and Pareto solutions at the concave zones of the convex border of the admissible search space. Moreover, in dominance-based approaches, the quality of a solution is assessed in relation to all population and no absolute value is assigned to them. These procedures are the best to explore the front of Pareto regardless of its shape or continuity. However, it is challenging to test for non-dominance in a set of feasible solutions [29, 90].

MOGA (multi-objective genetic algorithm): the ordenated classification of a certain individual corresponds to the number of chromosomes of the current population that dominates it. The main reported disadvantage of this algorithm is that the fitness distribution is performed in the space of the objective function values, which implies that two solutions with the same objective function value cannot be simultaneously in the population. Therefore, the designer does not know which design variables combinations result in the same desired fitness value. On the other hand, this algorithm is extremely efficient and easy to implement [29, 90].

NSGA (Non-dominated Sorting Genetic algorithm): this algorithm was proposed by *N.Srinivas* and *Kalyanmoy Deb* and is based on a sorted selection method aiming to emphasise non-dominated current solutions and in a niching generation procedure whose main goal is to keep the population's diversity. They differ from the standard genetic algorithm only in the selection operator [29, 90].

NSGA-II: the NSGA variation was proposed by Deb et al., an improved elitist version. This algorithm creates niches at a prescribed crowding distance by using the selection operator in order to keep the population's diversity at the Pareto's front [29, 90].

- **Indicator-based approaches**: The performance of dominance-based algorithms rapidly becomes worse when the number of objective functions increases (above 4) due to the loss of selection pressure. The indicator-based algorithms use quality indicators which are functions that assess the approximation sets. These algorithms claim the following advantages: the designer preferences can be easily incorporated into the optimization algorithm; the diversity is implicitly taken into account in the performance indicator definition; less sensibility regarding discontinuities and non-convexity at the front of Pareto and less parameters to define and tune. There are several types of performance indicators, including the cardinality indicators, which measure the number of non-dominated points provided by an algorithm; the convergence indicators quantifying how close a set of non-dominated points is from the Pareto front in the objective space; the distribution and spread indicators, wherein the distribution of Pareto front approximations is assessed, being particularly useful when there are multiple solutions in the Pareto set that correspond to different objective vectors; and the convergence and distribution indicators mixing both properties of convergence and distribution ones. Their main applications range from a straightforward comparison between algorithms for multi-objective optimization to the definition of stopping criteria or the assessment of the diversity present in a given approximation set [29, 93].

2.7.3 Constraint multi-objective evolutionary algorithms

The constraint multi-objective optimization algorithms can be divided into the following categories [29]:

- in this first method, the one-optimization techniques for constrained problems are applied. The algorithm preserves non-admissible elitist solutions to connect disconnected admissible regions and the stochastic ranking is performed in order to balance objectives and constraints;
- the second one manipulates the constraints, treating them as additional goals;
- this method is based on sorting of priorities for the admissible and non-admissible solutions;
- the fourth method uses a genetic reparation scheme in order to reproduce admissible solutions or solutions less violated than the original ones;
- the last one creates mechanisms aiming to guide the admissible solutions to the front of Pareto and the non-admissible ones to the admissible solutions space.

The multi-objective evolutionary algorithms assessment must be done by more than one performance indicator. Diversity preservation strategies must be incorporated in those algorithms. The main idea under each one of them is to penalise closed solutions in the design space and even in the objective functions space, because the target is to obtain solutions well distributed at the Pareto's front. The most important techniques are the kernel method, nearest neighbour procedure and histogram or grids [29, 93].

2.7.4 Multi-objective optimization applied to composite structures

Due to the complex loading cases and required reliability, multi-objective optimization procedures are paramount for the design of complex stiffened composite structures, such as the one that is studied here. Therefore, over the years several studies had been carried out regarding this theme.

Irisarri et al. (2009) performed a multi-objective evolutionary-based optimization procedure in a composite panel subjected to compression and shear loads, in order to obtain the stacking sequence that corresponds to the maximum of the buckling margins under several loading conditions and, at the same time, to the minimum of weight. The algorithm was run for 300 different loading scenarios, resulting for each one of them a particular front of Pareto. Then, the optimization was guided in order to comply with pre-established constraints and preferred guidelines [94].

The same goals were sought by Ehsani and Dalir (2019) in the optimization of a grid stiffened plate. They used the ε-constraint method together with a genetic algorithm embedded in an artificial neural network arrangement in order to accurately predict the variables under analysis. The buckling load was considered as the main goal, whereas the weight of the structure was incorporated as an additional constraint, wherein the ε value was increased gradually in order to obtain the Pareto-frontier curve. The data to train and test the ANN was obtained by them using the *Mindlin* plate theory and the *Ritz* method. The design variables were the number, width, thickness and angle of each one of the two sets of ribs [95].

Seyyedrahmani et al. (2022) performed several combinations of natural frequencies, buckling load and cost as objective functions for the optimization of a composite sandwich panel and

utilised a genetic algorithm to achieve the optimal lamination parameters and thicknesses. The *Chebyshev* polynomials associated with *Hamilton*'s principle were used to determine the mechanical responses, which had a significant effect on the reduction of the computational time due to their meshless nature. The optimal results are presented in the form of 2D and 3D (three objectives) Pareto-frontier curves. The individuals were sorted according to their ranking and crowding distance and an elitist strategy combined with the crowding distance were used to select the best individuals for the successive generations [96].

Composite sandwich plates were also optimised by Kheirikhah (2020) regarding their weight and deflection under a transverse load or their weight and buckling load subjected to in-plane loads. Additionally, a third-order shear deformation theory together with the *Hamilton*'s principle and *Navier*'s equations were used to predict the variables under analysis, due to the necessity to ensure the displacement and transverse shear stresses continuity at the core/face sheets interfaces, to have zero transverse shear stresses at the top and bottom surfaces of the plate and to account for the transverse flexibility and transverse normal strain and stress of the core. The multi-objective optimization was performed using a genetic algorithm and Pareto's fronts were achieved according to the dominance concept [97].

Kalita et al. (2019) worked with skew composite plates, aiming to maximise both the fundamental natural frequency and the difference between the first two natural frequencies by changing the plies angles. Three different evolutionary-based algorithms were used, the genetic algorithm (GA), a particle swarm optimization (PSO) variant and a cuckoo search (CS) variant as well. The weight summation method was applied in the genetic-based algorithm in order to transform the multi-objective problem into several mono-objective problems. It was verified that the use of the CS variant led to better results regarding the absolute maxima achievement. Moreover, that optimization procedure has less tuning parameters than the other two, which led to a reduction in the development time [98].

Ganesh et al. (2021) implemented, as well, the multi-objective optimization of the fundamental natural frequency and the difference between the first two natural frequencies, using NSGA-III (non-dominated sorting genetic algorithm) and RPSOLC (repulsive particle swarm optimization with local search and chaotic perturbation), a memetic version of the conventional PSO, to obtain the Pareto-frontier curves. It was observed a more uniform and less spread front of Pareto for the genetic-based algorithm results [99].

H. An et al. (2018) aimed to maximise the fundamental natural frequency of a composite stiffened panel, seeking to minimise its mass as well. The design variables were the stacking sequences and plies thicknesses for the panel skin and stiffeners and the stiffeners number and respective positions along the panel. A genetic-based algorithm was developed and the weight summation method was employed to consider the two objectives simultaneously [100].

A multi-objective optimization procedure was performed by Murugesan et al. (2015) in order to efficiently design a composite stiffened panel subjective to a compressive load, maximising its critical buckling load and, at the same time, minimising its interlaminar shear stress and structural mass. The failure of a stiffened composite plate generally starts at the interface between the panel

skin and stiffeners due to the stress concentrations. These investigators tried to improve the stress distribution in those areas by using cover-skin layups around them to increase the bending stiffness and decrease the risk of delamination [101].

With the thicknesses, orientations, and dimensions of the stiffeners as design variables, Conceição António (2013) carried out an optimization procedure with regard to the minimization of both the weight and strain energy of an hybrid composite structure subject to constraints related to its structural integrity (stress, buckling and displacement). The constraints are imposed on the critical load factor, λ_{crit}, and on the critical displacement, d_{crit}. MOHGA (multi-objective hierarchical genetic algorithm), a self-adaptive genetic search technique that incorporates Pareto dominance and an elitist approach based on individual age control and the survival of non-dominated solutions, is employed with co-evolution of multi-populations. In age-structured populations, the quantity and longevity of non-dominated individuals are crucial for building the global Pareto front [102].

Conceição António and Hoffbauer (2016) and António and Neves Carneiro (2018) implemented a bi-objective optimization procedure, aiming to minimise the structure's weight and the variability of structural response with feasibility robustness of design constraints, which is assessed by the determinant of the variance-covariance matrix representing the joint effects of the propagation of uncertainties. Optimality is defined as the minimization of the structural weight and robustness as the minimization of the determinant of the variance-covariance matrix of the structural responses, being acknowledged by the tolerance to the input uncertainties. The Pareto front is built using an hierarchical genetic algorithm with co-evolution of populations, denoted by MOGA-2D, wherein the evolution is based on the exchange data between two populations using the crossover operator, a small population (SP) using local dominance as fitness measure and elitism and an enlarged population (EP) to store the non-dominated solutions. The presence of two parallel populations is essential for the method to successfully converge because it enables the reduction of the number of non-dominated solutions stored in the SP while preserving that information in the EP, allowing the evolutionary search to progress while attempting to maintain diversity and the best Pareto-optimal front [103, 104]. The same procedure was adopted by Conceição António (2015), using the Co-Dominance-based genetic algorithm with two levels of dominance concepts and two exchanging-populations connected by the crossover operator with selective mating selection of parents taking into account the dominance at the enlarged population [105].

2.8 Design of composite structures

Even though they have high specific stiffness and strength, structures in composite materials are usually thin, then susceptible to buckle and, regardless of their thickness, to enter into resonance conditions when the excitation frequencies are similar to the natural ones and, therefore, there is an amplification of the amplitude of vibration, particularly for lightly damped structures. Optimization of composite plates to maximise buckling loads is essential nowadays with the increasing use

of composite materials in the most varied industries. Due to the existence of design flexibility, the design of composite laminates frequently integrates the plies thicknesses and orientations as design variables. For buckling design, it is often suggested that the outer plies have +/-45° orientation, which enhances the composite laminate behaviour under in-plane compressive loads and for damage tolerance requirements [11, 83, 106–108]. The ability of a structure to withstand the design load and continuing to fulfill its intended purpose in the presence of cracks and other types of damage is known as damage tolerance. Damage reduces particularly the compression strength. Four different approaches were identified by Boeing to reduce the negative impact of damage: develop damage tolerant structure; improve quality control to reduce fabrication damage; improve non-destructive evaluation methods for detecting damage during manufacturing; and implement in-service inspection methods that ensure the detection of critical service damage. Composite panels are usually reinforced with stiffeners in order to increase their out-of-plane stiffness and improve their buckling behaviour. The optimization of their shape, size and location is very important on global buckling of the wing panel, because local buckling of the wing skin may occur for low load levels even before the wing panel reaches its own critical buckling load, whether they are not properly arranged. Panels with skins consisting ultimately of 45° plies are more damage tolerant due to the low load level in the skin, which retards the skin-stiffener separation due to the absence of buckling at design ultimate loads. Moreover, in order to prevent early disbonding or delamination resulting from transverse strain differentials, the skin-stiffener interface should have a reduced Poisson's ratio mismatch [83, 106–108]. The benefit that results from the fibre angles optimization is the changing of the structure's stiffness which, consequently, has an influence on the modes of vibration [56–58, 61, 62, 83].

2.9 Summary

In this chapter, the state of the art regarding the optimization techniques suitable for application in the aerospace industry, particularly in the composite laminates design, was presented and discussed. Emphasis was given to the genetic algorithms embedded in an ANN arrangement. Firstly, the main characteristics associated to the artificial neural networks were deeply discussed, highlighting their advantages and drawbacks and describing why their use could improve the algorithm's performance. It was concluded that accurate results may be achieved in the predictions of the fundamental natural frequency and critical buckling load, physical variables under analysis, saving significantly the computational time required by FEM simulations. Afterwards, the main ANN's training processes were analysed, the gradient-based and the evolutionary-based optimization algorithms. The genetic algorithms are zero-order optimization procedures, that is, they do not need derivatives of the objective functions to be calculated, which reduces considerably the time necessary to obtain notable results. However, the tuning of their parameters are an extremely time-consuming task based on a trial and error procedure. On the other hand, the derivatives are necessary for the implementation of the gradient-based procedures, what increases the development time despite being algorithms with a good performance. Finally, particular attention was

given to the multi-objective optimization algorithms, which are procedures extremely relevant for the optimization of structures like the one studied here, wherein the optimization of several variables simultaneously, such as the maximisation of the critical buckling load and, at the same time, the minimisation of the mass, is a key aspect in order to obtain the best structure as possible for those high-responsibility applications. The main methods were presented and compared in relation to their inherent complexity, computational time and performance.

Chapter 3

Mathematical model

3.1 Introduction

In this chapter, the constitutive relations and equilibrium equations regarding the behaviour of a composite laminated plate are presented. Besides that, the fundamental equations to determine the natural frequencies and buckling loads of the considered structure are deduced, according to the *Lévy* and *Rayleigh-Ritz* methods.

Lastly, it was tried to derive the differential equations of motion for a stiffened composite plate in order to predict its fundamental natural frequency and, therefore, to verify the FEM model created for that effect.

3.2 Composite materials

The composite panel under analysis is a thin plate composed of several CFRP plies stacked together. Each layer has unidirectional fibres supported by a polymeric matrix. The matrix assembles all the fibres, keeping them together, acting as a load-transfer and protecting them from the environment.

Firstly, the constitutive relations are described in the material principal directions for each lamina k (see Figure 3.1). The material referential is oriented of an angle θ in relation to the main referential O_{xyz}. Only the macromechanical behaviour of a lamina is considered and it is assumed that the generalised $Hooke$'s law remains valid. Moreover, the material is taken as orthotropic, that is, there are three mutually orthogonal planes of symmetry. Therefore, the number of independent material parameters is reduced to 9 (E_1, E_2, E_3, G_{12}, G_{13}, G_{23}, ν_{12}, ν_{13} and ν_{23}). In this formulation, the thickness of each layer is constant, the strains and displacements are small and, according to the thin plate theory, the transverse shear stresses are neglected [109, 110].

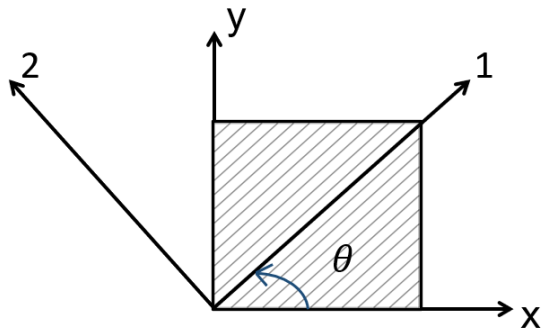

Figure 3.1 – Material principal directions.

The number 1 refers to the fibre direction, therefore the maximum stiffness direction, whereas the number 2 indicates, obviously, the direction perpendicular to the fibres' direction, so it points out the direction with the lowest *Young* modulus.

Assuming that the material is homogeneous, their layers are perfectly bonded together and either orthotropic or transversely isotropic, the relations between the stresses and deformations for each lamina k are given by

$$\begin{Bmatrix} \sigma_{11} \\ \sigma_{22} \\ \sigma_{12} \end{Bmatrix}^{(k)} = \frac{1}{1 - \nu_{12} \cdot \nu_{21}} \begin{bmatrix} E_1 & \nu_{12} \cdot E_2 & 0 \\ \nu_{21} \cdot E_1 & E_2 & 0 \\ 0 & 0 & G_{12} \cdot (1 - \nu_{12} \cdot \nu_{21}) \end{bmatrix} \begin{Bmatrix} \varepsilon_{11} \\ \varepsilon_{22} \\ \gamma_{12} \end{Bmatrix}^{(k)}, \tag{3.1}$$

$$\begin{Bmatrix} \sigma_{13} \\ \sigma_{23} \end{Bmatrix}^{(k)} = \begin{bmatrix} G_{13} & 0 \\ 0 & G_{23} \end{bmatrix} \begin{Bmatrix} \gamma_{13} \\ \gamma_{23} \end{Bmatrix}^{(k)}, \tag{3.2}$$

wherein E_1 corresponds to the *Young* modulus at the fibre direction, E_2 to the same elastic property in the direction perpendicular to the fibres, the *Poisson*'s coefficient $\nu_{ij} = -\frac{\varepsilon_j}{\varepsilon_i}$ regards the strains' ratio when a load is applied through the i direction and G corresponds to the shear modulus. Usually, the laminate is considered transversely isotropic if the fibres are randomly disposed at each ply.

For thin plates, the segments normal to the medium non-deformed plane remain approximately straight and perpendicular to that deformed surface, therefore γ_{13}=γ_{23}=0 and, consequently, the shear stresses are also null according to equations 3.2. Moreover, those segments do not stretch, which leads to $\varepsilon_{33} = 0$. The normal stress regarding the transverse direction is also considered null, because it takes a value significantly lower in comparison with the in-plane normal stresses [109, 110].

Using the matrix which allows the transformation of the stresses from the principal/local referential to the referential O_{xyz}, the following equations regarding the relationships between stresses and deformations are achieved for each lamina k:

$$\begin{Bmatrix} \sigma_{xx} \\ \sigma_{yy} \\ \sigma_{xy} \end{Bmatrix}^{(k)} = \begin{bmatrix} \bar{Q}_{11} & \bar{Q}_{12} & \bar{Q}_{16} \\ \bar{Q}_{12} & \bar{Q}_{22} & \bar{Q}_{26} \\ \bar{Q}_{16} & \bar{Q}_{26} & \bar{Q}_{66} \end{bmatrix}^{(k)} \begin{Bmatrix} \varepsilon_{xx} \\ \varepsilon_{yy} \\ \gamma_{xy} \end{Bmatrix}^{(k)} ; \tag{3.3}$$

$$\begin{Bmatrix} \sigma_{yz} \\ \sigma_{xz} \end{Bmatrix}^{(k)} = \begin{bmatrix} \bar{Q}_{44} & \bar{Q}_{45} \\ \bar{Q}_{45} & \bar{Q}_{55} \end{bmatrix}^{(k)} \begin{Bmatrix} \gamma_{yz} \\ \gamma_{xz} \end{Bmatrix}^{(k)} .$$

All stress, deformation and displacement variables depend, in general, on their spatial coordinates (x,y,z) and time t, except the midplane ones which do not depend upon the transverse coordinate. By simplification, these dependencies are omitted. The reduced stiffness coefficients $\bar{Q}_{ij}$ are obtained according to the following equations:

$$\begin{aligned}
\bar{Q}_{11} &= Q_{11} \cdot m^4 + 2 \cdot (Q_{12} + 2 \cdot Q_{66}) \cdot m^2 \cdot n^2 + Q_{22} \cdot n^4; \\
\bar{Q}_{12} &= (Q_{11} + Q_{22} - 4 \cdot Q_{66}) \cdot m^2 \cdot n^2 + Q_{12} \cdot \left(m^4 + n^4\right); \\
\bar{Q}_{16} &= -m \cdot n^3 \cdot Q_{22} + m^3 \cdot n \cdot Q_{11} - m \cdot n \left(m^2 - n^2\right) \cdot (Q_{12} + 2 \cdot Q_{66}); \\
\bar{Q}_{22} &= Q_{11} \cdot n^4 + 2 \cdot (Q_{12} + 2Q_{66}) \cdot m^2 \cdot n^2 + Q_{22} \cdot m^4; \\
\bar{Q}_{26} &= -m^3 \cdot n \cdot Q_{22} + m \cdot n^3 \cdot Q_{11} + m \cdot n \cdot \left(m^2 - n^2\right) \cdot (Q_{12} + 2Q_{66}); \\
\bar{Q}_{44} &= Q_{44} \cdot m^2 + Q_{55} \cdot n^2; \\
\bar{Q}_{45} &= (Q_{55} - Q_{44})\, mn; \\
\bar{Q}_{55} &= Q_{55} \cdot m^2 + Q_{44} \cdot n^2; \\
\bar{Q}_{66} &= (Q_{11} + Q_{22} - 2Q_{12}) \cdot m^2 \cdot n^2 + Q_{66} \cdot \left(m^2 - n^2\right)^2;
\end{aligned} \tag{3.4}$$

$$m = \cos\theta \quad ; \quad n = \sin\theta .$$

The coefficients Q_{ij} are denominated by stiffness coefficients and depend only upon the elastic properties:

$$Q_{11} = \frac{E_1}{1 - \nu_{12} \cdot \nu_{21}} \quad ; \quad Q_{22} = \frac{E_2}{1 - \nu_{12} \cdot \nu_{21}} \quad ; \quad Q_{12} = \frac{\nu_{12} \cdot E_2}{1 - \nu_{12} \cdot \nu_{21}} = \frac{\nu_{21} \cdot E_1}{1 - \nu_{12} \cdot \nu_{21}}; \tag{3.5}$$

$$Q_{66} = G_{12} \quad ; \quad Q_{44} = G_{23} \quad ; \quad Q_{55} = G_{13} .$$

The relations between the deformations and displacements, neglecting some higher order terms (*Von-Kármán*'s equations), are described below:

$$
\begin{aligned}
\varepsilon_{xx} &= \frac{\partial u}{\partial x} + \frac{1}{2}\left(\frac{\partial w}{\partial x}\right)^2 \quad ; \quad \varepsilon_{xy} = \frac{1}{2}\left(\frac{\partial u}{\partial y} + \frac{\partial v}{\partial x} + \frac{\partial w}{\partial x}\frac{\partial w}{\partial y}\right); \\
\varepsilon_{xz} &= \frac{1}{2}\left(\frac{\partial u}{\partial z} + \frac{\partial w}{\partial x}\right) \quad ; \quad \varepsilon_{yy} = \frac{\partial v}{\partial y} + \frac{1}{2}\left(\frac{\partial w}{\partial y}\right)^2; \\
\varepsilon_{yz} &= \frac{1}{2}\left(\frac{\partial v}{\partial z} + \frac{\partial w}{\partial y}\right) \quad ; \quad \varepsilon_{zz} = \frac{\partial w}{\partial z}; \\
\varepsilon_{xy} &= \frac{1}{2}\gamma_{xy} \quad ; \quad \varepsilon_{xz} = \frac{1}{2}\gamma_{xz} \quad ; \quad \varepsilon_{yz} = \frac{1}{2}\gamma_{yz}.
\end{aligned}
\tag{3.6}
$$

For a thin plate according to the classical laminated plate theory, the in-plane and transverse displacements can be calculated according to the expressions below as a function of the midplane displacements u_0, v_0 and w_0:

$$
\begin{aligned}
u &= u_0 - z \cdot \frac{\partial w_0}{\partial x}; \\
v &= v_0 - z \cdot \frac{\partial w_0}{\partial y}; \\
w &= w_0.
\end{aligned}
\tag{3.7}
$$

The membrane forces per unit length and the bending and twisting moments can be written as

$$
\left\{ \begin{array}{c} \mathbf{N} \\ \mathbf{M} \end{array} \right\} = \left[\begin{array}{cc} \mathbf{A} & \mathbf{B} \\ \mathbf{B} & \mathbf{D} \end{array} \right] \left\{ \begin{array}{c} \boldsymbol{\varepsilon}_o^m \\ \boldsymbol{\varepsilon}_o^b \end{array} \right\}; \tag{3.8}
$$

$$
(A_{ij}, B_{ij}, D_{ij}) = \sum_{k=1}^{n_L} \int_{h_{k-1}}^{h_k} \left(1, z, z^2\right) \bar{Q}_{ij}^{(k)} \mathrm{d}z \quad i, j = 1, 2 \text{ or } 6;
$$

$$
\boldsymbol{\varepsilon} = \left\{ \begin{array}{c} \boldsymbol{\varepsilon}_o^m \\ \boldsymbol{\varepsilon}_o^b \end{array} \right\} = \left\{ \begin{array}{c} \varepsilon_x^0 \\ \varepsilon_y^0 \\ \gamma_{xy}^0 \\ \chi_{xx} \\ \chi_{yy} \\ \chi_{xy} \end{array} \right\} \quad ; \quad \mathbf{N} = \left\{ \begin{array}{c} N_x(x,y,t) \\ N_y(x,y,t) \\ N_{xy}(x,y,t) \end{array} \right\} \quad ; \quad \mathbf{M} = \left\{ \begin{array}{c} M_x(x,y,t) \\ M_y(x,y,t) \\ M_{xy}(x,y,t) \end{array} \right\};
$$

$$
\left\{ \begin{array}{c} \varepsilon_{xx}(x,y,z,t) \\ \varepsilon_{yy}(x,y,z,t) \\ \gamma_{xy}(x,y,z,t) \end{array} \right\} = \left[\begin{array}{cccccc} 1 & 0 & 0 & -z & 0 & 0 \\ 0 & 1 & 0 & 0 & -z & 0 \\ 0 & 0 & 1 & 0 & 0 & -z \end{array} \right] \left\{ \begin{array}{c} \boldsymbol{\varepsilon}_o^m(x,y,t) \\ \boldsymbol{\varepsilon}_o^b(x,y,t) \end{array} \right\},
$$

wherein A_{ij} is an extensional stiffness coefficient, B_{ij} a bending-extensional stiffness coefficient and D_{ij} the bending stiffness coefficient. The matrix $\mathbf{B}$ is null if the laminate is symmetric about its midplane. Moreover, n_L represents the number of layers whose height is equal to $h_{(k)}$ - $h_{(k-1)}$. $\boldsymbol{\varepsilon}_o^m$ corresponds to the membrane strains at the middle surface, whereas $\boldsymbol{\varepsilon}_o^b$ represents the curvatures.

The composite panel under analysis is arranged symmetrically from both a geometric and material property standpoint. The constitutive relations can be written as:

$$\begin{Bmatrix} N_{xx} \\ N_{yy} \\ N_{xy} \end{Bmatrix} = \begin{bmatrix} A_{11} & A_{12} & 0 \\ A_{12} & A_{11} & 0 \\ 0 & 0 & A_{66} \end{bmatrix} \begin{Bmatrix} \varepsilon_x^0 \\ \varepsilon_y^0 \\ \gamma_{xy}^0 \end{Bmatrix};$$
$$\begin{Bmatrix} M_{xx} \\ M_{yy} \\ M_{xy} \end{Bmatrix} = \begin{bmatrix} D_{11} & D_{12} & D_{16} \\ D_{12} & D_{11} & D_{26} \\ D_{16} & D_{26} & D_{66} \end{bmatrix} \begin{Bmatrix} \chi_{xx} \\ \chi_{yy} \\ \chi_{xy} \end{Bmatrix}. \tag{3.9}$$

For this particular laminate, the bending-stretching coupling coefficients B_{ij} and extensional stiffness coefficients A_{16} and A_{26} are zero, due to symmetry conditions and the interchange between $+\theta$/-θ plies. This means that bending–stretching coupling are not present in such laminates, B_{ij}=0. Therefore, in-plane loads does not generate bending and twisting curvatures which cause out-of-plane warping, and bending moments does not produce an extension of the middle surface. This characteristic is particular desirable for structures subjected to hygrothermal forces due to changes in environmental conditions, wherein those forces could lead to undesirable warping in nonsymmetric laminates. On the other hand, there is no coupling between direct stresses and shear strains, that is, A_{16}=A_{26}=0, because the layup is balanced, for every layer with a $+\theta$ orientation there is a similar one with -θ orientation. The bending-twisting coefficients D_{16} and D_{26} tend to zero as the number of layers increases for multilayered symmetric and balanced laminates. Thus, for a large number of layers, they can be neglected because their magnitude is significantly lower in comparison with the other bending-twisting coefficients [2, 111–113].

The equilibrium equations deduced for the isotropic materials are also valid for non-isotropic ones. By equilibrium of forces and moments:

$$\frac{\partial}{\partial x}\left(\frac{\partial M_{xx}}{\partial x} + \frac{\partial M_{yx}}{\partial y}\right) + \frac{\partial}{\partial y}\left(\frac{\partial M_{yy}}{\partial y} + \frac{\partial M_{xy}}{\partial x}\right) = -p;$$
$$\frac{\partial N_x}{\partial x} + \frac{\partial N_{yx}}{\partial y} = 0; \tag{3.10}$$
$$\frac{\partial N_y}{\partial y} + \frac{\partial N_{xy}}{\partial x} = 0.$$

In the next figure, Figure 3.2, the membrane forces per unit length and the torsional and bending moments are represented along x and y.

3.3 Equations of motion for an unstiffened composite plate

3.3.1 *Hamilton*'s variational principle

The equations of motion of the composite plate can be achieved by using the *Hamilton*'s variational principle. According to this principle, the sum of the variations of the kinetic and strain energies plus the work done by the non-conservative forces during any time interval $[t_1, t_2]$ is null:

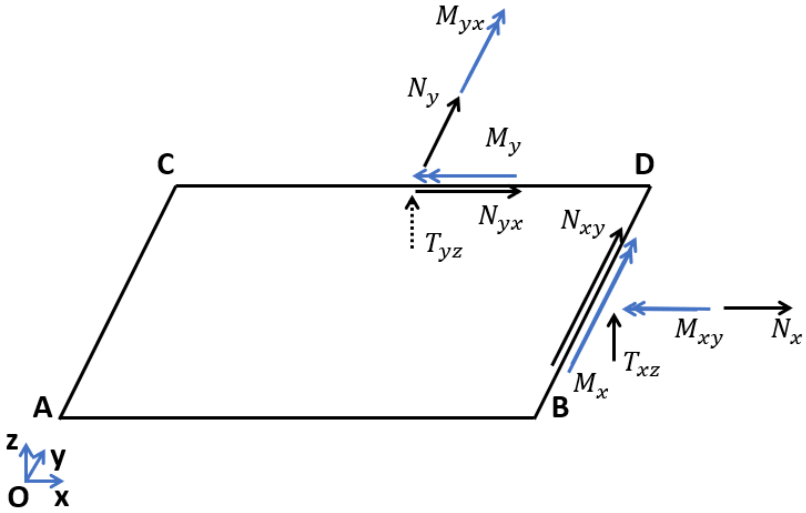

Figure 3.2 – Representation of the membrane forces and moments acting on the composite panel.

$$\delta \int_{t_1}^{t_2} [T - (F + U)] \mathrm{d}t = 0 \tag{3.11}$$

The variable T and U are, respectively, the kinetic and strain energies and F is here related to the external forces acting on the panel, being δF the virtual work of those forces. These variables are calculated according to the following expressions,

$$\begin{aligned} T &= \int_V \frac{\rho}{2} \frac{\partial \mathbf{u}}{\partial t} \cdot \frac{\partial \mathbf{u}}{\partial t} \mathrm{d}V, \quad U = \int_V U_0 \mathrm{d}V \\ \delta F &= -\left(\int_V \mathbf{f} \cdot \delta \mathbf{u} \mathrm{d}V + \int_A \hat{\mathbf{t}} \cdot \delta \mathbf{u} \mathrm{d}A \right), \end{aligned} \tag{3.12}$$

wherein $\delta \mathbf{u}$ represents the virtual displacement vector, $\mathrm{d}V$ and $\mathrm{d}A$ the infinitesimal volume and surface elements, $\mathbf{f}$ the body forces vector and $\hat{\mathbf{t}}$ the tractions acting on the panel's surface.

3.3.2 Equations of motion

Taking into account all simplifications performed in section 3.2, the physical quantities involved in the variational principle described above are written as:

$$\begin{aligned} \delta U &= \int_S \int_{-\frac{h}{2}}^{\frac{h}{2}} (\sigma_{xx} \delta \varepsilon_{xx} + \sigma_{yy} \delta \varepsilon_{yy} + 2\sigma_{xy} \delta \varepsilon_{xy}) \mathrm{d}z \mathrm{d}x \mathrm{d}y; \\ \delta F &= -\int_S \left[q_t(x,y,t) \delta w \left(x, y, \frac{h}{2} \right) + q_b(x,y,t) \delta w \left(x, y, -\frac{h}{2} \right) \right] \mathrm{d}x \mathrm{d}y \end{aligned} \tag{3.13}$$

$$
\begin{aligned}
&-\int_{\Gamma_\sigma}\int_{-\frac{h}{2}}^{\frac{h}{2}}\left[\hat{\sigma}_{nn}\delta u_n+\hat{\sigma}_{ns}\delta u_s+\hat{\sigma}_{nz}\delta w\right]\mathrm{d}z\mathrm{d}s;\\
&\delta T=\int_S\int_{-\frac{h}{2}}^{\frac{h}{2}}\rho\left[\left(\dot{u}_0-z\frac{\partial\dot{w}}{\partial x}\right)\left(\delta\dot{u}_0-z\frac{\partial\delta\dot{w}}{\partial x}\right)\right]\mathrm{d}z\mathrm{d}x\mathrm{d}y\\
&+\int_S\int_{-\frac{h}{2}}^{\frac{h}{2}}\rho\left[\left(\dot{v}_0-z\frac{\partial\dot{w}}{\partial y}\right)\left(\delta\dot{v}_0-z\frac{\partial\delta\dot{w}}{\partial y}\right)+\dot{w}\delta\dot{w}\right]\mathrm{d}z\mathrm{d}x\mathrm{d}y.
\end{aligned}
$$

Regarding equations 3.13, q_t is the distributed force per unit area at the top ($z=h/2$) of the laminate, q_b is the distributed force per unit area at the bottom ($z=-h/2$), $(\sigma_{nn},\sigma_{ns},\sigma_{nz})$ are the stress components on the portion Γ_σ of the boundary Γ and $(\delta u_n,\delta u_s)$ are the virtual displacements along the normal and tangential directions, respectively, of the boundary Γ.

Substituting equations 3.13 into *Hamilton*'s principle, expression 3.11, considering expressions 3.6, 3.7 and 3.8, the non-existence of forces acting on the boundary Γ and that $q(x,y,t)=q_t(x,y,t)+q_b(x,y,t)$, because $\delta w\left(x,y,\frac{h}{2}\right)=\delta w\left(x,y,-\frac{h}{2}\right)=\delta w(x,y)$ and then applying an integration by parts to relieve the virtual displacements $(\delta u_0,\delta v_0,\delta w_0)$ in S of any differentiation results an expression which depends upon all components of the virtual displacement vector. The *Euler-Lagrange* equations,

$$
\begin{aligned}
\delta u_0:\quad &\frac{\partial N_{xx}}{\partial x}+\frac{\partial N_{xy}}{\partial y}=I_0\frac{\partial^2 u_0}{\partial t^2}-I_1\frac{\partial^2}{\partial t^2}\left(\frac{\partial w}{\partial x}\right),\\
\delta v_0:\quad &\frac{\partial N_{xy}}{\partial x}+\frac{\partial N_{yy}}{\partial y}=I_0\frac{\partial^2 v_0}{\partial t^2}-I_1\frac{\partial^2}{\partial t^2}\left(\frac{\partial w}{\partial y}\right),\\
\delta w_0:\quad &\frac{\partial^2 M_{xx}}{\partial x^2}+2\frac{\partial^2 M_{xy}}{\partial y\partial x}+\frac{\partial^2 M_{yy}}{\partial y^2}+\mathcal{N}(w)+q=I_0\frac{\partial^2 w}{\partial t^2}\\
&-I_2\frac{\partial^2}{\partial t^2}\left(\frac{\partial^2 w}{\partial x^2}+\frac{\partial^2 w}{\partial y^2}\right)+I_1\frac{\partial^2}{\partial t^2}\left(\frac{\partial u_0}{\partial x}+\frac{\partial v_0}{\partial y}\right),
\end{aligned}
\tag{3.14}
$$

result from equalizing the coefficients of each individual virtual displacement to zero due to their complete independence, wherein:

$$
\begin{aligned}
&\mathcal{N}(w)=\frac{\partial}{\partial x}\left(N_{xx}\frac{\partial w}{\partial x}+N_{xy}\frac{\partial w}{\partial y}\right)+\frac{\partial}{\partial y}\left(N_{xy}\frac{\partial w}{\partial x}+N_{yy}\frac{\partial w}{\partial y}\right);\\
&\left\{\begin{array}{c}I_0\\I_1\\I_2\end{array}\right\}=\int_{-\frac{h}{2}}^{\frac{h}{2}}\rho\cdot\left\{\begin{array}{c}1\\z\\z^2\end{array}\right\}\mathrm{d}z.
\end{aligned}
\tag{3.15}
$$

The variables I_0, I_1 and I_2 are the terms relative to the mass moments of inertia. Then, taking into account the relationship between forces and moments per unit length and membrane strains and curvatures at the middle surface given by the systems of equations 3.9 and the relation of the last ones with the in-plane and transverse displacements, the replacement of those relationships in the *Euler-Lagrange* equation relative to $w_0=w$ results in:

$$-D_{11}\frac{\partial^4 w}{\partial x^4}-D_{12}\frac{\partial^4 w}{\partial x^2\partial y^2}-4D_{66}\frac{\partial^4 w}{\partial x^2\partial y^2}-D_{12}\frac{\partial^4 w}{\partial x^2\partial y^2}-D_{22}\frac{\partial^4 w}{\partial y^4}+\mathscr{N}(w)+q$$
$$-\left(\frac{\partial^2 M_{xx}}{\partial x^2}+2\frac{\partial^2 M_{xy}}{\partial y\partial x}+\frac{\partial^2 M_{yy}}{\partial y^2}\right)=I_0\frac{\partial^2 w}{\partial t^2}-I_2\frac{\partial^2}{\partial t^2}\left(\frac{\partial^2 w}{\partial x^2}+\frac{\partial^2 w}{\partial y^2}\right)+I_1\frac{\partial^2}{\partial t^2}\left(\frac{\partial u_0}{\partial x}+\frac{\partial v_0}{\partial y}\right) \tag{3.16}$$

3.4 Calculation of the mechanical responses

Here, the eigenvalue problems that allow the calculation of the natural frequencies in a completely free panel; and the buckling loads under in-plane loads in a simply supported unstiffened composite plate at the edges $x=0$ and $x=L$, are presented.

3.4.1 Natural frequencies

The *Rayleigh-Ritz* energy approach is employed to obtain the approximate natural frequencies of the rectangular laminate with all free edges as boundary conditions. The vibration analysis leads to a generalised eigenvalue problem [114]. Moreover, the fundamental natural frequency can be obtained according to the principle of *Rayleigh*: "if the vibrating system is conservative (no energy is added or lost), then the maximum kinetic energy, T_{max}, must be equal to the maximum potential (strain) energy, U_{max}" [115].

As results from equation 3.12, when the mass is symmetrically distributed with respect to the middle plane, the kinetic energy is calculated in accordance with the following expression,

$$T=\frac{1}{2}\cdot h\cdot\int_A\left[\rho\cdot\left(\dot{u_0}^2+\dot{v_0}^2+\dot{w}^2\right)\right]\mathrm{d}A, \tag{3.17}$$

wherein u_0, v_0 and w correspond to the in-plane and transverse displacements, respectively. The inertia relative to the rotations of perpendicular lines to the middle plane is disregarded from here on. Considering that the plate is subjected to harmonic oscillations with frequency ω, the displacements are expressed as

$$\begin{aligned} u_0(x,y,t)&=U(x,y)\sin(\omega t),\\ v_0(x,y,t)&=V(x,y)\sin(\omega t),\\ w(x,y,t)&=W(x,y)\sin(\omega t), \end{aligned} \tag{3.18}$$

and then the replacement of them into equation 3.17 results in:

$$T=\frac{1}{2}\cdot\omega^2\cdot h\cdot\cos^2(\omega t)\cdot\int_A\left[\rho\cdot\left(U^2+V^2+W^2\right)\right]\mathrm{d}A. \tag{3.19}$$

From the equation above, clearly the maximum kinetic energy is represented as

$$T_{max}=\frac{1}{2}\cdot\omega^2\cdot h\cdot\int_A(\rho\cdot W^2)\mathrm{d}A, \tag{3.20}$$

considering that the contribution of the in-plane displacements is much lower than the transverse displacement one.

Regarding the strain energy, it assumes the largest value when the deflection of the plate is maximum. That occurs for $\sin(\omega t)$=1 and for a certain point (x,y). Taking into account the simplifications already performed with regard to the stiffness coefficients:

$$\begin{aligned} U_s = & \frac{1}{2}\int_A \left[A_{11}\cdot(\varepsilon_x^0)^2 + A_{22}\cdot(\varepsilon_y^0)^2 + A_{66}\cdot(\varepsilon_{xy}^0)^2 + 2\cdot A_{12}\cdot\varepsilon_x^0\cdot\varepsilon_y^0\right]\ \mathrm{d}A \\ & + \frac{1}{2}\int_A \left[D_{11}\cdot\chi_x^2 + D_{22}\cdot\chi_y^2 + D_{66}\cdot\chi_{xy}^2 + 2\cdot D_{12}\cdot\chi_x\cdot\chi_y\right]\ \mathrm{d}A; \end{aligned} \tag{3.21}$$

$$\begin{aligned} U_{s,max} = & \frac{1}{2}\iint\left\{A_{11}\cdot\left(\frac{\partial U}{\partial x}\right)^2 + A_{22}\cdot\left(\frac{\partial V}{\partial y}\right)^2 + A_{66}\cdot\left(\left(\frac{\partial U}{\partial y}\right)^2 + 2\cdot\left(\frac{\partial U}{\partial x}\cdot\frac{\partial V}{\partial y}\right) + \left(\frac{\partial V}{\partial x}\right)^2\right)\right\}\mathrm{d}x\,\mathrm{d}y \\ & + \frac{1}{2}\iint\left\{2\cdot A_{12}\cdot\left(\frac{\partial U}{\partial x}\cdot\frac{\partial V}{\partial y}\right) + D_{11}\cdot\left(\frac{\partial^2 W}{\partial x^2}\right)^2 + D_{22}\cdot\left(\frac{\partial^2 W}{\partial y^2}\right)^2\right\}\mathrm{d}x\,\mathrm{d}y \\ & + \frac{1}{2}\iint\left\{2\cdot D_{12}\cdot\left(\frac{\partial^2 W}{\partial x^2}\right)\left(\frac{\partial^2 W}{\partial y^2}\right) + D_{66}\cdot\left(\frac{\partial^2 W}{\partial x\partial y}\right)^2\right\}\mathrm{d}x\,\mathrm{d}y. \end{aligned} \tag{3.22}$$

Applying the *Rayleigh*'s principle, the fundamental natural frequency, ω_1, can be achieved:

$$U_{s,\max} = T_{\max} \tag{3.23}$$

$$\omega_1^2 = \frac{2U_{s,\max}}{\rho\cdot h\cdot\int_A W^2(x,y)\mathrm{d}A} \tag{3.24}$$

Since we arbitrarily stiffened the plate by assuming a modal shape, increasing its frequency, the approximate lowest or fundamental natural frequency determined from Rayleigh's principle is always higher than the "exact" values. The spatial displacements are written in the form of a series,

$$\begin{aligned} U(x,y) &= \sum_{i=1}^{n} A_i U_i(x,y), \\ V(x,y) &= \sum_{i=1}^{n} B_i V_i(x,y), \\ W(x,y) &= \sum_{i=1}^{n} C_i W_i(x,y), \end{aligned} \tag{3.25}$$

and the unknown coefficients are determined according to the minimum total energy principle. The application of the following equation for each unknown coefficient,

$$\frac{\partial\left(U_{s,\max} - T_{\max}\right)}{\partial k_i} = 0 \quad (i = 1,2,3,\ldots,n), \tag{3.26}$$

results in a system of homogeneous linear algebraic equations in k_i (general unknown variable), wherein in order for at least one coefficient be different from zero, the determinant of the coefficients' matrix must be null ($\left[\mathbf{K}-\omega^2\mathbf{M}\right]$)=0. The resultant equation is denominated by frequency or characteristic equation, which enables to obtain the natural frequencies of a given plate.

Regarding the approximation functions, they may be assumed as a sum of power series functions, which were approved by many researchers for isotropic and laminated plates having only free edges,

$$\begin{aligned} U(\zeta,\eta) &= \sum_0^i\sum_0^j a_{ij}\cdot\zeta^i\cdot\eta^j, \\ V(\zeta,\eta) &= \sum_0^k\sum_0^l b_{kI}\cdot\zeta^k\cdot\eta^l, \\ W(\zeta,\eta) &= \sum_0^m\sum_0^n c_{mn}\cdot\zeta^m\cdot\eta^n, \end{aligned} \tag{3.27}$$

where $\zeta=\frac{x}{L}-\zeta_0$, $\eta=\frac{y}{b}-\eta_0$ and L, b and h corresponds to the length, width and total thickness of the composite laminate, respectively. For $\zeta=\frac{L}{2}$ and $\eta=\frac{b}{2}$, the referential is centered at point A (see Figure 3.2). The coefficients i, j, k, l, m and n are selected according to the desired number of mode shapes, because the number of used shape functions is directly related to the number of natural frequencies, and degree of accuracy [114, 116, 117]. On the other hand, a good alternative, even though with a harder mathematical treatment, consists in using the mode shapes relative to the transversal vibration of beams with the same boundary conditions.

3.4.2 Buckling loads

Under compressive loads, the plate's behaviour is stable until a certain load is reached. The lowest value of this load is designated by critical buckling load. From this point on, the plate seeks an alternative equilibrium configuration while a stiffness variation occurs. That phenomena is denominated by bifurcation. Buckling of laminates is an instability that is characterised by excessive transverse deflections under in-plane compressive or shear forces [110, 111].

Lévy's method can be used to determine the buckling loads of a rectangular laminate with two parallel edges simply supported and the two remaining ones with arbitrary boundary conditions. For plates with any boundary conditions, the *Ritz* method is the preferred choice as long as suitable approximation functions are found for the problem [110].

The equation of motion governing buckling under in-plane normal forces per unit length N_{xx} (N_{yy}=N_{xy}=M_{xx}=M_{yy}=M_{xy}=q=0) is given by further simplification of expression 3.16:

$$D_{11}\cdot\frac{\partial^4 w}{\partial x^4}+2\cdot(D_{12}+2D_{66})\cdot\frac{\partial^4 w}{\partial x^2\partial y^2}+D_{22}\cdot\frac{\partial^4 w}{\partial y^4} \tag{3.28}$$

$$-N_{xx}\cdot\frac{\partial^2 w}{\partial x^2}+I_0\cdot\frac{\partial^2 w}{\partial t^2}-I_2\frac{\partial^2}{\partial t^2}\left(\frac{\partial^2 w}{\partial x^2}+\frac{\partial^2 w}{\partial y^2}\right)+I_1\frac{\partial^2}{\partial t^2}\left(\frac{\partial u_0}{\partial x}+\frac{\partial v_0}{\partial y}\right)=0.$$

According to the *Lévy* method, the partial differential equation 3.28 is reduced to an ordinary differential equation in y by assuming a solution in the form of a single *Fourier* series,

$$w(x,y) = \sum_{n=1}^{\infty} W_n(y) \cdot \sin(\beta x), \quad \beta = \frac{n\pi}{L}, \tag{3.29}$$

which satisfies the boundary conditions of a simply supported plate along the edges $x = 0$ and $x = L$ (equation 3.30). The boundary and loading conditions regarding the buckling problem studied here are illustrated later on, in Figure 6.2.

$$w = 0 \quad ; \quad M_{xx} = D_{11} \cdot \chi_{xx} + D_{12} \cdot \chi_{yy} = 0. \tag{3.30}$$

Considering only the first term of the *Fourier* series present in 3.29 and replacing it and its derivatives into equation 3.28, considering $N_{xx} = -N_x$, not accounting for the inertia terms and for any x ($\sin(\beta x) \neq 0$):

$$\beta^4 \cdot D_{11} \cdot W_n - 2 \cdot \beta^2 \cdot (D_{12} + 2D_{66}) \cdot \frac{\mathrm{d}^2 W_n}{\mathrm{d}y^2} + D_{22} \cdot \frac{\mathrm{d}^4 W_n}{\mathrm{d}y^4} - N_x \cdot W_n \cdot \beta^2 = 0. \tag{3.31}$$

Assuming the general solution ([110])

$$W_n(y) = A_n \cdot \cosh(\lambda_1 \cdot y) + B_n \cdot \sinh(\lambda_1 \cdot y) + C_n \cdot \cos(\lambda_2 \cdot y) + D_n \cdot \sin(\lambda_2 \cdot y), \tag{3.32}$$

where λ_i are the roots of the following characteristic function

$$\beta^4 \cdot D_{11} - 2 \cdot \beta^2 \cdot (D_{12} + 2D_{66}) \cdot \lambda^2 + D_{22} \cdot \lambda^4 - N_x \cdot \beta^2 = 0 \tag{3.33}$$

and are given by:

$$\lambda_1^2 = \frac{\beta^2}{D_{22}} \cdot \left((D_{12} + 2 \cdot D_{66}) + \sqrt{(D_{12} + 2 \cdot D_{66})^2 - D_{22} \cdot D_{11} + D_{22} \cdot \frac{N_x}{\beta^2}} \right); \tag{3.34}$$

$$\lambda_2^2 = \frac{\beta^2}{D_{22}} \cdot \left((D_{12} + 2 \cdot D_{66}) - \sqrt{(D_{12} + 2 \cdot D_{66})^2 - D_{22} \cdot D_{11} + D_{22} \cdot \frac{N_x}{\beta^2}} \right)$$

The constants A_n, B_n, C_n and D_n must be determined according to the boundary conditions at the edges $y = 0$ and $y = b$. Those edges are free, therefore the bending moment and the transverse force are null at each one. A system of equations which depends also on λ_i results from those conditions. In order for the system to have nontrivial solutions ($A_n \neq 0 \vee B_n \neq 0 \vee C_n \neq 0 \vee D_n \neq 0$), the determinant of the matrix of coefficients must be null, which leads to an equation which establishes a relationship between λ_1 and λ_2. From this one and equations 3.34, the critical buckling load N_{xx} can be determined, even though with a complex manipulation of the expressions.

3.4.3 Derivation of the differential equations of motion for a stiffened composite plate

The laminated plates and shells with stiffeners or stringers have an unquestionable importance in the aerospace industry and other modern engineering fields. Therefore, theoretical, numerical and experimental analysis of these structures became even more fundamental for their static and dynamic understanding.

Here, the objective is to derive the differential equations of motion and to obtain the eigenvalue problem capable of determining the natural frequencies of a stiffened composite plate. The longitudinal stiffeners are made of aluminium, which is an isotropic material. The mass and stiffness of the aluminium stiffeners must be added to the overall mass and stiffness matrices of the structure, taking into consideration a suitable referential.

Qing et al. considered separately the plate and stiffeners contribution. The created model takes into account the compatibility of displacements and stresses at the interfaces between the composite and the aluminium longitudinal stiffeners, not neglecting neither the transverse shear deformation nor the rotary inertia [118]. Moreover, *Xue* and *Wang* modelled the panel and stiffeners according to the classical theories of the plate and beam's behaviour, calculating and adding their kinetic and strain energies, and joining them afterwards using the equations of displacements' compatibility. They claimed that there are two approaches to consider the stiffeners contribution. One consists in the transformation of the stiffened plate into and equivalent orthotropic one and the other considers the stiffeners as a grid attached to the plate [119].

Regarding the shape functions used to approximate the displacements and rotations, they are often power series, as referred above, such as the *Jacobi* polynomials, a type of orthogonal functions in the interval [-1,1]. It is worth to mention that only the linear displacements are considered here, because the plate is thin. These functions are of easier mathematical treatment in comparison with the more complicated trigonometrical functions. Besides that, when the *Ritz* method is used, they do not promote ill-conditioning issues when the number of terms increases. Other well-known polynomials can be obtained by the adjustment of their parameters, such as the *Gegenbauer*, *Legendre* or *Chebychev* polynomials. In order to make their treatment easier, it is performed a transformation from the global (x,y) to a local referential (ξ,η), pointing out their orthogonal properties [120] .

Based on the classical theory of plates, the maximum strain and kinetic energies of the composite panel can be obtained by expressions 3.22 and 3.20, respectively, considering also the coupling between bending and stretching effects due to the presence of stiffeners, that is, $B_{ij} \neq 0$, and taking into account that the maximum strain energy occurs for the instant whose deflection is highest:

$$
\begin{aligned}
U_s = & \frac{1}{2}\int_A \left[A_{11}\cdot\varepsilon_{xx}^2 + A_{22}\cdot\varepsilon_{yy}^2 + A_{66}\cdot\varepsilon_{xy}^2 + 2\cdot A_{12}\cdot\varepsilon_{xx}\cdot\varepsilon_{yy}\right]\ \mathrm{d}A \\
& + \frac{1}{2}\int_A \left[D_{11}\cdot\chi_x^2 + D_{22}\cdot\chi_y^2 + D_{66}\cdot\chi_{xy}^2 + 2\cdot D_{12}\cdot\chi_x\cdot\chi_y\right]\ \mathrm{d}A \\
& + \frac{1}{2}\int_A \left[B_{11}\cdot\varepsilon_{xx}\cdot\chi_x + B_{22}\cdot\varepsilon_{yy}\cdot\chi_y + B_{66}\cdot\varepsilon_{xy}\cdot\chi_{xy} + 2\cdot B_{12}\cdot(\varepsilon_{xx}\cdot\chi_y + \varepsilon_{yy}\cdot\chi_x)\right]\ \mathrm{d}A;
\end{aligned}
\tag{3.35}
$$

$$
\begin{aligned}
U_{max,p} = & \frac{1}{2}\iint\left\{A_{11}\cdot\left(\frac{\partial U}{\partial x}\right)^2 + A_{22}\cdot\left(\frac{\partial V}{\partial y}\right)^2 + A_{66}\cdot\left(\left(\frac{\partial U}{\partial y}\right)^2 + 2\cdot\left(\frac{\partial U}{\partial x}\cdot\frac{\partial V}{\partial y}\right) + \left(\frac{\partial V}{\partial x}\right)^2\right)^2\right\}\mathrm{d}x\,\mathrm{d}y \\
& + \frac{1}{2}\iint\left\{2\cdot A_{12}\cdot\left(\frac{\partial U}{\partial x}\cdot\frac{\partial V}{\partial y}\right) + D_{11}\cdot\left(\frac{\partial^2 W}{\partial x^2}\right)^2 + D_{22}\cdot\left(\frac{\partial^2 W}{\partial y^2}\right)^2\right\}\mathrm{d}x\,\mathrm{d}y \\
& + \frac{1}{2}\iint\left\{2\cdot D_{12}\cdot\left(\frac{\partial^2 W}{\partial x^2}\right)\left(\frac{\partial^2 W}{\partial y^2}\right) + D_{66}\cdot\left(\frac{\partial^2 W}{\partial x\partial y}\right)^2 + B_{11}\cdot\left(\frac{\partial U}{\partial x}\cdot\frac{\partial^2 W}{\partial x^2}\right)\right\}\mathrm{d}x\,\mathrm{d}y \\
& + \frac{1}{2}\iint\left\{B_{22}\cdot\left(\frac{\partial V}{\partial y}\cdot\frac{\partial^2 W}{\partial y^2}\right) + B_{66}\cdot\left(\left(\left(\frac{\partial U}{\partial y}\right)^2 + 2\cdot\left(\frac{\partial U}{\partial x}\cdot\frac{\partial V}{\partial y}\right) + \left(\frac{\partial V}{\partial x}\right)^2\right)^2\cdot\frac{\partial^2 W}{\partial x\partial y}\right)\right\}\mathrm{d}x\,\mathrm{d}y \\
& + \frac{1}{2}\iint\left\{2\cdot B_{12}\cdot\left(\frac{\partial U}{\partial x}\cdot\frac{\partial^2 W}{\partial y^2} + \frac{\partial V}{\partial y}\cdot\frac{\partial^2 W}{\partial x^2}\right)\right\}\mathrm{d}x\,\mathrm{d}y;
\end{aligned}
\tag{3.36}
$$

$$
T_{max,p} = \frac{1}{2}\cdot\omega^2\cdot h\cdot\int_A(\rho\cdot W^2)\mathrm{d}A. \tag{3.37}
$$

The cross-sectional dimensions of the stiffeners are considerably lower than their length, thus the longitudinal stiffeners are modelled as a beam firmly attached to the plate's midplane. Moreover, the transverse strain is negligible taking into account the classical beam's theory.

Using the equations of compatibility of displacements, the plate and a certain stiffener are incorporated together. The transverse stiffener's displacement is expressed as a function of the plate's displacement $w = w(x, y = y_s, t)$, where y_s represents the spatial localization of the stiffener along the Oy axis. Therefore, the expressions of the stiffener's maximum strain and kinetic energies, when the composite stiffened plate oscillate in one of its modes of vibration, can be obtained:

$$
U_{max,s} = \frac{1}{2}\cdot E\cdot I\int_0^L\left[\frac{\partial^2}{\partial x^2}W(x, y_s)\right]^2\mathrm{d}x; \tag{3.38}
$$

$$
T_{max,s} = \frac{1}{2}\cdot\omega^2\cdot\rho\cdot L\cdot\int_A W^2\mathrm{d}A. \tag{3.39}
$$

The total energy of the stiffened plate is given by

$$\Pi = U_p + T_p + \sum_{i=1}^{N_{stiff}} (U_{i,s} + T_{i,s}), \tag{3.40}$$

where N_{stiff} represents the number of stiffeners and the subscripts p and s represent plate and stiffener, respectively.

A prediction of the fundamental natural frequency can be obtained according to the *Rayleigh*'s principle, equation 3.24.

On the other hand, the in-plane and transverse displacements are represented as a series of complete, orthogonal polynomials according to the *Ritz* method in order to obtain the eigenvalue problem which allows to obtain the structure's natural frequencies in accordance with the *Rayleigh-Ritz* procedure described at the end of subsection 3.4.1. The shape functions must comply with the geometric boundary conditions, be linearly independent, continuous and with a continuous derivative until at least the order of derivatives necessary to obtain the total potential energy, and form a complete series [109].

The in-plane and transverse displacements may be then represented as a sum of adequately weighted *Jacobi* polynomials [120], wherein W can be replaced by U or V without loss of generality,

$$W(\xi,\eta) = \sum_{i=0}^{i}\sum_{j=0}^{j} c_{ij} \cdot \psi_i(\xi) \cdot \psi_j(\eta), \tag{3.41}$$

$$\begin{aligned} \psi_n(l) &= A(l) \cdot P_n^{(\alpha,\beta)}(l) \\ A(l) &= (1-l)^{\alpha} \cdot (1+l)^{\beta} \\ l &= \xi, \eta, \end{aligned} \tag{3.42}$$

for $\alpha, \beta > -1$. These coefficients are assigned to the weighting function $A(l)$, which is used to enforce the boundary conditions at each edge.

The *Jacobi* polynomials form a complete orthogonal system in the interval $[-1,1]$ with respect to the weighting function $A(l)$. The three-term recursive formula for the *Jacobi* polynomials is given by

$$\begin{aligned} 2 \cdot n \cdot c_n \cdot c_{2n-2} \cdot P_n^{(\alpha,\beta)}(l) = c_{2n-1} \cdot \left(c_{2n-2} \cdot c_{2n} \cdot l + \alpha^2 - \beta^2\right) \cdot P_{n-1}^{(\alpha,\beta)}(l) \\ -2 \cdot (n-1+\alpha)(n-1+\beta) \cdot c_{2n} \cdot P_{n-2}^{(\alpha,\beta)}(l), \end{aligned} \tag{3.43}$$

where

$$\begin{aligned} c_n &= n + \alpha + \beta, \\ P_0^{(\alpha,\beta)}(l) &= 1, \\ P_1^{(\alpha,\beta)}(l) &= \frac{\alpha-\beta}{2} + \left(1 + \frac{\alpha-\beta}{2}\right) \cdot l. \end{aligned} \tag{3.44}$$

3.5 Finite Element Method

In this section, the mathematical formulation associated to the discretisation of the domain inherent to a finite element model is undertaken.

In order to apply the h-version FEM, the continuum domain Ω_0 must be splitted into n_e smaller domains Ω_0^e, where n_e represents the number of elements.

$$\Omega^0 \approx \Omega_h^0 = \bigcup_{e=1}^{n_e} \Omega_e^0 \tag{3.45}$$

The subscript h regards to the FE approximation of some physical quantity. The displacement solution $\boldsymbol{w}_e$, at each instant, is obtained by the consideration of each node displacement through shape functions N_k, as expressed in the following equation,

$$\boldsymbol{w}_e\left(\boldsymbol{x}^0,t\right) \approx \boldsymbol{w}_{e,h}\left(\boldsymbol{x}^0,t\right) = \sum_{k=1}^{n_{\text{nod}}} N_k\left(\boldsymbol{x}^0\right)\boldsymbol{d}_k(t), \tag{3.46}$$

where n_{nod} is the number of nodes of a particular finite element e, $\boldsymbol{x}^0$ the reference position vector and $\boldsymbol{d}_k$ represents the nodal displacement vector. At each node, only one shape function, the one assigned to that specific node, has unitary value and it has a non-null value at only one determined node. If isoparametric elements are used, the same shape functions are used to interpolate any physical quantity, such as the displacement, and the Cartesian's coordinates:

$$\begin{aligned} \boldsymbol{w}_{e,h}(\xi,\eta,t) &= \sum_{k=1}^{m} N_k(\xi,\eta)\cdot\boldsymbol{d}_k(t); \\ \boldsymbol{x}_{e,h}(\xi,\eta,t) &= \sum_{k=1}^{m} N_k(\xi,\eta)\cdot\boldsymbol{x}_k(t). \end{aligned} \tag{3.47}$$

3.6 Final remarks

In this chapter, the main goal is to clarify the reader about the main equations regarding the physical behaviour of a composite plate. Firstly, the constitutive relations and equilibrium equations were derived and presented for a simple composite plate. Then, applying the *Hamilton*'s variational principle, the differential equation of motion relative to the transverse displacement was established. The *Rayleigh-Ritz* procedure was proposed to obtain the plate's natural frequencies. In turn, in order to predict the buckling loads for the same simpler structure, the *Lévy*'s method was implemented. Lastly, the *Rayleigh-Ritz* approach was presented as a clear hypothesis to obtain the natural frequencies of the stiffened composite plate. The transverse displacement was approximated by using *Jacobi* polynomials.

Chapter 4

Wing representative structure's description

4.1 Introduction

In this chapter, the airplane wing representative structure under analysis is deeply described, including its geometry and all materials and respective involved mechanical properties. Furthermore, the discretisation of the structure for the finite element models is presented, highlighting the type of elements used to discretise each individual part.

4.2 Wing representative structure's geometry

The main structure components are illustrated in the figure below, Figure 4.1. The connections between the majority of the individual parts are assured by bolts except the connection between the stiffeners and the panels. Araldite® 420 A/B is used between them.

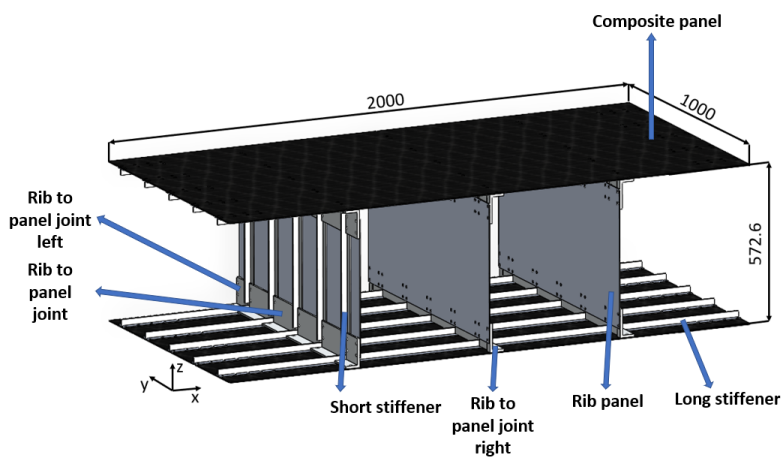

Figure 4.1 – Airplane wing representative structure and its components. Provided by Cardiff School of Engineering.

The number of items of each part as well as its material are specified in the table below.

Table 4.1 – List of items and their materials.

Item	Quantity	Material
Composite panel	2	USN150B: 18 plies By default: [-45/0/45/0/90/0/-45/0/45]s
Long stiffener	10	Aluminium 6063AT6
Short stiffener	15	Aluminium 6063AT6
Rib panel	3	Aluminium 6082AT6
Rib to panel joint	24	Aluminium 6082AT6
Rib to panel joint left	6	Aluminium 6082AT6
Rib to panel joint right	6	Aluminium 6082AT6

Due to the scope of this thesis, only the elastic behaviour of the described materials is considered.

4.3 Elastic materials

The mechanical properties and density of the adhesive and aluminium alloys necessary for the development of the finite element models are presented in Table 4.2 [5].

Table 4.2 – Elastic properties of the adhesive and aluminium alloys.

Material	σ_y /MPa	E /MPa	ν	ρ /g $\cdot$ cm^{-3}
Aluminium 6063AT6	170	70000	0.33	2.70
Aluminium 6082AT6	260			
Araldite ® 420 A/B	27	1850	0.3	1.2

Regarding the composite panel, it is a symmetric plate made up by 18 plies stacked together of USN150B, which is a transversely isotropic carbon fibre-epoxy material. It is composed by SKYFLEX K51 matrix and TR50S15L fibres. *Henriques* (2021) performed a micromechanics-based model in order to predict the elastic properties of that composite, because they are not available in the literature. Using the elastic properties of a similar material, which differs only in the fibre content, the USN150B elastic properties were achieved. The missing elastic properties were calculated according to the *Voigt* model of the Rule of Mixtures, which assumes that the fibre's and matrix's strain is equal under longitudinal loading conditions, and the model for transverse modulus based on the unit cell [5].

The following assumptions were made to predict the unknown elastic properties according to the referred models: the composite is only composed by its fibres and matrix, which are bonded perfectly (no voids); the fibres are disposed in an uniform and unidirectional way; the polymeric

matrix is isotropic; composite material is transversely isotropic, that is, the properties are constant in the plane perpendicular to the fibre direction, assuming that the fibres are randomly disposed; and the resulted properties are calculated in relation to the material's principal axes [5].

Therefore, taking into account that the resin content is about 33% and the remainder is composed by carbon fibres, the elastic properties of the transversely isotropic material were calculated using the models already explained (see Table 4.3):

Table 4.3 – Elastic properties of USN150B.

E_{11} [GPa]	131	X_t [MPa]	2000
$E_{22} = E_{33}$ [GPa]	8	$Y_t = Z_t$ [MPa]	61
$G_{12} = G_{13}$ [GPa]	4.5	X_c [MPa]	2000
G_{23} [GPa]	3.5	$Y_c = Z_c$ [MPa]	200
$\nu_{12} = \nu_{13}$	0.29	$S_{12} = S_{13}$ [MPa]	70
ν_{23}	0.47	S_{23} [MPa]	40
ρ [g $\cdot$ cm^{-3}]	1.544	t_{ply} [mm]	0.194444

The coordinate system 123 refers to the material's principal axes; X, Y, Z are the normal strengths in those directions; S is the shear strength and the subscripts t and c refers to tensile and compressive, respectively.

4.4 Finite element method

As it will be explained and demonstrated later on, all FEM simulations are carried out only in a substructure of the stiffened composite panel. Therefore, here only the discretisation processes associated with the composite panel and the longitudinal stiffeners are presented and discussed. Moreover, no bolts or holes are considered in order to make the mesh construction easier and to simplify the analysis of the results.

The discretisation process consists in the transformation of the continuous structure into an assembly of discrete finite elements accurately interconnected.

Each finite element is characterised by the following classes according to Abaqus® software [121]:

- **family**: continuum (solid), shell, beam, rigid, membrane, infinite, springs and dashpots or truss elements;
- **number of degrees of freedom**;
- **number of nodes**: the number of nodes at each edge is related to the order of interpolation used to interpolate the desired variables in other points;

- **formulation**: is related to the mathematical theory used to characterise the element's behaviour;
- **integration**: numerical techniques used to calculate several quantities over the volume of the element, replacing the expensive direct integration (e.g. *Gauss* quadrature). The elements may use full or reduced integration, being the last one identified by the letter R at the end of the element's description.

The continuum elements are suitable for a wide range of structure's shapes subjected to any loading, due to their simple nature. Their names begin with the letter C ("**C**ontinuum"), followed by two letters which indicate the dimensionality (**3D** indicate a three-dimensional element, **AX** an axisymmetric element, for example), next the number of active degrees of freedom is appointed and the last one, if necessary, a letter indicates whether it is used an incompatible mode formulation (**I**) or an hybrid element formulation (**H**). The incompatible mode elements are used to surpass the shear locking phenomena in fully integrated, first-order ones, with high accuracy and low computational cost. Additional degrees of freedom are introduced to improve the deformation gradient of the element. The stiffeners were modelled with 8-node hexahedral continuum solid elements with incompatible nodes, C3D8I. The elimination of the shear locking problem, by using reduced integration, and the volumetric locking alleviation are some of the advantages of those elements. Furthermore, they assure a faster and better convergence in comparison with the tetrahedral elements and their geometry is suitable for rectangle structures, like this one [121].

The thickness of the composite panel is significantly lower than their in-plane dimensions, therefore this structure is modelled as a shell. The standard 3D shell elements may be general-purpose, thin-only or thick-only. The thick shell problems assume the effects of the transverse shear deformation, whereas the others neglect that. A general-purpose element with hourglass control denominated by reduced integrated 8-node continuum shell element, SC8R, is used. These elements are similar to the C3D8I continuum solid, differing in their constitutive and kinematic behaviours. They are first-order interpolation elements which have lighter computational effort, no aspect ratio issues and allow the stress assessment through the material thickness by attaching one element per layer [5, 121–123].

Both types of elements considered for the panel and stiffeners have only displacement degrees of freedom, so they can be interconnected without any kinematical transition. The connection between the meshes, the mesh developed for the panel and for each stiffener, is established by a tie constraint, which connects two surfaces avoiding the relative motion between them. It is worth to mention that the meshes between parts could be non-conformal, that is, there are nodes belonging to a certain mesh that are placed along the edges of the other mesh, without a perfect bonding/matching between the nodes. This phenomena is not relevant for the simulations to perform, because the contact between the several parts is not a critical point within this work.

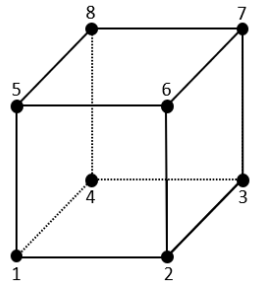

Figure 4.2 – SC8R and C3D8I elements: linear degrees of freedom.

In the next figure, the meshes of the composite panel under analysis as well as their connections are presented.

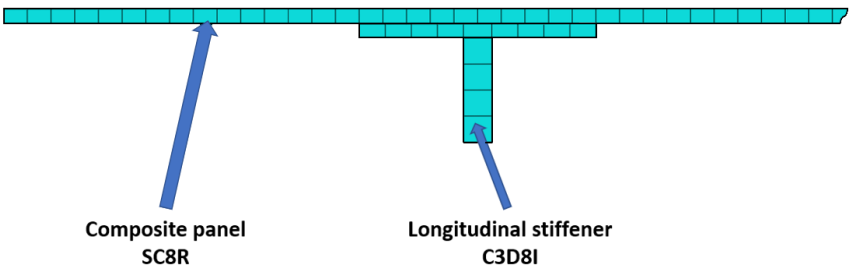

Figure 4.3 – Stiffened composite plate's mesh.

For the elaboration of this work, the adhesive's behaviour which connects the composite panel and the longitudinal stiffeners is not accounted for. This decision is based on the main objectives pre-established for this dissertation which do not include the study of the delamination at the interfaces or the cohesive failure in those areas. Therefore, it was possible to simplify the created Abaqus® model, reducing considerably the computational time.

4.5 Final remarks

Due to the essence of the simulations to perform, only a substructure of the overall one is considered. Moreover, no bolts or holes are considered and only the elastic behaviour is taken into account in the prediction of the fundamental natural frequency and the critical buckling load for the several configurations. The aluminum stiffener is a rectangle-like shape structure, therefore it is modelled by a continuum element, C3D8I. The thickness of the composite panel is considerably lower in comparison to their in-plane dimensions, so a shell element is employed. In order to reduce shear locking effects and improve the model's performance, the shell element chosen was the SC8R.

Chapter 5

Optimization of the airplane wing representative structure for vibration

5.1 Introduction

In this chapter, an assessment of the wing representative structure's behaviour is performed, Figure 1.1, under free conditions, that is, without any loading and with null forces and moments at all extremities. Therefore, the structure's fundamental natural frequency for a set of experiences which differ only in the values of the considered design variables is obtained, aiming to achieve the best structure's configuration regarding the maximisation of that output value. As referred above, this optimization problem is extremely relevant in order to keep the amplitude of vibration within a desired gap.

The airplane wing representative's structure is composed by two similar composite panels and by transversal and longitudinal aluminium stiffeners. In a first instance, the main goal is to achieve the composite fibres orientations which result in the highest value for the fundamental natural frequency. Then, a similar procedure is performed, adding the layers' thicknesses as design variables. Therefore, the analysed structure is simplified into a simple composite panel, because all design variables are related to them and, as referred, the two panels are identical concerning the number of plies, stacking sequence and plies thicknesses and orientations. Moreover, no bolts or holes are considered with the aim of simplifying the creation of the model, particularly its mesh, and posterior analysis.

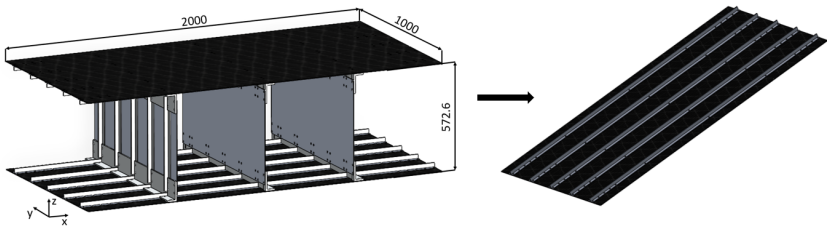

Figure 5.1 – Analysed substructure of the airplane wing representative structure.

The CAD Model, provided by the School of Engineering at Cardiff University, was simplified accordingly and then imported to Abaqus® software, version 6.20-1. The simulations were performed in a computer with the following characteristics: 8 CPUS AMD Ryzen 7 5700G with Radeon Graphics 3.80 GHz; 16 GB of RAM, 475 GB hard drive. The required mechanical properties to create the models are provided in the previous chapter.

The optimization code was developed in the Visual Basic environment and then the FORTRAN language was used to compile it. The developed code is based on a genetic algorithm, an evolutionary-based approach, and an artificial neural network was built to predict the natural frequencies values for a particular set of design variables, avoiding the use of more finite element simulations, significantly reducing the computational time.

In Section 5.2, a complete description of the developed genetic-based code and the artificial neural network arrangement is done, presenting all steps relative to each one of the procedures, as well as all the involved parameters.

In Sections 5.3 and 5.4, the optimization results related to each one of them are presented and deeply analysed. A study regarding the evolution of the absolute and relative errors and the influence of the several code parameters on the output results is performed. Moreover, the results obtained by FEM simulations, that is, the structure's main modes of vibration, are exhibited and compared.

Lastly, in Section 5.5, some final conclusions are drawn related to the work developed throughout the chapter.

5.2 Description of the optimization algorithm

In this section, the model capable of optimising the substructure's fundamental natural frequency and critical buckling load, altering the composite fibres orientations and layers' thicknesses, is presented.

The procedure is divided into three stages: firstly several FEM simulations to train and test the developed network are carried out; thereafter a learning algorithm is applied to the ANN which is then validated; finally a genetic algorithm is employed with the aim of achieving the best configuration regarding the design variables, the fibres orientations and layers' thicknesses, depending on the considered problem.

In order to reduce the number of required FEM simulations, the relationship between the design variables and the mechanical output response was achieved by the development of an ANN. The set of experiments necessary to train the network, that is, achieve its best configuration regarding the synaptic weights and biases, were planned according to the Uniform Design Method due to its high representativeness of the domain under analysis. The UDM's experimental points are taken out from specific tables. An accessory table is always provided in order to consult the right columns, being that right choice related to a minimum discrepancy value in the representation. Moreover, considering the design points and their corresponding output values obtained by FEM simulations, the best ANN's architecture was achieved by the implementation of a genetic-based

algorithm. Lastly, all experiments were feedforwarded in the optimal ANN and the outcomes were compared with those from FEM simulations, aiming to validate the developed network.

In a second phase, using the developed neural network to predict the output values and applying again a genetic algorithm, it was possible to achieve the best design variables and correspondent optimised mechanical variable, under several constraints. It is worth to mention that the genetic parameters used to achieve the best ANN's configuration and to optimise the mechanical responses are completely independent.

Lastly, the *Sobol* indices for global sensitivity analysis are calculated to establish the importance of each particular design variable on the structural response, implementing an ANN-based Monte Carlo Simulation. In this approach, the *Sobol* indices are calculated using the conditional variance and the total system variance. The MCS is used to calculate those statistical values, whereas the output mechanical values are predicted by the artificial neural network. Statistically, an individual *Sobol* index could be defined as the contribution of the variance of a certain design variable for the total variability of the fundamental natural frequency or critical buckling load response. The different development stages referred above are schematised in the figure below, Figure 5.2. The achievement of the best ANN's architecture is referred as learning process, whereas the optimization of the mechanical variables is denoted as optimization process and the sensitivity measurement as global sensitivity analysis.

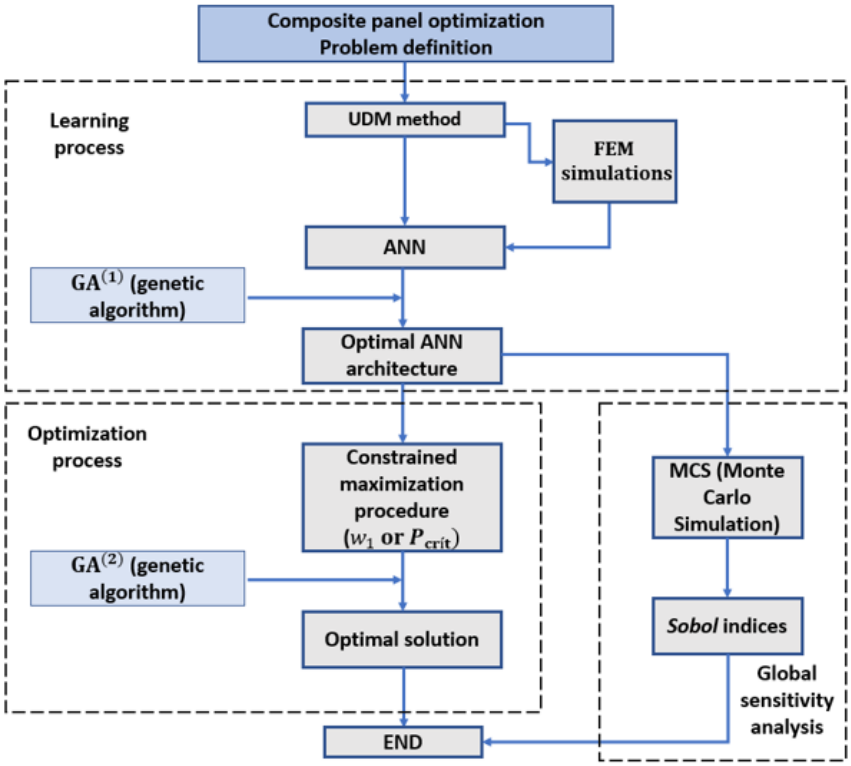

Figure 5.2 – Flow diagram of the optimization framework. Adapted from [124–126].

5.2.1 Uniform Design Method

The sets of design variables were planned according to the UDM. This procedure involves reducing the variation in a process through a robust design of experiments. In this work, the design of experiments was implemented using the table $L_{27}(3^{13})$. These tables are presented later on, when a particular optimization problem is introduced and deeply analysed. Therefore, 27 experiments are necessary for each optimization procedure.

5.2.2 ANN model development

The optimal configuration of the artificial neural network is achieved by minimising the error between the simulated network outputs and the outputs resulted from FEM simulations, for the set of 27 experimental points provided by UDM. In this stage, the design variables are the synaptic weights, $\mathbf{W}_{ji}^{(L)}$ and biases, $\mathbf{r}^{(L)}$. The errors are back-propagated using a genetic algorithm, denominated $\mathbf{GA}^{(1)}$, with appropriated genetic parameters (see Figure 5.3). A population of binary-coded solutions for ANN configuration, denominated by $\mathbf{P}^{(t)}$, is considered for each t-generation. If pre-established criteria regarding the obtained errors is not attained, a new generation is created by the crossover operation of the genetic algorithm and the feedforward process is repeated until the best ANN configuration is achieved.

In order to completely define this first optimization procedure, the following parameters must be specified and characterized:

- ANN architecture: number of hidden layers and the number of nodes in each layer: input layer, hidden layer(s) and output layer;
- experimental points (UDM);
- normalisation range for the input and output variables;
- genetic operators: dimension of the population, mutation and elite percentages, maximum number of generations, crossover operator, similarity control method;
- range of values and number of bits for the synaptic weights and biases at each connection;
- activation functions and respective parameters.

The data used to build the ANN needs to be normalised in order to avoid numerical error propagation during the learning process. The data normalisation is done according to the following equation,

$$\overline{d}_k = (d_k - d_{\min}) \cdot \frac{d_N^{\max} - d_N^{\min}}{d_{\max} - d_{\min}} + d_N^{\min}, \tag{5.1}$$

in which d_k represents the real value of a certain variable before normalisation, $d_{\min}$ and $d_{\max}$ their minimum and maximum values, respectively, and $d_N^{\max}$ and $d_N^{\min}$ the range of normalisation, which

is particular for each set of similar variables. The vector containing all signals at the input of each p-layer is calculated as follows,

$$\mathbf{i}^{(p)} = \mathbf{W}^{(p)}\mathbf{y}^{(p-1)} + \mathbf{r}^{(p)}, \tag{5.2}$$

wherein $\mathbf{i}^{(p)}$ represents the input vector of the p-layer and $\mathbf{y}^{(p-1)}$ represents the output of the layer $p-1$.

Regarding the activation functions, whose main function is to introduce non-linearity to the network, the ones related to each one of the optimization procedures are presented in the opportune sections. It is worth to mention that if a linear function is used, no bias must be considered. In order to achieve the best ANN configuration, the errors between the network outputs and FEM simulations must be compared and back-propagated, aiming to minimise those values during the learning procedure. Therefore, several error measures are presented and combined in a fitness function:

- root-mean-square error,

$$RMSE = \frac{1}{n_{\text{exp}} \cdot OUT} \sqrt{\sum_{i=1}^{n_{exp}} \sum_{j=1}^{OUT} \left(O_{ij}^{sim} - O_{ij}^{ANN} \right)^2}, \tag{5.3}$$

  where O represents the values of the output variables provided both by the FEM model and ANN.

- relative error

$$RE = \frac{1}{n_{\text{exp}} \cdot OUT} \sqrt{\sum_{i=1}^{n_{exp}} \sum_{j=1}^{OUT} \left(\frac{O_{ij}^{sim} - O_{ij}^{ANN}}{O_{ij}^{sim}} \right)^2}. \tag{5.4}$$

- error component which takes into account the influence of the biases, Γ_{error},

$$\Gamma_{error} = \frac{1}{n_{\text{exp}}} \sum_{i=1}^{n_{\text{exp}}} \left[\frac{1}{N_{\text{hid}}} \sum_{k=1}^{N_{\text{hid}}} \left(r_k^{(1)} \right)^2 + \frac{1}{OUT} \sum_{j=1}^{OUT} \left(r_j^{(2)} \right)^2 \right], \tag{5.5}$$

  where N_{hid} represents the number of hidden nodes.

Then, the errors are aggregated into

$$F_1 = c_1 \cdot RMSE + c_2 \cdot RE + c_3 \cdot \Gamma_{error}, \tag{5.6}$$

in which c_1, c_2, c_3 are user-defined values, aiming to stabilize the numerical procedure due to the difference in the magnitude of each parcel. A fitness function is defined straight away in order to implement a genetic algorithm, whose main goal is to minimise F_1,

$$Maximise \;\; FIT^1 = K^1 - F_1, \tag{5.7}$$

where K^1 is a user-defined constant large enough to keep that expression positive. The evolutionary-based approach is considered for the ANN architecture optimization, because the probability of reaching local optima is lower compared to the gradient-based algorithms. As referred above, the design variables are initially binary-coded to simplify the computer calculations. Then, a decoding process is executed, aiming to obtain the fitness value of each particular individual belonging to the pre-established population.

5.2.3 Optimal design procedure

During this last stage, the fundamental natural frequency or the critical buckling load are maximised under certain pre-specified constraints. The design variables are, now, the fibres orientations and/or layers thicknesses and the fitness assessment is performed using the optimal ANN architecture developed earlier in the process. The optimal design procedure is carried out using an evolutionary-based algorithm, genetic one, denoted by $\mathbf{GA}^{(2)}$ in the scheme, see Figure 5.3, with independent genetic parameters from those related with the first one. A population of binary-coded solutions, denominated by $\mathbf{X}^{(t)}$, is considered for each t-generation. The optimization process is repeated until pre-established convergence criteria is met. In this case, a maximum number of generations is prescribed.

The fitness function results from the combination of the objective value and the penalties, which could be graded, due to constraint(s) violation. Moreover, constant values are associated to each parcel, with the aim of stabilizing the numerical procedure through magnitude equality. Note that the size constraints are imposed directly on the design space in the binary coding.

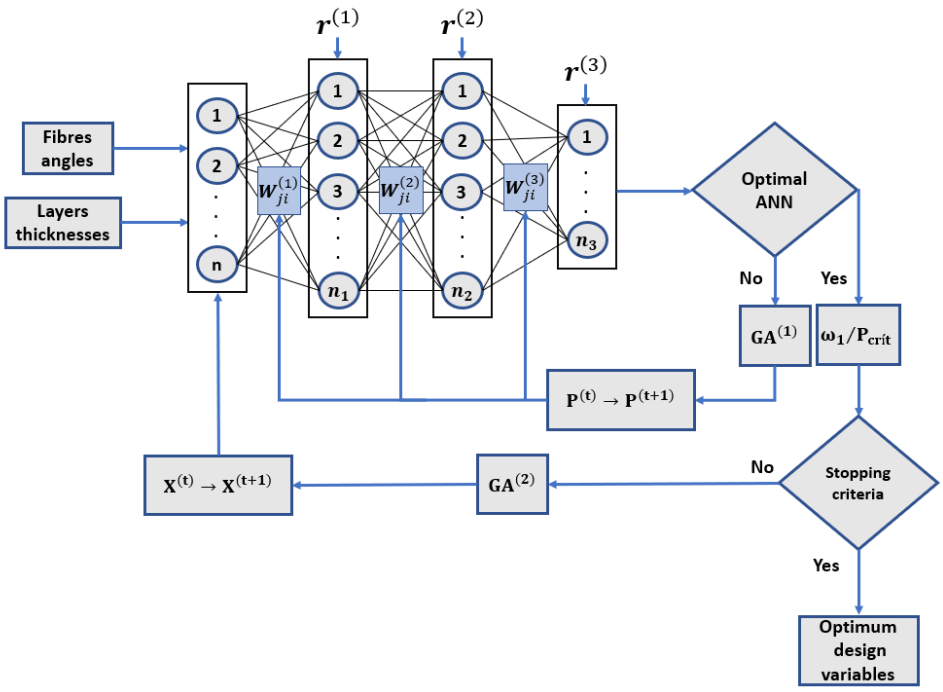

Figure 5.3 – ANN learning and optimization procedure. Adapted from [124–126].

5.2.4 Genetic algorithm description

In this subsection, a deeper understanding of the implemented genetic algorithm is provided. The structure of the two algorithms, $\mathbf{GA}^{(1)}$ and $\mathbf{GA}^{(2)}$ is identical, differing only on the values of their genetic parameters. The basic genetic algorithm's performance consists on the binary coding of the design variables, the assessment of the individuals based on a suitable fitness function and in applying successively genetic operators, such as selection, crossover, similarity control elimination/replacement and mutation, to generate new individuals. The complete steps are schematised in Figure 5.4 and summarised below:

- Step 1: The initial population, $\mathbf{P}^K$, is randomly created according to a certain statistical distribution. The individuals are binary-coded.
- Step 2: The individuals are ranked in the original population based on their fitness values. Selection. Two individuals are selected for crossover: one belonging to the highly fitted group, elite group, and another from the least fitted set.
- Step 3: Crossover. The individuals that resulted from the crossover operator make part of the offspring group, $\mathbf{B}$. The crossover operator acts on the descendent chromosome, assigning to each one of the genes a value equal to the one presented in the same bit of a certain parent. That distribution is performed according to a certain criteria characteristic of each crossover operator (see subsection 2.6.4). Moreover, a certain probability can be assigned to this genetic operator. Lastly, the offspring group joins the initial population, forming the enlarged population, $\mathbf{P}^K \cup \mathbf{B}$.
- Step 4: The enlarged population is ranked according to their fitness values. Elimination/Replacement control. A certain similarity control mechanism is applied, phenotype-based (by variable) or genotype-based (by gene), and the similar individuals are taken out from the population in order to preserve its diversity and are replaced by new random ones.
- Step 5: Due to the introduction of new individuals, a ranking procedure is performed. Now, the dimension of the population can be lower than the pre-specified value. Therefore, a mutation operator is used to reestablish the population's dimension. Moreover, this operator is fundamental to induce population's diversity, avoiding premature convergence resulting from the anchorage at local optimum. After this operator, the new population, $\mathbf{P}^{K+1}$ is created and the process is repeated until the pre-specified convergence criteria is followed.
- Step 6: Convergence criteria. The adopted convergence criteria is a maximum number of generations. However, there are many more, including a certain fitness value achievement, the difference between those values between a prescribed number of generations or the perception of a evolution stagnation. The main ones can be revisited in subsection 2.6.6.

The next figure exemplifies the sequential procedure described above, Figure 5.4.

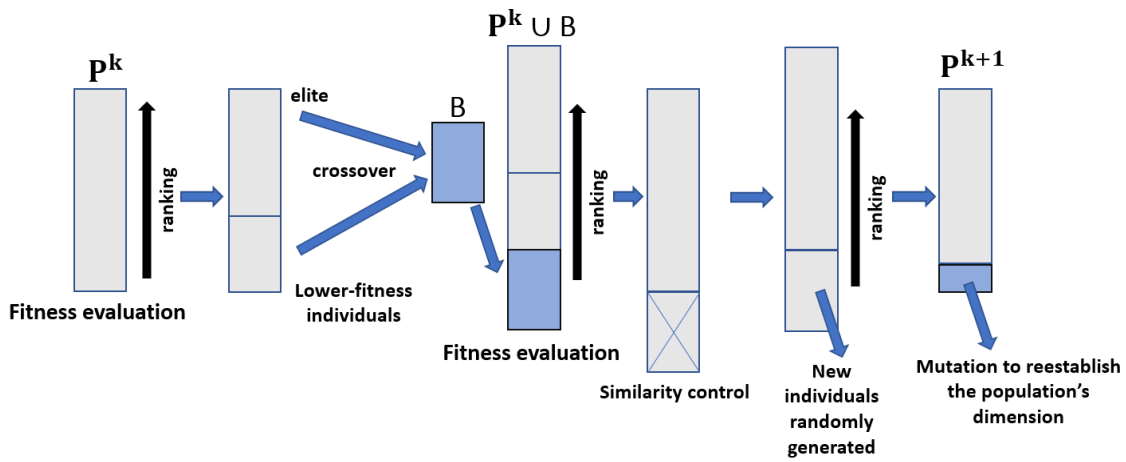

Figure 5.4 – Genetic algorithm's description. Adapted from [124–126] .

5.2.5 Global sensitivity analysis

The relative importance of each design variable is calculated by a global sensitivity analysis according to variance-based methods. The GSA is based on the first order *Sobol* indices and relative sensitivities. The output response uncertainty is accordingly divided among the input variables. In comparison with the local sensitivity analysis, this technique does not require strong model assumptions, which is relevant for unknown systems. Thus, assuming that the variables are independent, the variance of the conditional expectation, $var(E\langle O \mid x_i\rangle)$, is a measure of each design variable relative importance on the output variable (denoted by O) response. Then, the *Sobol* indices are calculated:

$$S_i^O = \frac{var(E\langle O \mid x_i\rangle)}{var(O)}. \tag{5.8}$$

In order for the computational requirements to become less expensive, the Monte Carlo Simulation together with the optimal artificial neural network arrangement are utilised to predict the *Sobol* indices. The conditional and system variances are calculated according to the following procedure [88, 124]:

- Step 1: generation of a vector of the design variables, $\mathbf{x}$, according to the uniform probability distribution function $U \sim(0,1)$;

- Step 2: a set of random numbers, λ_j ($j = 1, \ldots, \mathrm{N}_f$), following a uniform probability distribution function, are used as fixed values for the design variable x_i;

- Step 3: a sample matrix, $\mathbf{J}_\alpha$, is generated for each design variable (apart from itself), by collecting samples of $INP-1$ random numbers following a uniform probability distribution function, where N_r represents the size of the sample;

$$\boldsymbol{J}_\alpha = \begin{bmatrix} \alpha_{1,1} & \dots & \alpha_{1,INP-1} \\ \vdots & \ddots & \vdots \\ \alpha_{k,1} & \dots & \alpha_{k,INP-1} \\ \vdots & \ddots & \vdots \\ \alpha_{N_r,1} & \cdots & \alpha_{N_r,INP-1} \end{bmatrix}$$

- Step 4: for each design and fixed variable, N_r combinations of each fixed value and a $\mathbf{J}_\alpha$ value are defined, placing each one of them along the respective domain. The output values are obtained for that defined input vectors, $\boldsymbol{out}_{ANN}$, using the optimised ANN. This procedure is repeated for each design variable. Then, the conditional expectation is estimated and their mean values calculated:

$$E\left\langle O \mid x_i \right\rangle \approx \bar{O}^j = \frac{1}{N_r} \sum_{k=1}^{N_r} out_{ANN,k}; \tag{5.9}$$

$$\overline{\bar{O}} = \frac{1}{N_f} \sum_{j=1}^{N_f} \bar{O}^j. \tag{5.10}$$

Fixing each design variable x_i, the variance of the conditional expectation is obtained. This process is repeated for each design variable;

$$\mathrm{var}\left(E\left\langle O \mid x_i \right\rangle\right) \approx \frac{1}{N_f - 1} \sum_{j=1}^{N_f} \left(\bar{O}^j - \overline{\bar{O}}\right)^2. \tag{5.11}$$

- Step 5: The total system variance, $\mathrm{var}(O)$ is estimated and then the *Sobol* indices are obtained using equation 5.8:

$$E\left\langle O \right\rangle = \frac{1}{INP \cdot N_f \cdot N_r} \sum_{i=1}^{INP} \sum_{j=1}^{N_f} \sum_{k=1}^{N_r} out_{ANN}(i,j,k); \tag{5.12}$$

$$\mathrm{var}(O) = \frac{1}{INP \cdot N_f \cdot N_r - 1} \sum_{i=1}^{INP} \sum_{j=1}^{N_f} \sum_{k=1}^{N_r} \left(out_{ANN}(i,j,k) - E\left\langle O \right\rangle\right)^2. \tag{5.13}$$

In the next sections, the procedures and results belonging to each one of the performed optimizations are presented.

5.3 Fundamental natural frequency: ply angles

In this section, the stiffened laminated composite panel is optimised regarding its fundamental natural frequency. The main goal is to maximise ω_1 by altering the orientation of the plies belonging to the composite panel. For now, the thicknesses remain constant. The stacking sequence and the design variables can be observed in the next figure in accordance with the panel provided by the COST action.

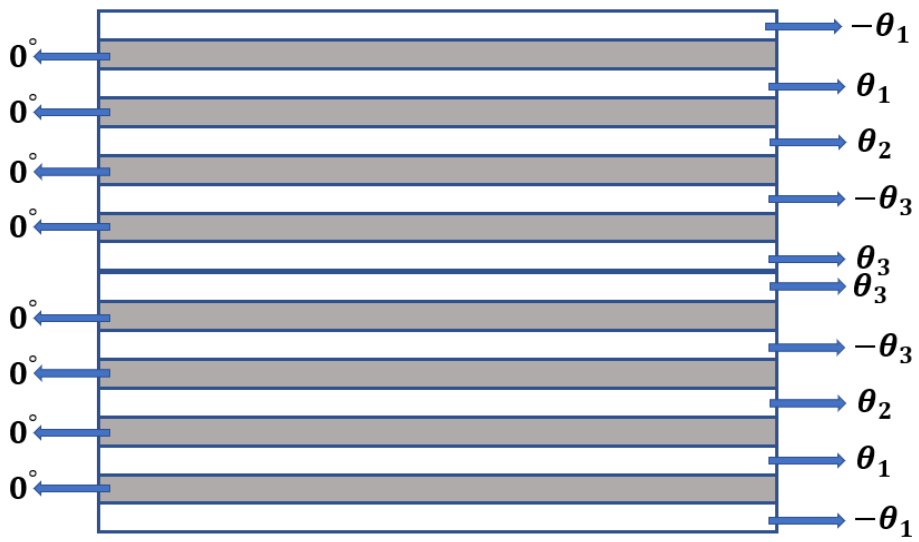

Figure 5.5 – Stacking sequence and design variables for the optimization of ω_1.

By the observation of the figure above, it is possible to verify that there are three design variables for this optimization problem, θ_1, θ_2 and θ_3. Moreover, the composite laminate is symmetric. In order to remain faithful to Cardiff School of Engineering design, it was chosen to preserve some layers with 0° of fibre's orientation. Aiming to obtain the composite laminate natural frequencies, a FEM model was constructed. The composite panel was built using the Abaqus® intrinsic tool designated by Composite Layup, in which are specified the orientation angle, thickness, material and the number of integration points for each individual layer. There are no prescribed boundary conditions besides null forces and moments at all extremities, or loading cases in this calculation. Ten natural vibration modes were requested, using the *Lanczos* eigensolver, being the first 6 corespondent to the rigid body modes, therefore of reduced importance.

5.3.1 Design of experiments

The design of experiments was implemented, as referred in subsection 5.2.1, using the table $L_{27}(3^{10})$, where 27 represents the number of experiments used for the ANN learning procedure, 3 corresponds to the number of levels of each factor and 10 the maximum number of columns,

that is, the maximum number of design variables (see Table 5.1). The right columns are selected according to Table 5.2.

Table 5.1 – Uniform design table, $L_{27}(3^{10})$.

No. of training datasets	**1**	**2**	**3**	**4**	**5**	**6**	**7**	**8**	**9**	**10**
1	1	5	9	11	13	15	17	19	25	27
2	2	10	18	22	26	2	6	10	22	26
3	3	15	27	5	11	17	23	1	19	25
4	4	20	8	16	24	4	12	20	16	24
5	5	25	17	27	9	19	1	11	13	23
6	6	2	26	10	22	6	18	2	10	22
7	7	7	7	21	7	21	7	21	7	21
8	8	12	16	4	20	8	24	12	4	20
9	9	17	25	15	5	23	13	3	1	19
10	10	22	6	26	18	10	2	22	26	18
11	11	27	15	9	3	25	19	13	23	17
12	12	4	24	20	16	12	8	4	20	16
13	13	9	5	3	1	27	25	23	17	15
14	14	14	14	14	14	14	14	14	14	14
15	15	19	23	25	27	1	3	5	11	13
16	16	24	4	8	12	16	20	24	8	12
17	17	1	13	19	25	3	9	15	5	11
18	18	6	22	2	10	18	26	6	2	10
19	19	11	3	13	23	5	15	25	27	9
20	20	16	12	24	8	20	4	16	24	8
21	21	21	21	7	21	7	21	7	21	7
22	22	26	2	18	6	22	10	26	18	6
23	23	3	11	1	19	9	27	17	15	5
24	24	8	20	12	4	24	16	8	12	4
25	25	13	1	23	17	11	5	27	9	3
26	26	18	10	6	2	26	22	18	6	2
27	27	23	19	17	15	13	11	9	1	1

Table 5.2 – Accessory table, $L_{27}(3^{10})$.

No. of design variables	**No. of columns**	**Discrepancy, D**
2	1,4	0.0600
3	1,3,6	0.1009
4	1,4,6,9	0.1189
5	2,5,7,8,10	0.1378

In order to obtain the minimum discrepancy value and taking into account that there are 3 design variables, the columns 1, 3 and 6 are chosen for the design of the experimental points

(see Table 5.2). Thus, the domain of the design variables, $\theta_i \in [0, \frac{\pi}{2}]$ rad is divided into 26 equal subdomains, being assigned to each one of them, by order, a number from 1 to 27. The first two natural frequencies are used to train the artificial neural network. The experimental points and respective FEM values are presented in Table 5.3.

Table 5.3 – Experimental points for the optimization of ω_1, having the plies orientations as design variables.

Experimental point	θ_1 /rad	θ_2 /rad	θ_3 /rad	ω_1 /rad $\cdot$ s^{-1}	ω_2 /rad $\cdot$ s^{-1}
1	0	0.48332	0.84581	44.96185	47.55177
2	0.06042	1.02706	0.06042	41.10711	56.76481
3	0.12083	1.57080	0.96664	45.02216	67.95265
4	0.18125	0.42291	0.18125	42.30343	44.69732
5	0.24166	0.96664	1.08747	47.17918	59.84043
6	0.30208	1.51038	0.30208	45.48649	66.08026
7	0.36249	0.36249	1.20831	47.13583	53.15575
8	0.42291	0.90623	0.42291	49.52407	57.63126
9	0.48332	1.44997	1.32914	49.14142	74.73221
10	0.54374	0.30208	0.54374	50.48602	55.37748
11	0.60415	0.84581	1.44997	52.31003	70.07637
12	0.66457	1.38955	0.66457	53.82742	78.83513
13	0.72498	0.24166	1.57080	51.27896	73.47557
14	0.78540	0.78540	0.78540	55.91532	78.06858
15	0.84581	1.32914	0	52.16740	90.30822
16	0.90622	0.18125	0.90623	53.77590	85.86601
17	0.96664	0.72498	0.12083	53.27890	91.64654
18	1.02706	1.26872	1.02706	53.59997	106.3052
19	1.08747	0.12083	0.24166	49.86713	99.55707
20	1.14789	0.66457	1.14789	52.58021	108.7305
21	1.20831	1.20831	0.36249	50.02295	116.2892
22	1.26872	0.06042	1.26872	47.02147	115.4221
23	1.32914	0.60415	0.48332	50.00159	116.5719
24	1.38955	1.14789	1.38955	45.94956	127.5172
25	1.44997	0	0.60415	46.77706	119.9837
26	1.51038	0.54374	1.51038	44.90593	124.9600
27	1.57080	1.08747	0.72498	48.56274	127.4544

The main goal of UDM is to ensure a high representativeness of the domain under consideration with minimum discrepancy, through a robust design of experiments. The representation of the training dataset shown in Figure 5.6 (3D representation) and Figure 5.7 (2D representations) helps to validate its intention. The entire design space is covered by experimental points, which can improve the genetic algorithm's performance in the extent that the possibility of reaching the global optima is higher.

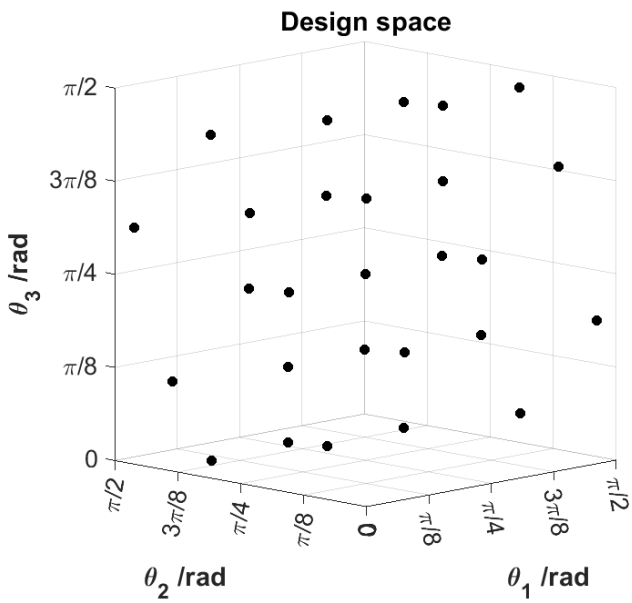

Figure 5.6 – 3D representation of the experimental points.

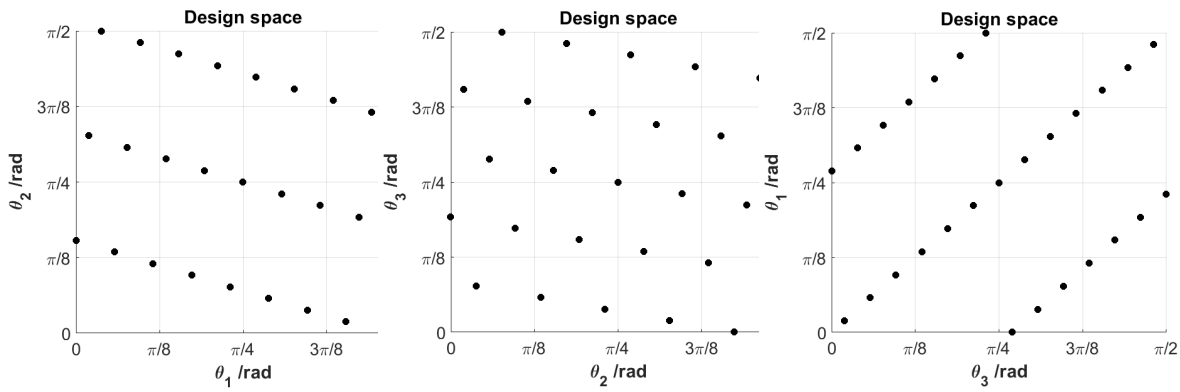

(a) Plane $0_{\theta_1\theta_2}$ (b) Plane $0_{\theta_2\theta_3}$ (c) Plane $0_{\theta_3\theta_1}$

Figure 5.7 – Representation of the experimental points in the three mutually orthogonal planes.

The representation of ω_1 for each experimental point is performed in the next figure, Figure 5.8, aiming to have an insight about its distribution along the domain under analysis and, ultimately, to draw some conclusions about possible activation functions to implement at the outermost layer of the ANN.

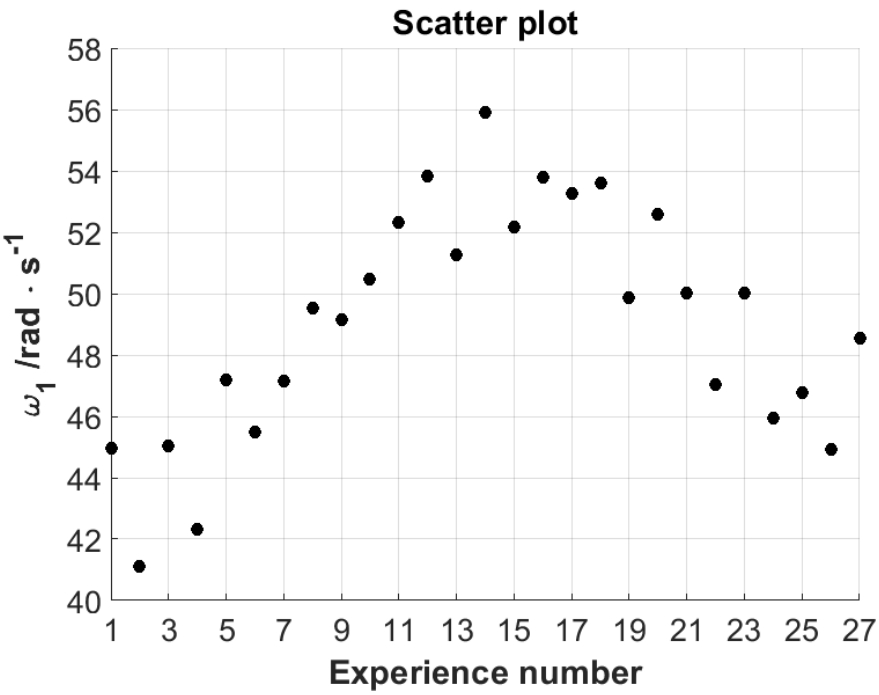

Figure 5.8 – Scatter plot of ω_1, having the plies orientations as design variables.

5.3.2 Modes of vibration

Here, the composite laminated plate modes of vibration are compared for 3 different design points, coinciding with a lower (see Figure 5.9), intermediate (see Figure 5.10) and higher (see Figure 5.11) value of the fundamental natural frequency, with the aim of comparing their configurations and ratios between their maximum and minimum displacements. It is worth to mention that the 7th, 8th, 9th and 10th modes of vibration here mentioned correspond, respectively, to the 1st, 2nd, 3rd and 4th non-rigid body modes.

Table 5.4 – Ratios between the extreme transverse displacements values of the natural vibration shapes.

Mode of vibration	Lower ω_1 value	Interm. ω_1 value	Higher ω_1 value
7th	2621	5590	5875
8th	259	170	178
9th	4775	4509	2954
10th	664	560	442

By the observation of the figures below, there are no differences between the vibration configurations for the 7th, 8th and 9th modes of vibration. The 8th, 9th and 10th modes of vibration are flexional ones, whereas the 7th is a torsional one. The only visible difference between them belongs to the 10th mode of vibration. For the lower value of the fundamental natural frequency, the spatial displacement is at the plane O_{yz}, whereas for the remaining ones the same occurs at the plane O_{xz}.

Moreover, it is possible to observe that in the 7th mode of vibration (torsional one), the composite panel extremities vibrate in phase opposition and there is a nodal line next to its centre; in the 8th mode of vibration (flexional one), the composite panel extremities vibrate in phase and in phase opposition with its centre. Besides that, there are two nodal lines in the O_{xz} plane next to the aluminium stiffeners; in the 9th mode of vibration (flexional one), the composite panel extremities vibrate in phase and in phase opposition with its centre (plane O_{yz}). In the plane O_{xz}, the panel extremities vibrate in phase opposition; lastly, in the 10^{th}mode of vibration (flexional one), for the configurations belonging to the panel with the intermediate and higher fundamental natural frequency value, the spatial displacement is, as referred above, at the plane O_{xz} and the composite panel extremities vibrate in phase and in phase opposition with its centre. There are, again, two nodal lines. The spatial displacement occurs at the plane O_{yz} for the lower ω_1 value configuration. There are four different parts which vibrate in phase opposition with the segments next to them. So, 3 nodal lines are observed in Figure 5.9d next to the three aluminium stiffeners. From the analysis of Table 5.4, the ratios between the extreme transverse displacements are similar for the 7th, 8th and 10th modes of vibration correspondent to the intermediate and higher ω_1 values configurations. The same is verified between the lower and intermediate ω_1 values configurations for the 9th mode of vibration.

Apart from the direct and difficult graphical comparison or using theoretic models, mode shapes might be compared using numerical correlations between an experimentally-measured mode shape, $\{\psi_X\}$, and a theoretically-predicted one, $\{\psi_A\}$ [127]. The Modal Assurance Criterion (*MAC*) is one of those parameters which quantifies the least-squares deviation of the points from the correlation along a straight line and it can be obtained according to the following expression:

$$MAC(A,X) = \frac{\left|\{\psi_X\}^T \{\psi_A\}\right|^2}{\left(\{\psi_X\}^T \{\psi_X\}\right)\left(\{\psi_A\}^T \{\psi_A\}\right)}. \tag{5.14}$$

In experimental modal analysis, the *MAC* value may be less than the expected one due to possible non-linearities in the test structure, noise on the measured data, poor modal analysis or even an inappropriate choice of the degrees of freedom to include in the correlation [127].

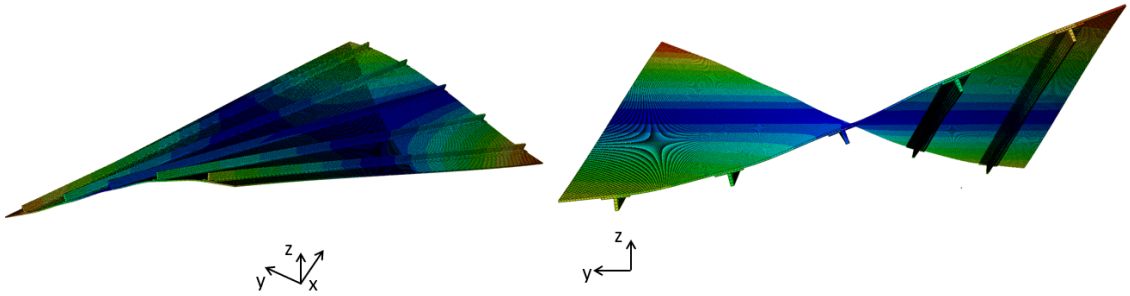

(a) 7th mode shape of the composite panel for $\omega = 41.1071$ rad $\cdot$ s^{-1}

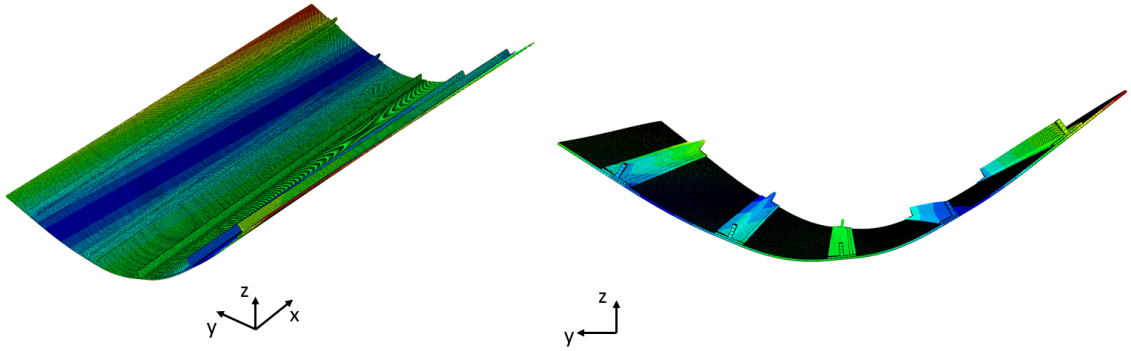

(b) 8th mode shape of the composite panel for $\omega = 56.7648$ rad $\cdot$ s^{-1}

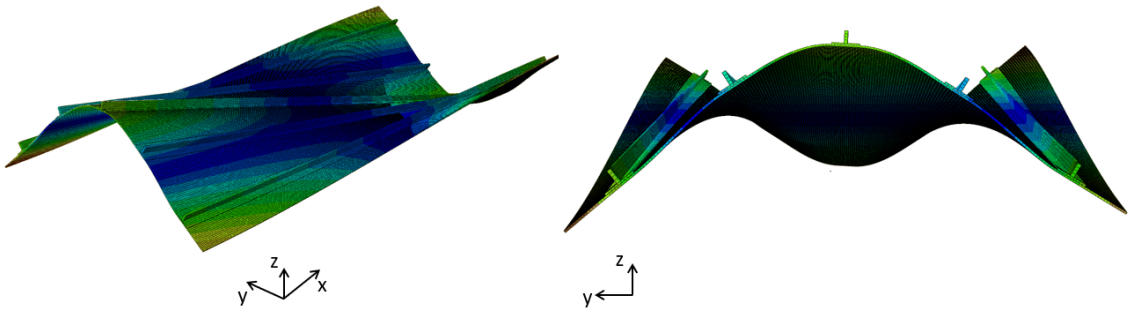

(c) 9th mode shape of the composite panel for $\omega = 102.8243$ rad $\cdot$ s^{-1}

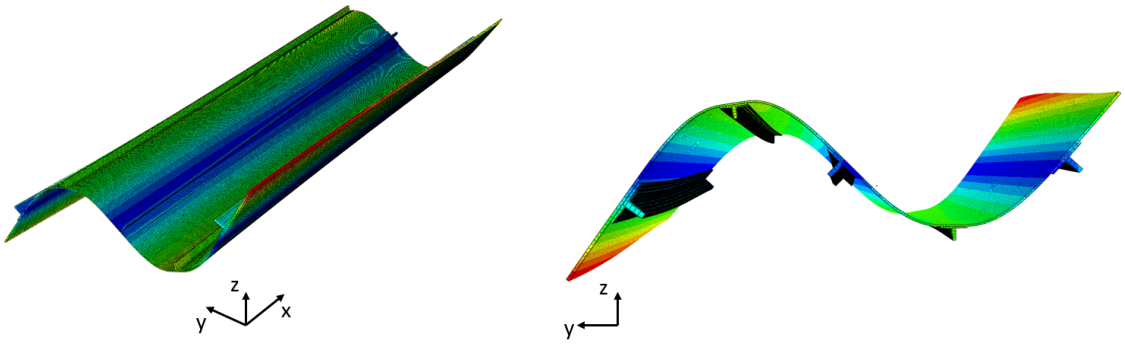

(d) 10th mode shape of the composite panel for $\omega = 159.6557$ rad $\cdot$ s^{-1}

Figure 5.9 – Vibration mode shapes of the composite panel for the lower fundamental natural frequency value.

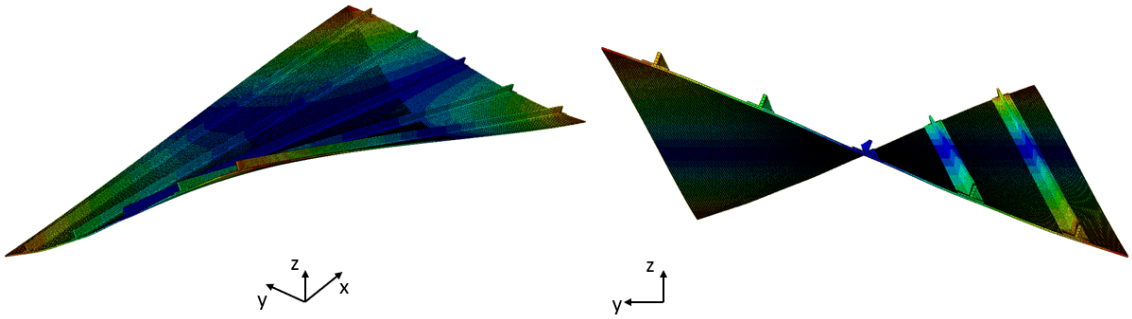

(a) 7th mode shape of the composite panel for $\omega = 48.5627$ rad $\cdot$ s^{-1}

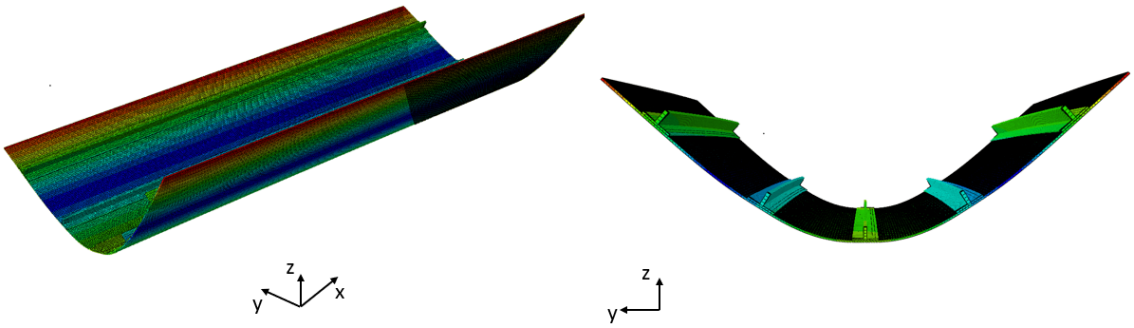

(b) 8th mode shape of the composite panel for $\omega = 127.4544$ rad $\cdot$ s^{-1}

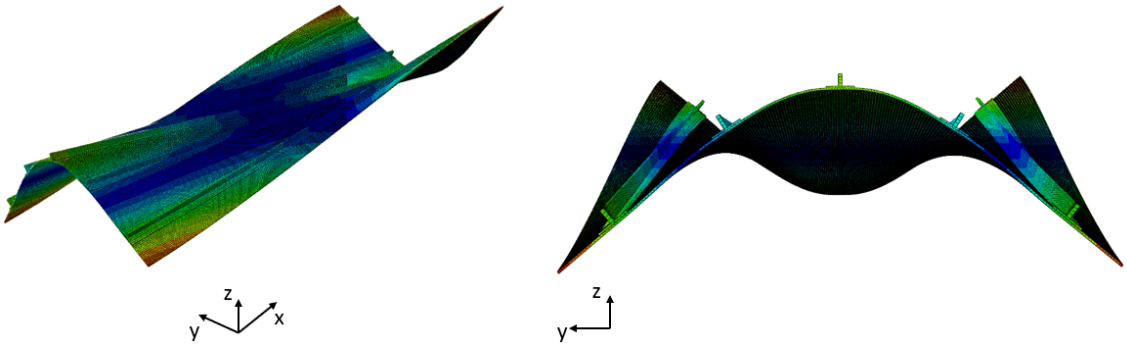

(c) 9th mode shape of the composite panel for $\omega = 162.0873$ rad $\cdot$ s^{-1}

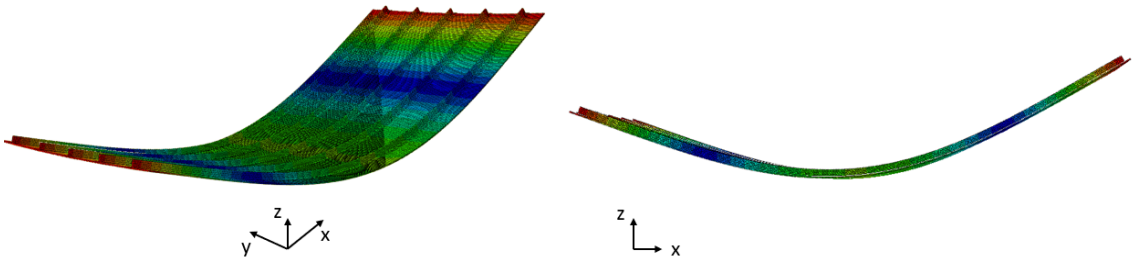

(d) 10th mode shape of the composite panel for $\omega = 200.5341$ rad $\cdot$ s^{-1}

Figure 5.10 – Vibration mode shapes of the composite panel for the intermediate fundamental natural frequency value.

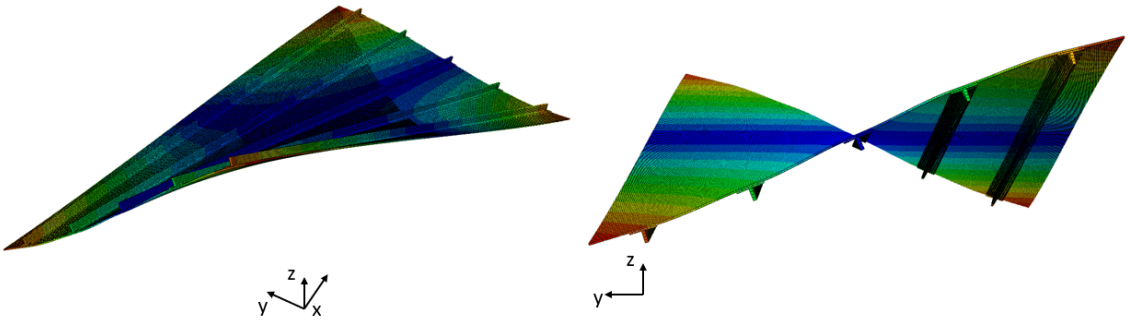

(a) 7th mode shape of the composite panel for $\omega = 55.9153$ rad $\cdot$ s^{-1}

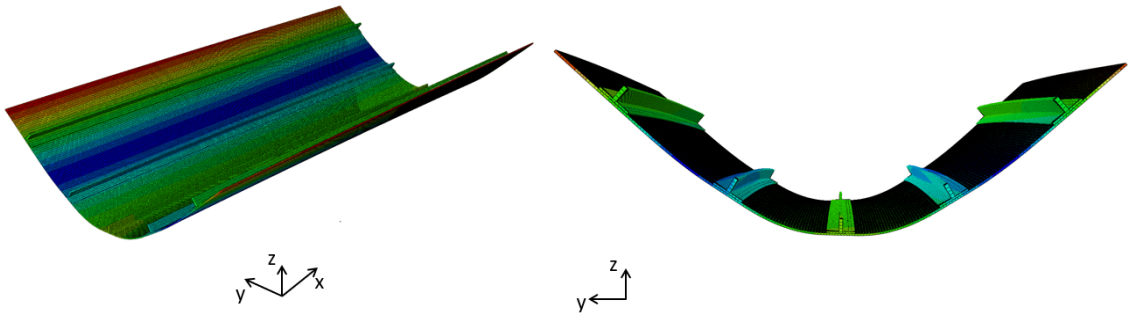

(b) 8th mode shape of the composite panel for $\omega = 78.0686$ rad $\cdot$ s^{-1}

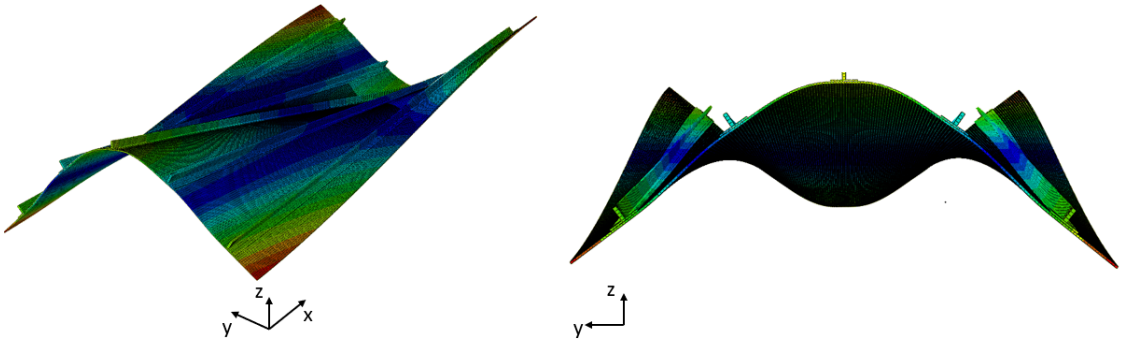

(c) 9th mode shape of the composite panel for $\omega = 139.7569$ rad $\cdot$ s^{-1}

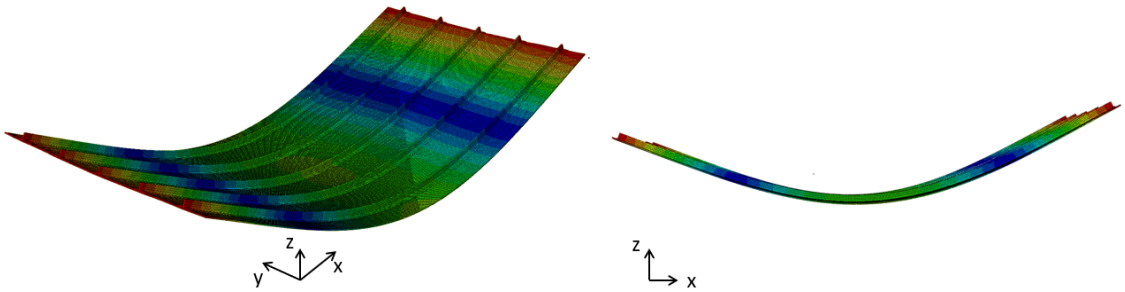

(d) 10th mode shape of the composite panel for $\omega = 200.4085$ rad $\cdot$ s^{-1}

Figure 5.11 – Vibration mode shapes of the composite panel for the higher fundamental natural frequency value.

Hereafter, the work done regarding the optimization procedures is presented. The diverse involved parameters and obtained results are clearly demonstrated.

5.3.3 ANN learning procedure

Firstly, with the values of Table 5.3 as inputs and outputs of the artificial neural network, wherein 27 experiences for minimum discrepancy and high representativeness of the domain under analysis are described, its learning procedure is carried out. In order to have a better sensitivity about the model obtained by the ANN to fit the required data, two natural frequencies were used to train the network.

After modifying consecutively and repeatedly several parameters concerning the genetic algorithm implementation and the ANN main configuration, such as the number of hidden layers, the similarity control mechanism, the range of the synaptic weights and biases, the parameterization ranges or the activation functions and respective parameters, the best ANN's architecture was achieved with regard to the synaptic weights and biases, design variables in this stage. Then, all design points were feedforwarded down the optimal ANN, with the aim of comparing the obtained results with those from FEM simulations. This first stage consists in the following optimization problem,

$$Maximise \;\; FIT^1 = K^1 - (c_1 \cdot RMSE + c_2 \cdot RE + c_3 \cdot \Gamma_{error}), \tag{5.15}$$

where RMSE is given by equation 5.3 and RE can be calculated according to equation 5.4.

After an iterative procedure, the following fitness function parameters were adopted:

- K^1= 5000;
- c_1= 50;
- c_2= 2500;
- c_3= 0.

Regarding the ANN architecture, the number of hidden neurons was set to 5 (only one hidden layer was considered), whereas the number of input and output neurons are constrained by the number of orientation angles to optimise and by the number of outputs chosen to train the network, respectively. As referred above, the employed genetic-based algorithm, $\mathbf{GA}^{(1)}$, is based on the maximisation of the expression 5.15. It was decided to normalise the input data between 0.01 and 0.99 and the output ones between 0 and 1. The synaptic weights and biases, design variables of the ANN-configuration optimization, are binary-coded with 4 digits at both interconnections (represents the number of genes belonging to each variable), input-hidden and hidden-output layers connections. Moreover, the chosen activation function was the sigmoidal one (see equation 2.2), with β_{sig}=1.5. Taking into account the activation function and the range of expected values for the output variables, the allowed range of values for the weights at the connection between the

input and hidden layers was set to [-3,3], whereas the interval [30,130] was chosen for the other interconnection. With the adopted ANN configuration, the number of variables at this first stage is

$$(INP+1)\cdot INT+(INT+1)\cdot OUT=(3+1)\cdot 5+(5+1)\cdot 2=32, \tag{5.16}$$

where INP, INT and OUT represent the number of input, hidden and output nodes, respectively.

The ANN learning process was performed by $\mathbf{GA}^{(1)}$ using a population with 21 individuals. The elite and mutation percentages were set to 0.333 and 0.1, respectively. Therefore, 7 individuals belong to the elite group, whereas 2 individuals make part of the mutation one. A mechanism of diversity control was used to avoid premature convergence due to the anchorage at local minima triggered by the loss of diversity. Each individual codifies the total number of variables and if there are at least 18 equal variables out of 32 between two selected individuals, one of them is taken out from the population and a new one is randomly created. The 18 value was set iteratively. Another procedure could be alternatively implemented, a genotype-based similarity control, wherein the control is performed gene by gene. The ANN learning procedure ends when the number of generations reaches 30000.

All these parameters were defined aiming to minimise the absolute and relative errors between the ANN simulated outputs and the results provided by FEM simulations and, at the same time, to assure a good performance of the second genetic algorithm. With all those referred parameters, an absolute error of 0.6015 rad $\cdot$ s^{-1} and a relative error of 1.012 % were achieved. The graphical representation of the evolution of these errors throughout the generations can be visualised in Figures 5.12 and 5.13.

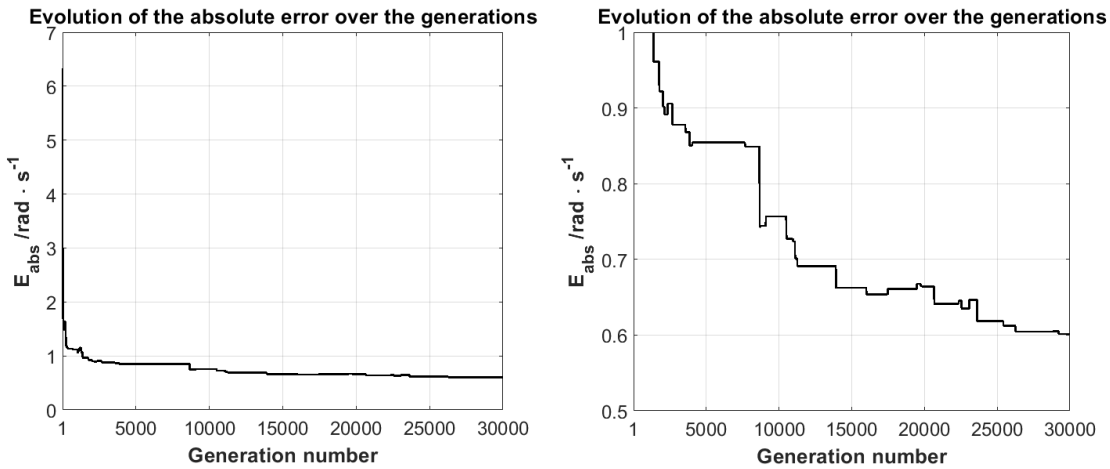

(a) Range: 6.33365 - 0.60147 /rad $\cdot$ s^{-1}

(b) Amplification

Figure 5.12 – Evolution of the ANN's absolute error over the generations, created to predict ω_1, having the plies orientations as design variables.

Regarding the absolute error, it ranges from 6.33365 to 0.60147 rad $\cdot$ s^{-1} and it is observed that it is lower than 0.85 for a population generation next to 5000. Therefore, the number of required generations for this particular problem is significantly lower than the selected one, so this value might be reduced in order to reduce the computational time. On the other hand, the relative error

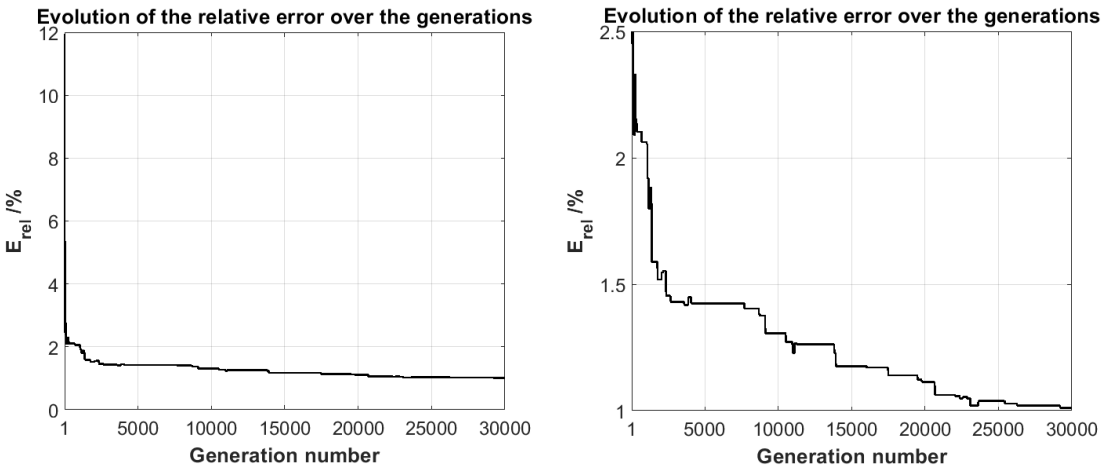

(a) Range: 11.96072 - 1.01151 %

(b) Amplification

Figure 5.13 – Evolution of the ANN's relative error over the generations, created to predict ω_1, having the plies orientations as design variables.

value ranges from 11.96072 to 1.01151 % and 1.4 % is achieved for the 5000-generation. Thus, the same conclusion could be drawn for this error measure.

Training dataset

The results from the ANN's feedforward propagation are summarised in Table 5.5 for the fundamental natural frequency and in Table 5.6 for the second one, in order to compare them with the ones obtained from the finite element model and, consequently, validate the optimization procedure:

Table 5.5 – Comparison between the ANN and FEM results for the training dataset of the ANN created to predict ω_1, having the plies orientations as design variables.

Experimental point	$\omega_{1,ANN}$ /rad $\cdot$ s^{-1}	$\omega_{1,FEM}$ /rad $\cdot$ s^{-1}	**Experimental point**	$\omega_{1,ANN}$ /rad $\cdot$ s^{-1}	$\omega_{1,FEM}$ /rad $\cdot$ s^{-1}
1	45.64452	44.96185	15	51.79937	52.16740
2	47.90133	41.10711	16	51.19009	53.77590
3	49.01579	45.02216	17	53.50983	53.27890
4	45.49247	42.30343	18	48.47966	53.59997
5	47.24915	47.17918	19	55.82395	49.86713
6	51.14879	45.48649	20	51.19974	52.58021
7	47.22847	47.13583	21	53.05606	50.02295
8	49.13863	49.52407	22	54.18602	47.02147
9	48.04862	49.14142	23	55.84095	50.00159
10	48.73653	50.48602	24	52.16061	45.94956
11	47.49203	52.31003	25	58.09557	46.77706
12	49.21503	53.82742	26	55.09857	44.90593
13	48.38178	51.27896	27	56.38224	48.56274
14	49.66955	55.91532			

Table 5.6 – Comparison between the ANN and FEM results for the training dataset of the ANN created to predict ω_2, having the plies orientations as design variables.

Experimental point	$\omega_{2,ANN}$ /rad $\cdot$ s^{-1}	$\omega_{2,FEM}$ /rad $\cdot$ s^{-1}	**Experimental point**	$\omega_{2,ANN}$ /rad $\cdot$ s^{-1}	$\omega_{2,FEM}$ /rad $\cdot$ s^{-1}
1	46.80422	47.55177	15	121.4140	90.30822
2	59.56270	56.76481	16	121.6518	85.86601
3	73.32385	67.95265	17	131.4480	91.64654
4	55.21610	44.69732	18	127.3755	106.3052
5	71.31625	59.84043	19	143.0398	99.55707
6	85.60586	66.08026	20	139.1420	108.7305
7	72.33492	53.15575	21	146.5099	116.2892
8	84.18888	57.63126	22	151.2297	115.4221
9	95.39920	74.73221	23	158.0376	116.5719
10	87.23812	55.37748	24	152.4278	127.5172
11	98.00761	70.07637	25	167.5123	119.9837
12	106.2943	78.83513	26	163.2419	124.9600
13	103.3084	73.47557	27	168.0319	127.4544
14	112.5139	78.06858			

Similar values for ω_1 were obtained, whereas for ω_2 that approximation does not happen. Despite of that distance, the relationship between two successive experimental points is practically the same for the two sets. The developed ANN clearly overestimates the values of ω_2 for all experimental points. However, no detailed attention will be given to that, since the ω_2 data was only used with the aim of obtaining reliable results concerning the ω_1 prediction.

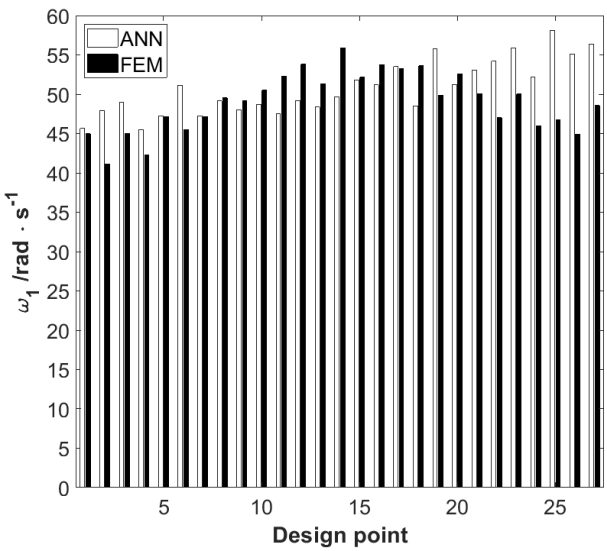

Figure 5.14 – Comparison between the ANN and FEM results for the training dataset of the ANN created to predict ω_1, having the plies orientations as design variables.

From the analysis of the figure above, Figure 5.14, good approximations were obtained between the ANN and FEM predictions, except for some experimental points at the right end of the bar graph. It is worth to mention that these kinds of still identifiable discrepancies are expected to be seen for data correlated by simple ANNs with an high dependency on the nature of the problem.

Hereafter, the influence of variations of the $\mathbf{GA}^{(1)}$ parameters and ANN's main architecture on the absolute and relative errors is studied in order to validate and explain the selected configuration.

Table 5.7 – Influence of the number of hidden nodes on the absolute and relative errors of the ANN learning procedure.

No. hidden nodes	$\mathbf{E}_{abs}$ /rad $\cdot$ s^{-1}	$\mathbf{E}_{rel}$ /%
3	0.70808	1.22870
4	0.44308	0.79978
5	0.60147	1.01151
6	0.52364	0.88697

Despite that from the observation of the table above, the number of chosen hidden nodes (5) does not lead to the lower error values, that value was selected because that ANN architecture led to a better balanced model, which improved the performance of $\mathbf{GA}^{(2)}$.

The output range was selected according to the values observed for the two first natural frequencies along the experimental points, because the activation function is linear at the output layer.

Table 5.8 – Influence of the range of weights at the hidden-output interconnection on the absolute and relative errors of the ANN learning procedure.

Output range	$\mathbf{E}_{abs}$ /rad $\cdot$ s^{-1}	$\mathbf{E}_{rel}$ /%
20 to 130	0.65162	1.14083
30 to 130	0.60147	1.01151
20 to 140	0.52198	0.94944
30 to 140	0.59059	1.00083

There are no significant differences between the several studied intervals. Others activation functions were also tested at the hidden layer, such as the hyperbolic tangent function or the Gaussian function. No improvements were observed for the first one (they became worst), whereas for the second one, whose representation is identical to the dispersion of the fundamental natural frequency (see Figures 2.3 and 5.8), the results were better regarding the magnitude of the error measures. However, problems arose in the optimization phase, $\mathbf{GA}^{(2)}$, wherein the model resulted from the first phase clearly overestimates the fundamental natural frequency value, in comparison with the result obtained from the FEM simulations for that specific set of design variables.

From Table 5.9, a higher population diversity causes the absolute and relative errors to decrease as population dimension increases. However, that improvement does not compensate the computational time enlargement, which is relevant when the number of variables and the number

Table 5.9 – Influence of the population's dimension on the absolute and relative errors of the ANN learning procedure.

$\mathbf{N}_{pop}$	$\mathbf{E}_{abs}$ /rad $\cdot$ s^{-1}	$\mathbf{E}_{rel}$ /%
18	0.65779	1.16205
21	0.60147	1.01151
24	0.44508	0.79486

of necessary model runs are high. The introduction of 3 more individuals leads to an increase of the CPU time up to 50 % of the previous value.

Table 5.10 – Influence of the mechanism of diversity control on the absolute and relative errors of the ANN learning procedure.

LIMDIF	$\mathbf{E}_{abs}$ /rad $\cdot$ s^{-1}	$\mathbf{E}_{rel}$ /%
14	0.53131	0.93712
16	0.68672	1.30230
18	0.60147	1.01151
20	0.67187	1.16235
22	0.63125	1.11406

In the genotype-based criteria, the parameter *LIMDIF* corresponds to the minimum number of equal genes between two individuals which leads to take one out from the population, replacing by another individual randomly created. On the other hand, the control may be done variable by variable and, again, between two different individuals, wherein a certain one is removed from the population if they have the same genotype regarding a minimum number of *LIMDIF* design variables. A lower value could lead to a loss of diversity, whereas the loss of better-fitness individuals may occur if that value is too high, resulting then in convergence at local optimal. Therefore, an intermediate value was selected.

Table 5.11 – Influence of the mutation percentage on the absolute and relative errors of the ANN learning procedure.

% **mutation**	$\mathbf{E}_{abs}$ /rad $\cdot$ s^{-1}	$\mathbf{E}_{rel}$ /%
0.05	0.45539	0.78129
0.1	0.60147	1.01151
0.2	0.49084	0.83327

As referred in others sections, the mutation operator is used to introduce variability to the population. An intermediate value was selected in order to create an optimised network which improves the performance of the second genetic algorithm. Although that this genetic operator is fundamental in introducing variability to the population, preventing early convergence, a value too high may lead, one more time, to the loss of individuals of higher fitness values.

5.3.4 Optimization of the ply angles

The objective of the implementation of this second genetic algorithm, $\mathbf{GA}^{(2)}$, is to achieve the best laminate configuration regarding the considered design variables, which leads to the higher fundamental natural frequency value, under prescribed constraints.

The second stage consists in the following optimization problem,

$$Maximise \;\; FIT^2 = OUT_{ANN} - \sum_{i=1}^{N} \alpha_i \Phi_i(\mathbf{x}), \tag{5.17}$$

where OUT_{ANN} corresponds to the lower output provided by the optimised artificial neural network, α_i is a user-tuned constant to weight each constraint in order to stabilize numerically the expression, Φ_i a particular constraint and $\mathbf{x}$ the vector of design variables.

The constraints related to this particular problem were directly imposed on the range of values suitable for each design variable. Therefore, the considered fitness function was merely

$$Maximise \;\; FIT^2 = OUT_{ANN}, \tag{5.18}$$

under the following constraints:

- balanced stacking sequence, that is, the same number of $-\theta$ and θ plies; and symmetric laminated about the midplane, in order to avoid shear-extension coupling (A_{16}=A_{26}=0) and extension-bending coupling (B_{ij}=0) (see Section 3.2). Those constraints are directly imposed by the laminate provided by the Cardiff School of Engineering (see Figure 5.5);

- contiguity constraint: in order to reduce matrix damage propagation up to a certain thickness, no more than 4 plies of the same orientation must be stacked together. This constraint was enforced by avoiding $\theta_3 = 0$;

- homogeneity constraint: each pair of $+\theta/-\theta$ plies should be located as closely as possible, aiming to minimise the bending-twisting coupling (D_{16}, D_{26}) and to improve the strength behaviour. This constraint is also verified by the initial provided stacking sequence design;

- damage tolerance requirements: the outer plies of the skin should always contain at least one set of +/- 45° [83, 106–108].

Considering the optimal ANN architecture came from the first optimization algorithm, the parameters chosen for this second genetic algorithm were N_{pop}=21; $\%_{elite}$=33 %; $\%_{mutation}$=10 %; $N_{generations}$=15000; θ_1=$\pm$0.7854 rad; $0 \leq \theta_2 \leq 1.5708$ rad; $0.1745 \leq \theta_3 \leq 1.5708$ rad. A certain individual is removed from the population if it codifies at least two variables ($LIMDIF$=2) with the same genotype, comparing with another individual from the population.

The following optimised configuration was achieved:

Table 5.12 – Optimised laminate configuration for vibration, considering the layers' orientations as design variables.

θ_1 /rad	θ_2 /rad	θ_3 /rad	$\omega_{1,ANN}$ /rad $\cdot$ s^{-1}	$\omega_{1,FEM}$ /rad $\cdot$ s^{-1}
0.7854	1.5708	0.1745	50.58	51.73

The resulted laminate configuration complies with the prescribed constraints. Moreover, the results obtained by the optimised ANN and by the FEM model, for the design variables came from the optimization procedure, are identical and next to the higher observed value for the fundamental natural frequency among the experimental points. The evolution of the ANN output value over the generations is plotted in the figure below.

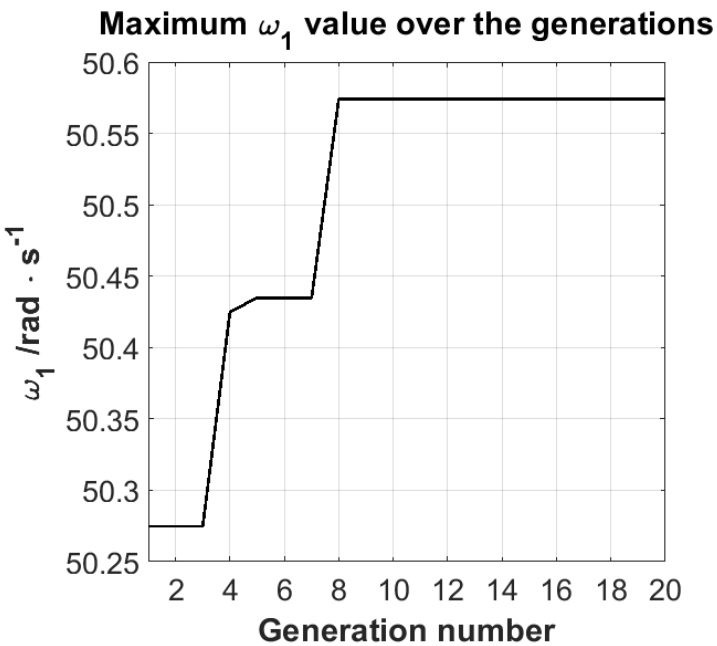

Figure 5.15 – Evolution of the maximised fundamental natural frequency over the generations, having the plies orientations as design variables.

No significant improvements on the obtained value are observed since the 1-generation, mainly due to the low number of design variables. The algorithm instantly achieved the optimal value at the 9-generation and that value does not change until the end of the optimization procedure. Moreover, the increase in the output value is reduced. It ranges only three tenths. Basically, only two jumps are observed, at the three and eight generations.

In order to study the influence of the damage tolerance constraint on the obtained results, an additional procedure was implemented. The allowable range for θ_1 was successively enlarged around 45° to perceive its influence upon the maximised obtained value for ω_1.

Table 5.13 – Influence of the allowable θ_1 range on the maximised obtained value for the fundamental natural frequency.

Allowable range	θ_1 /rad	θ_2 /rad	θ_3 /rad	$\omega_{1,ANN}$ /rad $\cdot$ s^{-1}	$\omega_{1,FEM}$ /rad $\cdot$ s^{-1}
0.7854	0.7854	1.5708	0.1745	50.58	51.73
0.5236 - 1.0472	1.0472	1.3614	0.1745	51.40	50.8
0.4363 - 1.3090	1.3090	0	0.1745	53.33	45.2
0.3491 - 1.2217	1.2217	0	0.1745	52.53	46.90
0.1745 - 1.3963	1.3963	0	0.1745	54.09	43.64
0 - 1.5708	1.5708	0	0.1745	55.49	42.18

From the table above, the prediction became worse as the available range increases. The ANN overpredicts the expected value due to a low sensibility of the developed model relatively to the orientation angle of the outermost layer.

5.3.5 *Sobol* indices

The *Sobol* indices are obtained according to the procedure described in subsection 5.2.5. For the optimization of the structure for vibration, having only the plies orientations as design variables, the following indices were obtained, altering the dimensions of the fixed values vector and sample matrix:

Table 5.14 – *Sobol* indices regarding the optimization of the structure for vibration, having only the plies orientations as design variables.

$\mathbf{N}_f$	$\mathbf{N}_r$	$S^O_{\theta_2}$	$S^O_{\theta_3}$	$\sum_{i=2,3} \mathrm{S}^O_{\theta_i}$	$\bar{S}^O_{\theta_2}$	$\bar{S}^O_{\theta_3}$
50	100	0.6007	0.4847	1.0854	0.5534	0.4466
25	50	0.7159	0.4770	1.1929	0.6001	0.3999
25	40	0.6993	0.5208	1.2201	0.5732	0.4268
25	100	0.5990	0.4780	1.0770	0.5562	0.4438
15	100	0.5653	0.4169	0.9822	0.5755	0.4245
20	100	0.6162	0.4399	1.0561	0.5835	0.4165
22	100	0.5909	0.4249	1.0158	0.5817	0.4183
23	100	0.6053	0.4441	1.0494	0.5768	0.4232
					0.5751	0.4249

The *Sobol* index relative to θ_1 is null as expected, because this variable is prescribed to 45°, therefore there is no contribution for the variance of the output response. Moreover, the indices are normalised in order for their sum to be unitary. The probable numerical error propagation during the algorithm's implementation led to a non-unitary value for the sum of all *Sobol* indices. Besides that, there are couplings between the design variables or, in other words, the individual effects on the variance of the output response are not summable. The dimensions of the $\boldsymbol{\lambda}_{fix}$ vector and $\boldsymbol{J}_\alpha$ matrix were changed in order to perceive their influence upon the obtained results.

Therefore, a simple mean calculation was performed to obtain the final indices' values: $\bar{S}^O_{\theta_2}$=0.5751 and $\bar{S}^O_{\theta_3}$=0.4249. So, the variables θ_2 and θ_3 have similar contributions for the variance of the fundamental natural frequency, with a slight higher value for θ_2, due to its proximity to the neutral axis of only an half of the symmetric laminate.

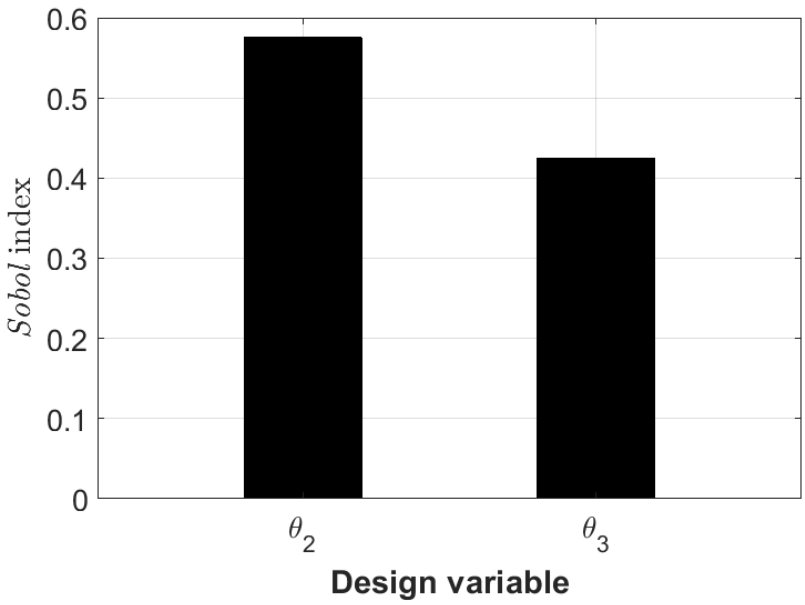

Figure 5.16 – *Sobol* indices corresponding to the ω_1 maximisation, having the plies orientations as design variables

5.3.6 Conclusions

For this concrete optimization problem, taking into account the chosen ANN's main architecture and genetic parameters, the following set of design variables was achieved (θ_1=0.7854 rad, θ_2=1.5708 rad and θ_3=0.1745 rad) for the second genetic algorithm. This input vector was forward propagated along the the optimised ANN, resulting ω_1=50.58 rad$\cdot$s^{-1}. The predicted value was ω_1=51.73 rad$\cdot$s^{-1} for the created finite element model, resulting a relative error of 2.22%. Moreover, that maximised value is placed around the higher values among the experimental points, as it can be depicted from Figure 5.8. However, from the same figure there are some combinations of the design variables which result in higher values for the fundamental natural frequency, compromising the assertiveness of the implemented algorithm. The network represents the training dataset, which contemplates the first two natural frequencies, with a relative error around 1.012%, Regarding the calculation of the *Sobol* indices, the θ_2 variable contributes around 58% for the total variance of the fundamental natural frequency and the remaining percentage concerns θ_3.

5.4 Fundamental natural frequency: ply angles and thicknesses

In this section, the same optimization procedure is performed, that is, the airplane wing representative structure is optimised regarding its fundamental natural frequency. Now, the thicknesses of the undefined layers are also design variables, altering the total plate's thickness. As demonstrated in Section 3.2, the stiffness coefficients are dependent on the thickness of each individual layer raised to the power of three. Therefore, in spite of the proportional increasing on the mass of the structure with the layers thicknesses, the stiffness has a bigger influence on the fundamental natural frequency. The stacking sequence and the unknown variables are represented in the next figure, Figure 5.17.

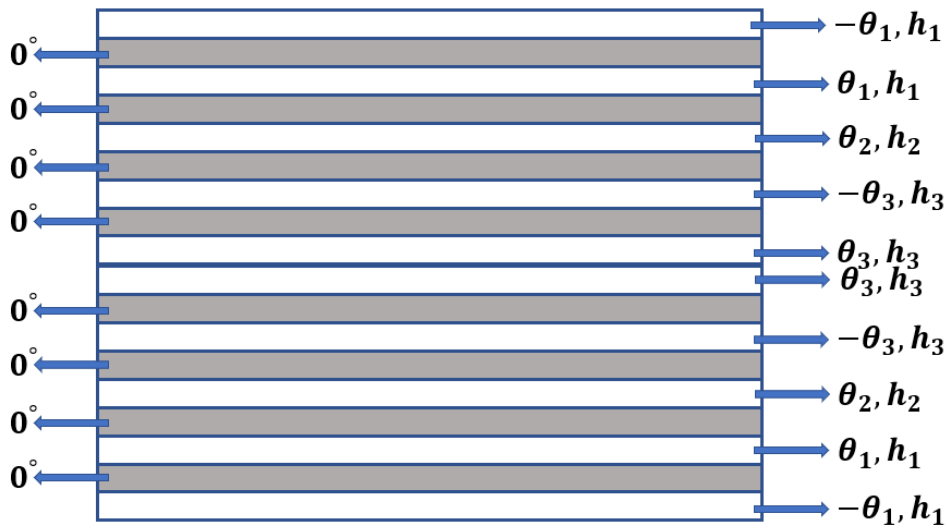

Figure 5.17 – Stacking sequence and design variables for the optimization of ω_1, including the plies thicknesses.

The same FEM model was used to predict the necessary data to train and build an artificial neural network.

5.4.1 Design of experiments

The design of experiments was now accomplished according to table $L_{27}(27^{11})$, in which 27 represents the number of experiments used for the ANN learning procedure, 27 corresponds to the number of levels of each factor and 11 to the maximum number of design variables (see Table 5.15). The accessory table, Table 5.16, is used to select the right columns, the columns 1, 2, 3, 6, 7 and 8.

The design variables domains, $\theta_i \in [0, \frac{\pi}{2}]$ rad and $h_i \in [0.1, 0.4]$ mm are, again, divided into 26 equal subdomains, being assigned to each one of them, by order, a number from 1 to 27. The first two natural frequencies are used again to train the artificial neural network. The experimental points and respective FEM values are presented in Table 5.17. The thicknesses' allowable range was defined taking into account recurrent values for carbon fiber reinforced polymer laminates.

Table 5.15 – Uniform design table, $L_{27}(27^{11})$.

No. of training datasets	**1**	**2**	**3**	**4**	**5**	**6**	**7**	**8**	**9**	**10**	**11**
1	1	4	7	8	10	13	16	19	20	22	25
2	2	8	14	16	20	26	5	11	13	17	23
3	3	12	21	24	3	12	21	3	6	12	21
4	4	16	1	5	13	25	10	22	26	7	19
5	5	20	8	13	23	11	26	14	19	2	17
6	6	24	15	21	6	24	15	6	12	24	15
7	7	1	22	2	16	10	4	25	5	19	13
8	8	5	2	10	26	23	20	17	25	14	11
9	9	9	9	18	9	9	9	9	18	9	9
10	10	13	16	26	19	22	25	1	11	4	7
11	11	17	23	7	2	8	14	20	4	26	5
12	12	21	3	15	2	21	3	12	24	21	3
13	13	25	10	23	22	7	19	4	17	16	1
14	14	2	17	4	5	20	8	23	10	11	26
15	15	6	24	12	15	6	24	15	3	6	24
16	16	10	4	20	25	19	13	7	23	1	22
17	17	14	11	1	8	5	2	26	16	23	20
18	18	18	18	9	18	18	18	18	9	18	18
19	19	22	25	17	1	4	7	10	2	13	16
20	20	26	5	25	11	17	23	2	22	8	14
21	21	3	12	6	21	3	12	21	15	3	12
22	22	7	19	14	4	16	1	13	8	25	10
23	23	11	26	22	14	2	17	5	1	20	8
24	24	15	6	3	24	15	6	24	21	15	6
25	25	19	13	11	7	1	22	16	14	10	4
26	26	23	20	19	17	14	11	8	7	5	2
27	27	27	27	27	27	27	27	27	27	27	27

Table 5.16 – Accessory table, $L_{27}(27^{11})$.

No. of design variables	**No. of columns**	**Discrepancy, D**
2	1,9	0.0710
3	1,9,10	0.1205
4	1,4,9,10	0.1673
5	1,4,9,10,11	0.2115
6	1,2,3,6,7,8	0.1378
7	1,2,3,5,6,7,8	0.1378

In Figure 5.18, the scatter plot of the fundamental natural frequency along the 27 experiences is illustrated, having the layers' orientations and thicknesses as design variables. A similar distribution is observed in comparison with the one represented in Figure 5.8.

Table 5.17 – Experimental points for the optimization of ω_1, having the plies orientations and thicknesses as design variables.

Point	θ_1 /rad	θ_2 /rad	θ_3 /rad	h_1 /mm	h_2 /mm	h_3 /mm	ω_1 /rad $\cdot$ s^{-1}	ω_2 /rad $\cdot$ s^{-1}
1	0	0.181246	0.362491	0.238462	0.273077	0.307692	41.67637	43.58834
2	0.060415	0.422907	0.785398	0.388462	0.146154	0.215385	43.62353	45.37277
3	0.120830	0.664566	1.208305	0.226923	0.330769	0.123077	44.44097	51.44169
4	0.181246	0.906229	0.181246	0.376923	0.203846	0.342308	42.59246	51.24943
5	0.241661	1.147890	0.422907	0.215385	0.388462	0.25	46.51631	70.61044
6	0.302076	1.389551	0.845813	0.365385	0.261538	0.157692	47.99034	61.64119
7	0.362491	0.181246	1.268720	0.203846	0.134615	0.376923	46.72868	63.87486
8	0.422907	0.241661	0.060415	0.353846	0.319231	0.284615	47.19992	50.01101
9	0.483322	0.483322	0.483322	0.192308	0.192308	0.192308	50.24286	52.51172
10	0.543737	0.724983	0.906229	0.342308	0.376923	0.1	54.60402	61.79261
11	0.604152	0.966644	1.329135	0.180769	0.25	0.319231	52.51298	78.64035
12	0.664568	1.208305	0.120830	0.330769	0.123077	0.226923	53.94806	73.31849
13	0.724983	1.449966	0.543737	0.169231	0.307692	0.134615	52.80389	88.22220
14	0.785398	0.060415	0.966644	0.319231	0.180769	0.353846	55.75196	79.24982
15	0.845813	0.302076	1.389551	0.157692	0.365385	0.261538	50.98491	92.77123
16	0.906229	0.543737	0.181246	0.307692	0.238461	0.169231	55.56032	92.77123
17	0.966644	0.785398	0.604152	0.146154	0.111538	0.388461	54.75231	84.64707
18	1.027059	1.027059	1.027059	0.296154	0.296154	0.296153	56.26969	109.8112
19	1.087474	1.268720	1.449966	0.134615	0.169231	0.203846	48.86496	106.9021
20	1.147890	1.510381	0.241661	0.284615	0.353846	0.111538	50.29187	124.7401
21	1.208305	0.120830	0.664568	0.123077	0.226923	0.330769	50.64875	93.09796
22	1.268720	0.362491	1.087474	0.273077	0.1	0.238461	50.23909	124.6458
23	1.329135	0.604152	1.510381	0.111538	0.284615	0.146153	48.07705	104.2506
24	1.389551	0.845813	0.302076	0.261538	0.157692	0.365385	48.23287	124.0364
25	1.449966	1.087474	0.724983	0.1	0.342308	0.273077	50.75117	111.3443
26	1.510381	1.329135	1.147890	0.25	0.215385	0.180769	45.46953	137.1117
27	1.570796	1.570796	1.570796	0.4	0.4	0.4	41.66694	148.1701

5.4.2 ANN learning procedure

The ANN learning process was undertaken using the data provided by Table 5.17 as inputs and outputs of the artificial neural network. The best ANN architecture was achieved taking into account the best possible generalisation of the relationship under analysis and by changing, again, several parameters regarding the genetic algorithm and the ANN configuration, such as the number of hidden layers, the similarity control mechanism, the range of the synaptic weights and biases, the parameterization ranges or the activation functions and respective parameters. The fitness function regarding this optimization phase was set to

$$Maximise \;\; FIT^1 = 5 \cdot 10^3 - (50 \cdot RMSE + 2500 \cdot RE), \tag{5.19}$$

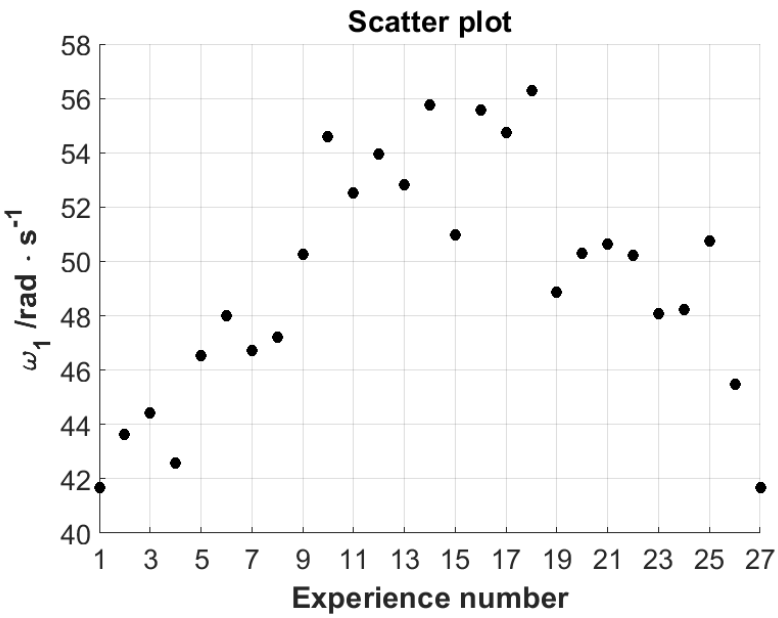

Figure 5.18 – Scatter plot of ω_1, having the plies orientations and thicknesses as design variables.

where RMSE is given by equation 5.3 and RE can be calculated according to equation 5.4. The weights for each parcel were chosen in order for them to have a similar contribution to the fitness assessment.

The same ANN architecture was selected to predict the output values in comparison with the one used when only the orientations of the layers were considered as design variables. The only difference is an addition on the number of input variables, which contemplate the layers' thicknesses as well. The applied genetic-based algorithm, $\mathbf{GA}^{(1)}$, is based on the maximisation of the expression 5.19. In order to avoid numerical error propagation, the input data was normalised between 0.01 and 0.99 and the output ones between 0 and 1. Here, the input data normalisation is even more fundamental, due to their different nature. Four digits are used in the binary-coded representation of the unknowns of this first optimization stage. The sigmoidal function was selected to introduce non-linearity at the hidden layer, with β_{sig}=1.7. The allowable range for the values of the weights at the connection between the input and hidden layers was set to [-3,3], whereas the interval [0,140] was selected for the other interconnection. The number of variables at this first stage is

$$(INP+1)\cdot INT+(INT+1)\cdot OUT=(6+1)\cdot 5+(5+1)\cdot 2=47. \tag{5.20}$$

This optimization phase was carried out using a population with 21 individuals, with 7 out of 21 belonging to the elite group and 2 to the mutation one. The similarity control is also phenotype-based, that is, if two individual picked from the population have the same genotype concerning at least 32 variables out of 47, then one of them is removed from the population and another one is randomly created. The ANN learning process ends up at the 30000-generation.

One more time, these referred parameters were set up through a trial and error procedure, aiming to universally represent the problem under analysis and, at the same time, to obtain the minimum values for the absolute and relative errors. Consequently, an absolute error of 0.912 rad $\cdot$ s^{-1} and a relative error of 1.204 % were achieved. The graphical representation of the evolution of these errors throughout the generations can be visualised in Figures 5.19 and 5.20.

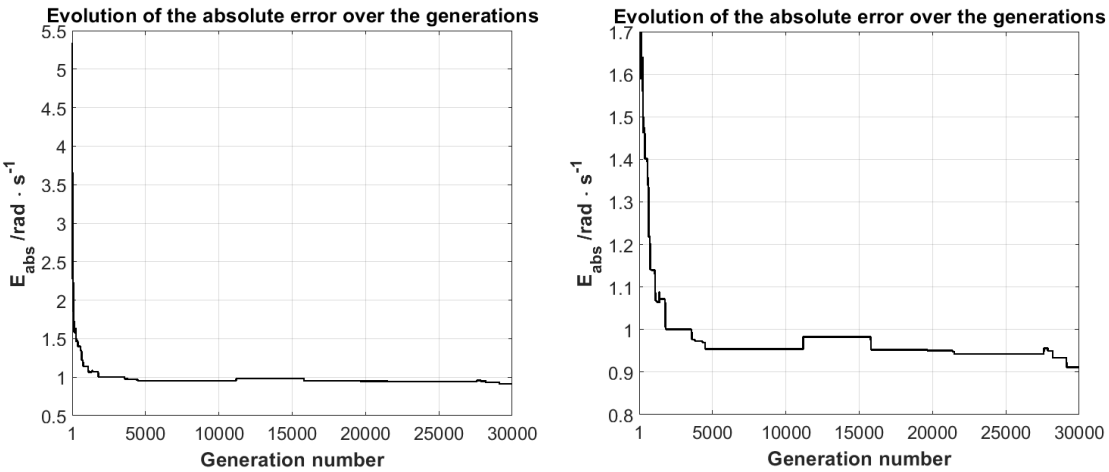

(a) Range: 5.293 - 0.912 /rad $\cdot$ s^{-1} (b) Amplification

Figure 5.19 – Evolution of the ANN's absolute error over the generations, created to predict ω_1, having the plies orientations and thicknesses as design variables.

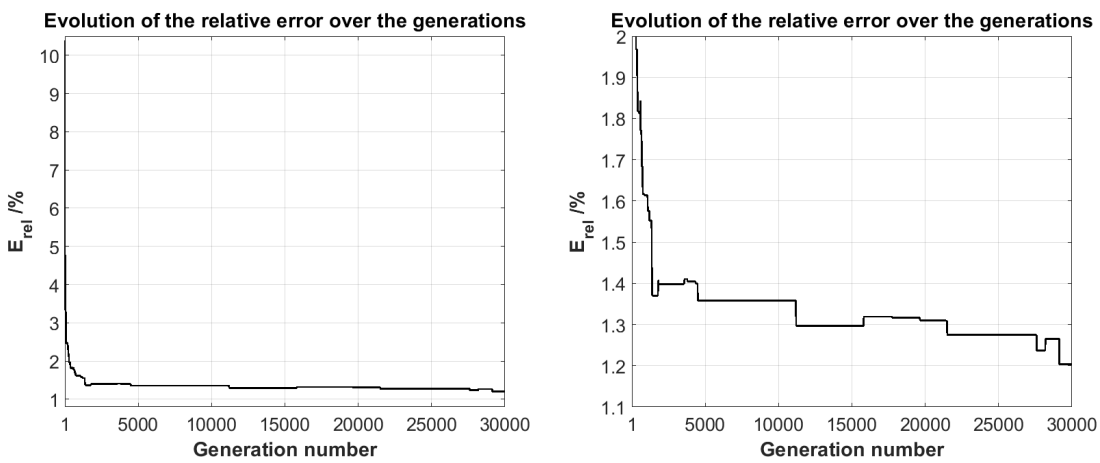

(a) Range: 10.394 - 1.204 % (b) Amplification

Figure 5.20 – Evolution of the ANN's relative error over the generations, created to predict ω_1, having the plies orientations and thicknesses as design variables.

During the evolution process, the absolute error fluctuates from 5.293 to 0.912 rad $\cdot$ s^{-1} and is lower than 1 rad $\cdot$ s^{-1} for a generation next to 2000, which points out a possible reduction in the number of generations, that is, promote the convergence criteria to happen earlier, whereas the relative error value ranges from 10.394 to 1.204 %. For the 2000-generation, this error is almost 1.4 %, thus the number of prescribed generations can be reduced in this concrete problem.

Training dataset

In the next two tables, the results from the ANN's feedforward propagation are presented for each experimental point, as well as their correspondent FEM predictions:

Table 5.18 – Comparison between the ANN and FEM results for the training dataset of the ANN created to predict ω_1, having the plies orientations and thicknesses as design variables.

Experimental point	$\omega_{1,ANN}$ /rad $\cdot$ s^{-1}	$\omega_{1,FEM}$ /rad $\cdot$ s^{-1}	**Experimental point**	$\omega_{1,ANN}$ /rad $\cdot$ s^{-1}	$\omega_{1,FEM}$ /rad $\cdot$ s^{-1}
1	46.15577	41.67637	15	51.42796	50.98491
2	48.57422	43.62353	16	50.77101	55.56032
3	48.27853	44.44097	17	48.51539	54.75231
4	51.84380	42.59246	18	48.43280	56.26969
5	52.54575	46.51631	19	48.17600	48.86496
6	51.76753	47.99034	20	50.76741	50.29187
7	49.37153	46.72868	21	51.52833	50.64875
8	49.54784	47.19992	22	50.16031	50.23909
9	52.41149	50.24286	23	51.30978	48.07705
10	51.61822	54.60402	24	48.52829	48.23287
11	54.10501	52.51298	25	47.18637	50.75117
12	48.85931	53.94806	26	46.84286	45.46953
13	47.83785	52.80389	27	46.74141	41.66694
14	51.85207	55.75196			

Table 5.19 – Comparison between the ANN and FEM results for the training dataset of the ANN created to predict ω_2, having the plies orientations and thicknesses as design variables.

Experimental point	$\omega_{2,ANN}$ /rad $\cdot$ s^{-1}	$\omega_{2,FEM}$ /rad $\cdot$ s^{-1}	**Experimental point**	$\omega_{2,ANN}$ /rad $\cdot$ s^{-1}	$\omega_{2,FEM}$ /rad $\cdot$ s^{-1}
1	41.54436	43.58834	15	112.4819	92.77123
2	48.13506	45.37277	16	125.0218	92.77123
3	50.09112	51.44169	17	124.9529	84.64707
4	73.79218	51.24943	18	132.0010	109.8112
5	78.27390	70.61044	19	133.1575	106.9021
6	81.52355	61.64119	20	138.5711	124.7401
7	61.25708	63.87486	21	134.5358	93.09796
8	68.75229	50.01101	22	136.2895	124.6458
9	82.53593	52.51172	23	137.7502	104.2506
10	91.31680	61.79261	24	139.4864	124.0364
11	103.4860	78.64035	25	139.3982	111.3443
12	99.15853	73.31849	26	139.1932	137.1117
13	112.0759	88.22220	27	139.5448	148.1701
14	104.6515	79.24982			

One more time, identical values were obtained for almost all experimental points regarding the fundamental natural frequency prediction. The same behaviour is identified for the second natural frequency in comparison with the tendency observed when only the fibres' orientations were considered as design variables.

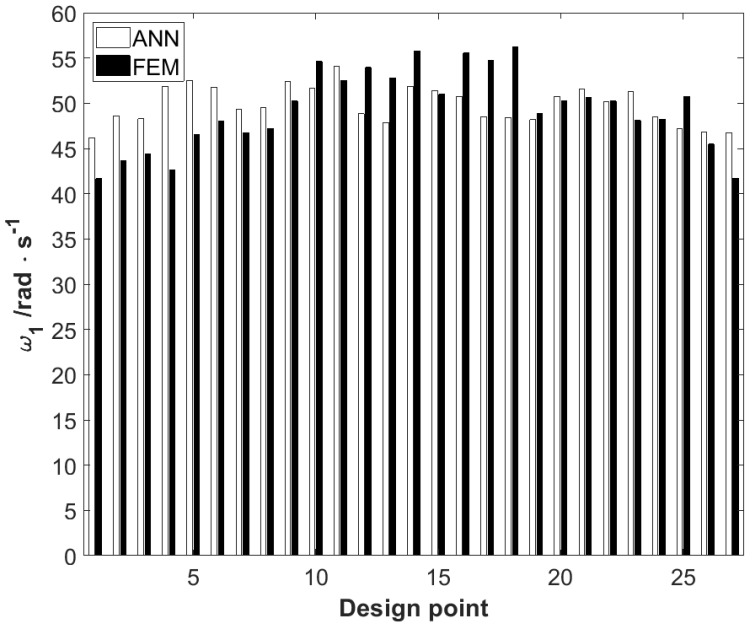

Figure 5.21 – Comparison between the ANN and FEM results for the training dataset of the ANN created to predict ω_1, having the plies orientations and thicknesses as design variables.

Apart from the design points at the left end of the bar graph (see Figure 5.21), the results for the fundamental natural frequency prediction are in good agreement.

The influence of the individual variations of the $\mathbf{GA}^{(1)}$ parameters and ANN's main architecture on the absolute and relative errors is studied from now on.

Table 5.20 – Influence of the number of hidden nodes on the absolute and relative errors of the ANN learning procedure.

No. hidden nodes	$\mathbf{E}_{abs}$ /rad $\cdot$ s^{-1}	$\mathbf{E}_{rel}$ /%
3	1.48896	2.34089
4	1.16351	2.09052
5	0.91192	1.20385
6	0.61901	1.01525

From the table above, the number of hidden nodes which corresponds to the highest fitness value is six. However, it was find out that 5 nodes are enough to predict accurately the output data. The output range was set iteratively in order to obtain the most balanced model. Some results are presented in the table below regarding its variation with no significant differences between the several ranges.

Table 5.21 – Influence of the range of weights at the hidden-output interconnection on the absolute and relative errors of the ANN learning procedure.

Output range	$\mathbf{E}_{abs}$ /rad $\cdot$ s^{-1}	$\mathbf{E}_{rel}$ /%
0 to 100	0.71521	1.14456
0 to 140	0.91192	1.20385
0 to 170	0.73818	1.11478
0 to 200	0.75395	1.02441

The same problems regarding the utilisation of others activation functions appeared in this optimization procedure. The hyperbolic tangent one does not introduce any improvements, whereas the Gaussian function, although its representation is similar to the ω_1 dispersion along the domain, clearly overestimates the maximised fundamental natural frequency value.

Table 5.22 – Influence of the population's dimension on the absolute and relative errors of the ANN learning procedure.

$\mathbf{N}_{pop}$	$\mathbf{E}_{abs}$ /rad $\cdot$ s^{-1}	$\mathbf{E}_{rel}$ /%
18	0.90732	1.42595
21	0.91192	1.20385
24	0.74988	1.16541

An intermediate dimension of the population was chosen in order to have a balance between the performance of both genetic algorithms and the the computational effort.

Table 5.23 – Influence of the mechanism of diversity control on the absolute and relative errors of the ANN learning procedure.

LIMDIF	$\mathbf{E}_{abs}$ /rad $\cdot$ s^{-1}	$\mathbf{E}_{rel}$ /%
28	0.60432	0.98904
30	0.73955	1.07686
32	0.91192	1.20385
34	0.70432	1.11582
36	0.74518	1.29772

The study upon the effect of the variation of the mechanism of diversity control was performed and showed here in order to demonstrate that the configurations with the lowest absolute and relative errors do not correspond always to the best one regarding the algorithm's overall performance. It could be a possible signal of overfitting phenomena.

The increase on the number of elite individuals makes that a higher number of moderate fitness members belongs to the elite group, therefore suitable for crossover, which leads to an improvement on the population's variability and could promote the search at others zones of the design space and the achievement of others local/global solutions. The obtained values, see Table 5.24, do not differ as much as expected. Then, it was chosen the one that improves the second genetic algorithm's performance.

Table 5.24 – Influence of the elite percentage on the absolute and relative errors of the ANN learning procedure.

% **elite**	$\mathbf{E}_{abs}$ /rad $\cdot$ s^{-1}	$\mathbf{E}_{rel}$ /%
0.1	0.63462	0.99702
0.2	0.74048	1.20697
0.33	0.91192	1.20385
0.5	0.62729	0.99113
0.6	0.85368	1.07671

5.4.3 Optimization of the layers' orientations and thicknesses

In this second genetic algorithm, $\mathbf{GA}^{(2)}$, the optimal laminate design is achieved, regarding the layers' thicknesses and orientations, aiming to maximise the fundamental natural frequency , ω_1, taking into account manufacturing constraints and, particularly, the ones which improve the laminate's strength behaviour and reduce the risk of delamination.

The second stage consists in the following optimization problem,

$$Maximise \;\; FIT^2 = OUT_{ANN}, \tag{5.21}$$

wherein the constraints are again imposed directly on the allowed bounds of the design variables and they are the same used for optimise the laminate taking into account only the orientation of the plies as design variables:

- balanced stacking sequence;
- contiguity constraint;
- homogeneity constraint;
- damage tolerance constraint.

The second optimization phase was carried out considering $\mathbf{P}^{opt}_{ANN}$ and the following genetic parameters: N_{pop}=21; $\%_{elite}$=33 %; $\%_{mutation}$=10 %; $N_{generations}$=15000. The similarity control mechanism established that a certain individual is removed from the population if it has the same genotype for at least 4 variables out of 6, comparing with another one from the population. Regarding the admissible domains for the design variables: $\theta_1 = \pm 0.7854$ rad; $0 \leq \theta_2 \leq 1.5708$ rad; $0.1745 \leq \theta_3 \leq 1.5708$ rad; $0.1 \leq h_1 \leq 0.4$ mm; $0.1 \leq h_2 \leq 0.4$ mm and $0.1 \leq h_3 \leq 0.4$ mm.

The optimised configuration is described in Table 5.25.

Table 5.25 – Optimised laminate configuration for vibration, considering the layers' orientations and thicknesses as design variables.

θ_1 /rad	θ_2 /rad	θ_3 /rad	h_1 /mm	h_2 /mm	h_3 /mm	$\omega_{1,ANN}$ /rad $\cdot$ s^{-1}	$\omega_{1,FEM}$ /rad $\cdot$ s^{-1}
0.7854	1.5708	0.9250	0.4	0.1	0.4	55.29	57.39

For the laminate configuration characterised in Table 5.25, the value provided by the optimised ANN lies in the range of the higher ω_1 values which appear among the experimental points. Besides that, the value provided by the developed FEM model is higher than those related with the training dataset, which allows to draw a conclusion about the authenticity of the created optimization procedure. Furthermore, the prescribed constraints are attained. The progression of the ANN prediction over the generations is plotted in Figure 5.22.

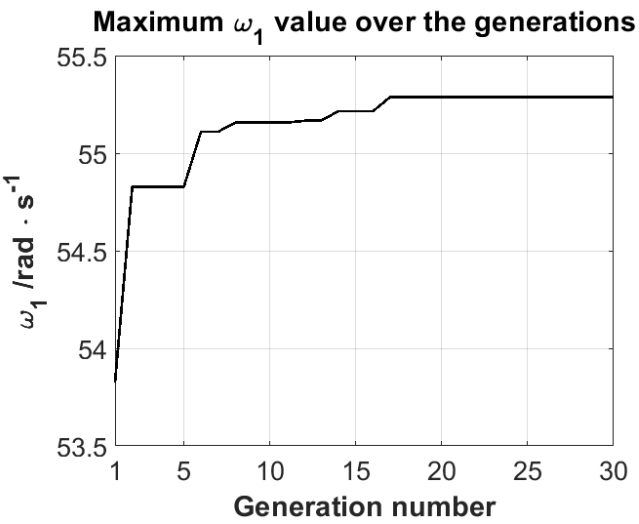

Figure 5.22 – Evolution of the maximised fundamental natural frequency over the generations, having the layers orientations and thicknesses as design variables.

During the evolution process, the maximised value for the fundamental natural frequency ranges from 53.83 to 55.29 rad $\cdot$ s^{-1}, thus there is just a slight variation to consider. Five jumps were observed, that is, five improvements on the optimised value. The optimization algorithm early reaches the final value, at the seventeen generation. Therefore, the number of required generations might be reduced to reduce the computational cost.

Changing only the constant of the sigmoidal function from $\beta_{sig} = 1.7$ to $\beta_{sig} = 1.5$, another optimised ANN network may be achieved. For this case, see Table 5.26, the value predicted by the artificial neural network overestimates the maximum ω_1 value, whereas the FEM solution is placed around the expected value.

Table 5.26 – Optimised laminate configuration for vibration, considering the layers orientations and thicknesses as design variables: other configuration.

θ_1 /rad	θ_2 /rad	θ_3 /rad	h_1 /mm	h_2 /mm	h_3 /mm	$\omega_{1,ANN}$ /rad $\cdot$ s^{-1}	$\omega_{1,FEM}$ /rad $\cdot$ s^{-1}
0.7854	1.5708	0.1745	0.4	0.1	0.1	60.34	55.87

Now, remembering that the thickness of each ply belonging to the panel provided by the Cardiff School of Engineering is t_{ply}= 0.194444 mm, it is worthwhile to compare the diverse optimal configurations with the standard one regarding the mass of the structure, taking into account

the total thickness of the optimised panel for each configuration.

Table 5.27 – Comparison between the total panel's thickness for each optimised configuration for vibration, having the plies orientations and thicknesses as design variables

Configuration	**Total thickness /mm**
Standard	3.50
$\beta_{sig} = 1.7$	4.96
$\beta_{sig} = 1.5$	3.76

The total thickness of the optimised configuration correspondent to $\beta_{sig} = 1.7$ is higher than the one relative to $\beta_{sig} = 1.5$ and, therefore, the fundamental natural frequency value provided by the created finite element model is bigger for the first one due to a higher stiffness increase, as expected (see Table 5.25 and Table 5.26).

5.4.4 *Sobol* indices

The contributions of the plies' orientations and thicknesses for the variance of the ω_1 response are summarised in the table below for several sets taking into consideration the dimensions of the random generated vector $\boldsymbol{\lambda}_{fix}$ and matrix $\boldsymbol{J}_{\alpha}$. The subscripts 1 to 3 refer to the plies' orientations, whereas the remaining ones regard the layers' thicknesses.

Table 5.28 – *Sobol* indices regarding the optimization of the structure for vibration, having the plies orientations and thicknesses as design variables.

$\mathbf{N}_f$	$\mathbf{N}_r$	S_2^O	S_3^O	S_4^O	S_5^O	S_6^O	$\sum_{i=2}^{6} S_i^O$
5	50	0.2231	0.0017	0.0530	0.4421	0.0082	0.7281
10	50	0.2924	0.0010	0.0735	0.6905	0.1513	1.2087
15	50	0.17	0.0088	0.0793	0.7596	0.1968	1.2145
5	100	0.1984	0.0363	0.0865	0.3231	0.1286	0.7729
10	100	0.2955	0.0507	0.1294	0.3933	0.1633	1.0322
15	100	0.2164	0.0349	0.1299	0.4675	0.1941	1.0428
20	100	0.1752	0.0356	0.1112	0.4168	0.1734	0.9122
25	100	0.1502	0.0326	0.0941	0.3879	0.1651	0.8299
		0.2290	0.0404	0.1235	0.4259	0.1769	0.9957

Considering only the experiences with N_r=100 and N_f=$\{10, 15, 20\}$ for the average of the *Sobol* indices corresponding to each design variable, because their sum is next to the unitary value, the following results were obtained: $\bar{S}_2^O$=0.2290; $\bar{S}_3^O$=0.0404; $\bar{S}_4^O$=0.1235; $\bar{S}_5^O$=0.4259 and $\bar{S}_6^O$=0.1769.

Due to the constraint relative to the θ_1 value, it does not contribute for the variance of the ω_1 response, as expected. The intermediate layers are the most important ones on the prediction of the fundamental natural frequency, as it is possible to prove from the table above, Table 5.28, due to the higher *Sobol* indices values. Furthermore, the thickness variable has a higher contribution

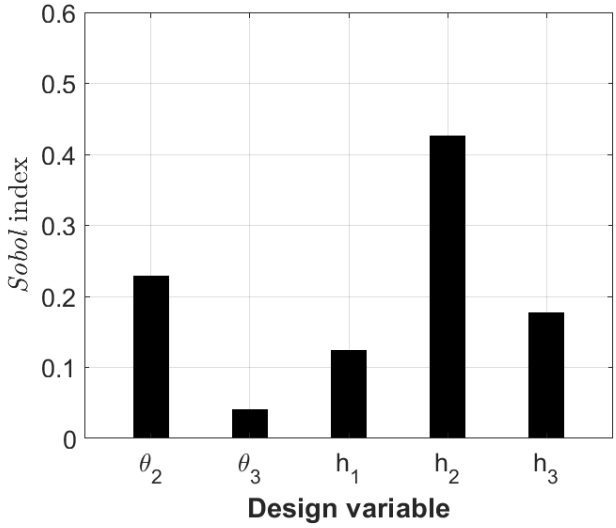

Figure 5.23 – *Sobol* indices corresponding to the ω_1 maximisation, having the plies orientations and thicknesses as design variables.

in comparison with the orientation of the same layer, which allows to draw a conclusion about the bigger influence that the plies' thickness has on the structure's stiffness and, consequently, on the fundamental natural frequency.

5.4.5 Conclusions

Here, the developed artificial neural network represents with a relative error of 1.2% the training data, which does not correspond exactly to the best configuration regarding the considered errors' measures. However, as explained above, this model is the one that better fits the relationship under analysis. Taking into account several constraints, the results from the second genetic algorithm were (θ_1=0.7854 rad, θ_2=1.5708 rad and θ_3=0.9250 rad; h_1=0.4 mm, h_2=0.1 mm and h_3=0.4 mm). The relative error between the predictions obtained from the optimised ANN and FEM simulation is 3.66%. Although the underprediction obtained from the artificial neural network, the FEM result is higher than all values among the experimental points, which further validates the optimization procedure.

Regarding the importance of each design variable upon the output response, it is worth to mention that there is a higher predominance of the thickness variables in comparison with the orientation ones.

5.5 Final remarks

The lower number of design variables allows to represent the relationship under analysis, using an artificial neural network, with a relative error next to 1%. For the first optimization problem, maximization of the fundamental natural frequency considering only the layers' orientations as design variables, the maximised ω_1 value is still a bit far from the higher values observed among the experimental points. The opposite occurred with the second one, wherein the layers' thicknesses were added as unknown variables and the implemented algorithm is further validated by the achievement of a value bigger than those obtained by FEM simulations for the training dataset. Regarding the design variables, only the orientation angle of the innermost layer changes between the two optimization problems, beside the thicknesses. In both optimization procedures, the intermediate layer has a slight bigger influence upon the variance of the output response, as it can be depicted from the first order *Sobol* indices analysis.

Chapter 6

Optimization of the airplane wing representative structure for buckling

In this section, the airplane wing representative structure is optimised with regard to its critical buckling load by changing the layers' orientations and thicknesses of the composite panels. It is challenging to investigate the behaviour of a certain structure pos-buckling, therefore the maximisation of the critical buckling load is fundamental in order for the structure to carry a bigger load and to ensure its safety. Furthermore, the sudden stiffness change due to buckling may lead to the immediate structure's failure, which is extremely dangerous for this demanding application. The stacking sequence and the design variables are illustrated below, in Figure 6.1.

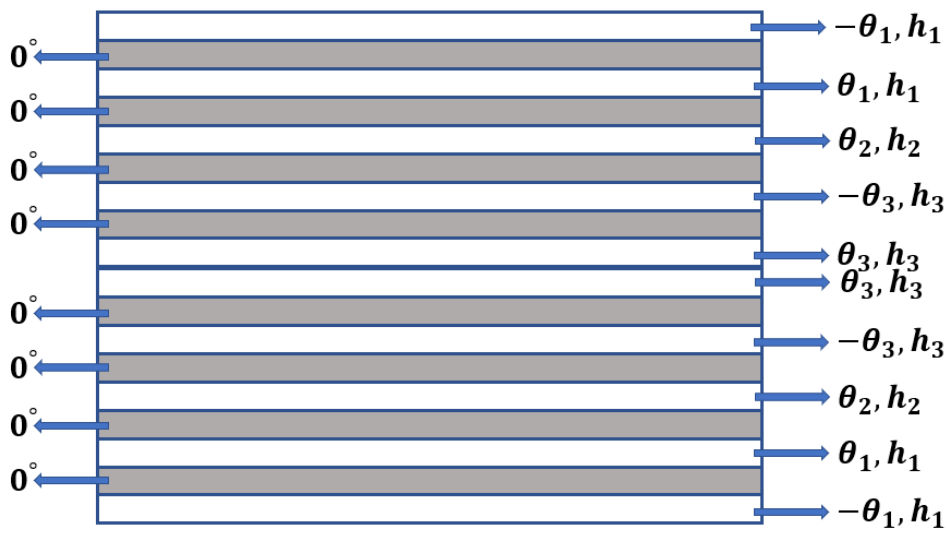

Figure 6.1 – Stacking sequence and design variables for the optimization of P_{crit}, including the plies thicknesses.

There are six design variables: θ_1, θ_2, θ_3, h_1, h_2 and h_3. A finite element model was developed in order to predict the buckling loads for each experimental point necessary to train the artificial neural network. The ANN was employed to reduce substantially the computational time which

could be necessary whether the FEM model was used along the genetic algorithm. The composite panel was built using the Abaqus® intrinsic tool designated by Composite Layup, in which are specified the orientation angle, thickness, material and the number of integration points for each individual layer.

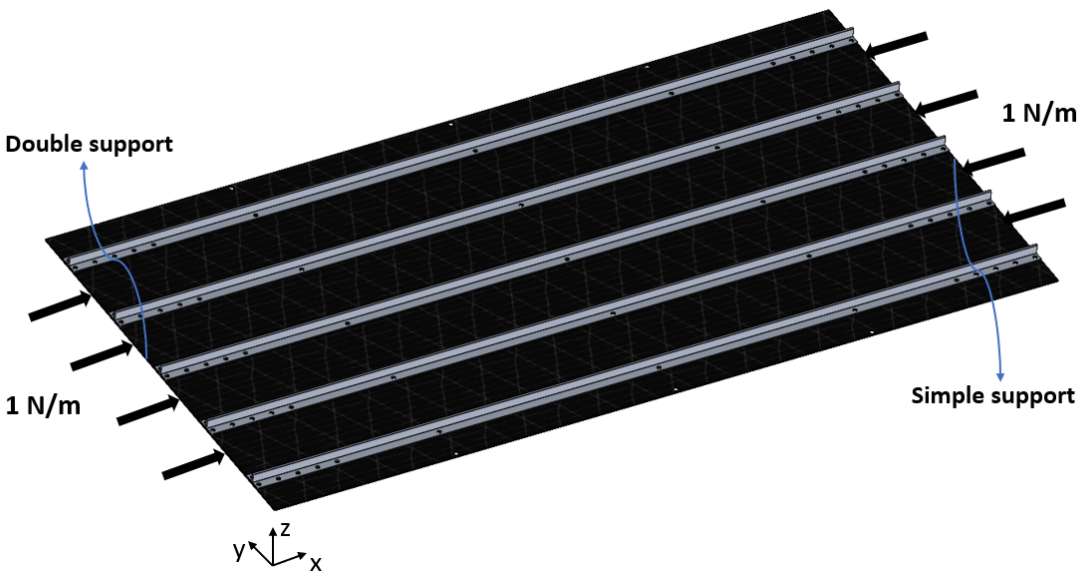

Figure 6.2 – FEM model for the critical buckling load prediction.

Regarding the boundary conditions, the Ox and Oz displacements are constrained at the edge $x = 0$ and there is not Oz displacement for $x = 2000$ mm. In order for the model to give directly the values of the critical buckling load, a unit load per unit length was assigned to those referred edges. Moreover, two additional constraints were artificially specified to the FEM model run the eigenvalue solver. In order to do not have rigid body motions along $0y$, two points characterised by their coordinates (0,0,0) and (2000,0,0) were restricted in their movements through the Oy axis. Then, a buckling step was created, using the subspace eigensolver and 5 eigenvalues were requested, that is, the first 5 buckling loads.

6.1 Design of experiments

The UDM was implemented using the tables already used in previous sections, $L_{27}(27^{11})$, Tables 5.15 and 5.16. The first two buckling loads resulted from the eigensolver are used to train the artificial neural network. The experimental points and respective FEM values are presented in Table 6.1.

Table 6.1 – Experimental points for the optimization of P_{crit}, having the plies orientations and thicknesses as design variables.

Point	θ_1 /rad	θ_2 /rad	θ_3 /rad	h_1 /mm	h_2 /mm	h_3 /mm	$P_{crit,1}$ /N · m^{-1}	$P_{crit,2}$ /N · m^{-1}
1	0	0.181246	0.362491	0.238462	0.273077	0.307692	37642	61549
2	0.060415	0.422907	0.785398	0.388462	0.146154	0.215385	38492	60920
3	0.120830	0.664566	1.208305	0.226923	0.330769	0.123077	59345	63872
4	0.181246	0.906229	0.181246	0.376923	0.203846	0.342308	47086	61437
5	0.241661	1.147890	0.422907	0.215385	0.388462	0.25	48536	60006
6	0.302076	1.389551	0.845813	0.365385	0.261538	0.157692	52915	59860
7	0.362491	0.181246	1.268720	0.203846	0.134615	0.376923	58966	68555
8	0.422907	0.241661	0.060415	0.353846	0.319231	0.284615	36941	60929
9	0.483322	0.483322	0.483322	0.192308	0.192308	0.192308	23952	59715
10	0.543737	0.724983	0.906229	0.342308	0.376923	0.1	21560	57807
11	0.604152	0.966644	1.329135	0.180769	0.25	0.319231	57083	69774
12	0.664568	1.208305	0.120830	0.330769	0.123077	0.226923	35293	59411
13	0.724983	1.449966	0.543737	0.169231	0.307692	0.134615	54082	58589
14	0.785398	0.060415	0.966644	0.319231	0.180769	0.353846	38204	57821
15	0.845813	0.302076	1.389551	0.157692	0.365385	0.261538	58243	67200
16	0.906229	0.543737	0.181246	0.307692	0.238461	0.169231	33063	58495
17	0.966644	0.785398	0.604152	0.146154	0.111538	0.388461	23847	57760
18	1.027059	1.027059	1.027059	0.296154	0.296154	0.296153	45753	54783
19	1.087474	1.268720	1.449966	0.134615	0.169231	0.203846	57150	71242
20	1.147890	1.510381	0.241661	0.284615	0.353846	0.111538	57095	64115
21	1.208305	0.120830	0.664568	0.123077	0.226923	0.330769	40000	59018
22	1.268720	0.362491	1.087474	0.273077	0.1	0.238461	56438	60642
23	1.329135	0.604152	1.510381	0.111538	0.284615	0.146153	58049	69841
24	1.389551	0.845813	0.302076	0.261538	0.157692	0.365385	53862	58805
25	1.449966	1.087474	0.724983	0.1	0.342308	0.273077	49343	57216
26	1.510381	1.329135	1.147890	0.25	0.215385	0.180769	55799	64923
27	1.570796	1.570796	1.570796	0.4	0.4	0.4	52363	62593

The distribution of P_{crit} throughout the experimental points domain is illustrated below, Figure 6.3. In opposite with what happened to the other two studied problems, see Figures 5.8 and 5.18, here the model that fits the represented data is more unpredictable.

Then, the basic steps of the ANN learning procedure and optimization phase are presented and discussed. The effect of the several genetic-based parameters on the obtained results is also studied.

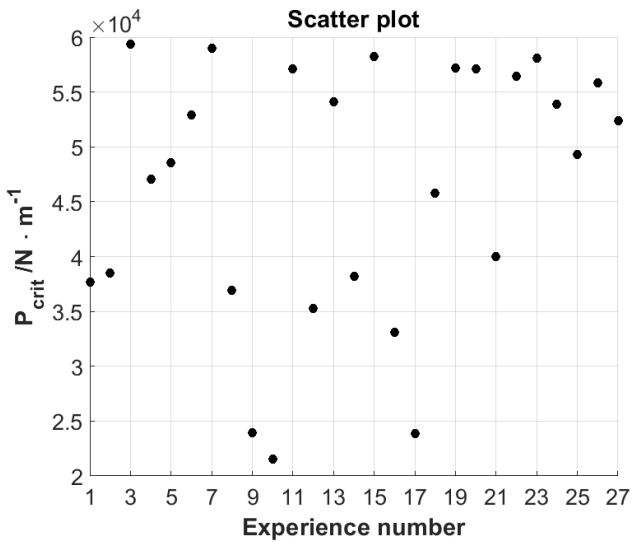

Figure 6.3 – Scatter plot of P_{crit}.

6.2 ANN learning procedure

The first stage of the optimization procedure consists in the achievement of the best ANN's configuration to predict the output values necessary for the fitness assessment in the second phase. The data presented in Table 6.1 was used as input and output of the artificial neural network. Two buckling loads are used to train the network in order to obtain the most accurate model representative of the problem under analysis. After analysing thoroughly the influence of the several genetic-based parameters and ANN's main architecture, the best configuration regarding the maximisation of the following fitness function, expression 6.1, was achieved:

$$Maximise \;\; FIT^1 = 5 \cdot 10^5 - (10 \cdot RMSE + 350000 \cdot RE). \tag{6.1}$$

Firstly, it was considered just one hidden layer and, after a tuning process (trial and error), the number of neurons in that layer was set to 5. Therefore, the following ANN's configuration was designed: 6-5-2. In order to avoid numerical error propagation throughout the network, the input data was again normalised between 0.01 and 0.99 and the output one between 0 and 1. A binary coding mechanism with 4 digits was used to code the synaptic weights and biases, design variables of the ANN-configuration optimization. The Gaussian function was established as activation function at the hidden layer (see equation 2.3), with c=50000 and $\kappa = \sqrt{110000000}$. The range of values for the weights at the connection between the input and hidden layer was fixed to [0,70000], whereas the interval [0,105000] was established for the other interconnection. The number of variables at this first stage is given by

$$(INP+1) \cdot INT + (INT+1) \cdot OUT = (6+1) \cdot 5 + (5+1) \cdot 2 = 47. \tag{6.2}$$

A population with 21 individuals was chosen by an iterative process for the implementation

of this first optimization procedure, $\mathbf{GA}^{(1)}$, with 7 individuals belonging to the elite group and 3 susceptible to mutation. The diversity control is performed variable by variable, that is, it is a phenotype-based procedure, specifying that a certain individual is removed from the population if it has the same genotype regarding at least 34 of the 47 variables, comparing with another one selected from the population. The ANN learning procedure ends up when the number of generations reaches 30000. One more time, an arrangement between the minimum values for the absolute and relative errors and the achievement of a balanced model was taken into account in the designing and choice of all these parameters. In the end of the evolution process, an absolute error of 1047.77 $\mathrm{N \cdot m^{-1}}$ and a relative error of 3.0773 % were obtained. The plot of the evolution of these errors throughout the generations can be visualised in Figures 6.4 and 6.5.

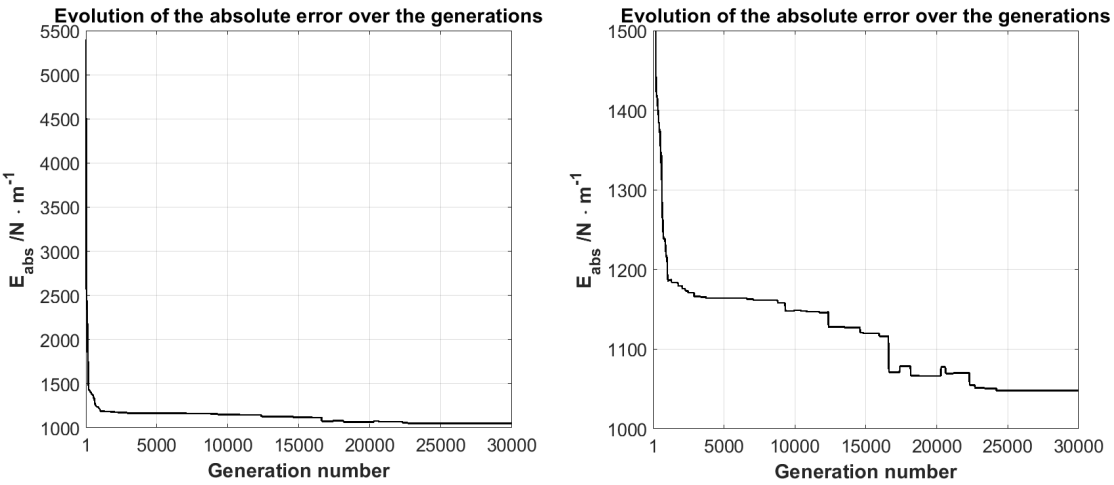

(a) Range: 5399.34 - 1047.77 /$\mathrm{N \cdot m^{-1}}$

(b) Amplification

Figure 6.4 – Evolution of the ANN's absolute error over the generations, created to predict P_{crit}, having the plies orientations and thicknesses as design variables.

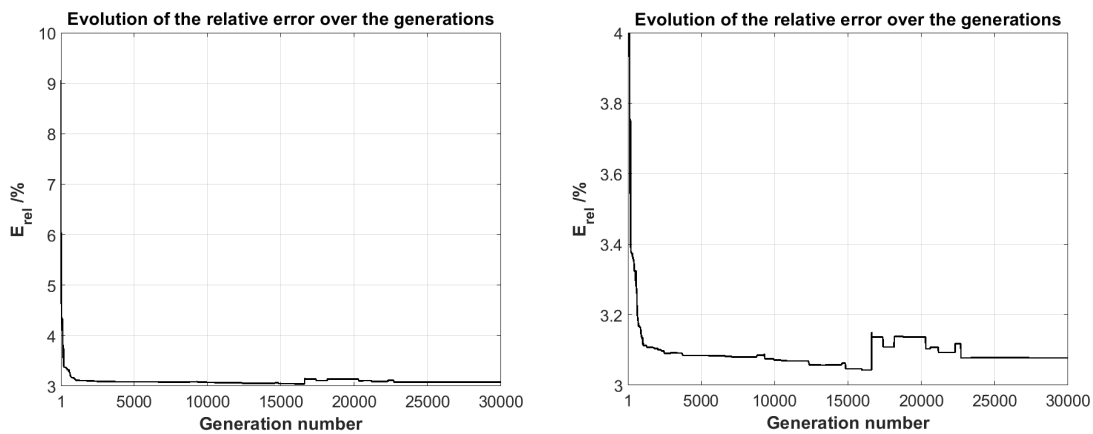

(a) Range: 9.0584 - 3.0773 %

(b) Amplification

Figure 6.5 – Evolution of the ANN's relative error over the generations, created to predict P_{crit}, having the plies orientations and thicknesses as design variables.

The absolute error ranges from 5399.34 to 1047.77 $\mathrm{N \cdot m^{-1}}$, whereas the relative error fluctuates from 9.0584 to 3.0773 %. Both error's measures converge to a certain value around the 23000-generation.

Training dataset

Table 6.2 – Comparison between the ANN and FEM results for the training dataset of the ANN created to predict P_1, having the plies orientations and thicknesses as design variables.

Experimental point	$P_{1,ANN}$ /$\mathrm{N \cdot m^{-1}}$	$P_{1,FEM}$ /$\mathrm{N \cdot m^{-1}}$	**Experimental point**	$P_{1,ANN}$ /$\mathrm{N \cdot m^{-1}}$	$P_{1,FEM}$ /$\mathrm{N \cdot m^{-1}}$
1	61164	37642	15	53746	58243
2	45589	38492	16	47799	33063
3	54305	59345	17	34967	23847
4	40213	47086	18	51605	45753
5	41847	48536	19	55315	57150
6	49703	52915	20	58751	57095
7	53889	58966	21	40279	40000
8	42474	36941	22	49269	56438
9	34887	23952	23	55366	58049
10	51773	21560	24	30304	53862
11	54054	57083	25	46412	49343
12	39727	35293	26	53172	55799
13	42920	54082	27	47334	52363
14	50243	38204			

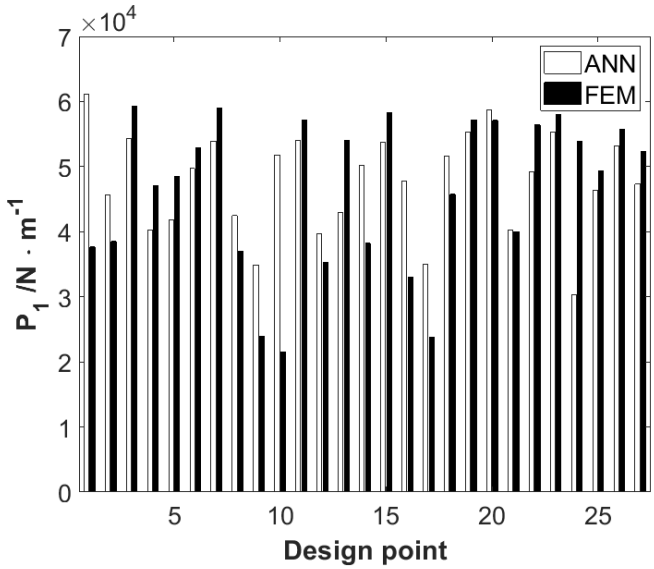

Figure 6.6 – Comparison between the ANN and FEM results for the training dataset of the ANN created to predict P_1, having the plies orientations and thicknesses as design variables.

Table 6.3 – Comparison between the ANN and FEM results for the training dataset of the ANN created to predict P_2, having the plies orientations and thicknesses as design variables.

Experimental point	$P_{2,ANN}$ /N · m^{-1}	$P_{2,FEM}$ /N · m^{-1}	**Experimental point**	$P_{2,ANN}$ /N · m^{-1}	$P_{2,FEM}$ /N · m^{-1}
1	69939	61549	15	77256	67200
2	68449	60920	16	45394	58495
3	80297	63872	17	51441	57760
4	60308	61437	18	75624	54783
5	65107	60006	19	82908	71242
6	75150	59860	20	60922	64115
7	80520	68555	21	60059	59018
8	52304	60929	22	72747	60642
9	49560	59715	23	82099	69841
10	76547	57807	24	45830	58805
11	79326	69774	25	71596	57216
12	36979	59411	26	79921	64923
13	65483	58589	27	61210	62593
14	76214	57821			

Here, the differences between the FEM and ANN predictions are more expectable and visible (see Figure 6.6), mainly due to the higher values correspondent to the buckling loads coupled with a bigger variation between their limit values. Therefore, a balanced model was tried to reach, as a compromise between underfitting and overfitting phenomena.

In relation to the following configuration which corresponds to the lowest values of the absolute and relative errors:

- 6-5-2 (five hidden nodes);
- 0.01-0.99 and 0-1 (normalisation range of the input and output variables, respectively);
- 4 bits for binary coding, 0-105000 as the suitable domain for the variables at the exterior interconnection, sigmoidal function with $\beta_{sig} = 1.5$ as activation function at the hidden layer, $LIMDIF$=34;
- $N_{pop} = 21$, % elite=33 %, % mutation=10 % and N_{gen}=30000.

Table 6.4 – Influence of the number of hidden nodes on the absolute and relative errors of the ANN learning procedure.

No. hidden nodes	E_{abs} /N · m^{-1}	E_{rel} /%
4	936.71	2.59
5	623.48	1.59
6	679.17	1.96
7	709.61	1.97

From Table 6.4, one more time the increase on ANN's complexity does not mean that better results concerning the different measures of the error are obtained due to, sometimes, oversaturation.

Taking into account the range of values that the first two buckling loads take, the allowable domain for the variables at the exterior interconnection was successively increased, Table 6.5, in order to perceive its influence upon the obtained results.

Table 6.5 – Influence of the range of weights at the hidden-output interconnection on the absolute and relative errors of the ANN learning procedure.

Output range	$\mathbf{E}_{abs}$ /N $\cdot$ m^{-1}	$\mathbf{E}_{rel}$ /%
0 to 30000	768	2.17
0 to 35000	654	1.69
0 to 40000	690	1.83
0 to 50000	691	1.87
0 to 60000	705	1.84
0 to 70000	792	1.86
0 to 80000	686	1.84
0 to 90000	794	2.15
0 to 100000	738	1.81
0 to 105000	623	1.59
0 to 110000	636	1.60
0 to 115000	660	2.05
0 to 120000	606	1.65
0 to 125000	670	1.57
0 to 130000	589	1.79
0 to 140000	767	2.30
0 to 150000	661	1.81
0 to 200000	812	2.31

The chosen interval is the one that corresponds to the lowest conjugation of the absolute and relative errors. However, the variation of the output range is more important for the performance of the second genetic algorithm, since it is directly related to the value provided by the optimised network.

Table 6.6 – Influence of the population's dimension on the absolute and relative errors of the ANN learning procedure.

$\mathbf{N}_{pop}$	$\mathbf{E}_{abs}$ /N $\cdot$ m^{-1}	$\mathbf{E}_{rel}$ /%
15	714	2.00
18	679	1.96
21	623	1.59
24	710	1.97

The increase on the population's dimension, see Table 6.6, did not correspond to the lowest error values, which allows to establish a balance point regarding the computational effort.

Table 6.7 – Influence of the mechanism of diversity control on the absolute and relative errors of the ANN learning procedure.

LIMDIF	$\mathbf{E}_{abs}$ /$\mathrm{N \cdot m^{-1}}$	$\mathbf{E}_{rel}$ /%
30	623	1.59
32	781	2.44
34	623	1.59
36	723	2.11
38	759	2.15

From the variation of the mechanism of diversity control, namely the parameter *LIMDIF*, see Table 6.7, none conclusions might be drawn due to the several observed fluctuations between consecutive values of that variable.

The three ANN design improvements discussed suggest that the Gaussian function is the one that better fits nonlinear and unknown data, despite the fact that using it results in higher absolute and relative errors between ANN and FEM predictions. For data with a superior magnitude order, which corresponds to this case, this activation function also performs well in the second optimization phase, which was a problem for the optimization of the airplane wing representative structure for vibration.

6.3 Optimization of the layers' orientations and thicknesses

The objective of the implementation of this second genetic algorithm, $\mathbf{GA}^{(2)}$, is to achieve the best laminate configuration, taking into account the design variables, which corresponds to the higher critical buckling load and, at the same time, minimum weight, under pre-specified constraints. Therefore, a multi-objective optimization procedure will be approached and developed. Particularly, in order to simplify this strategy, the linear aggregation method is used (see equation 2.22):

The second stage consists in the following optimization problem,

$$Maximise \;\; FIT^{(2)} = \sum_{i=1}^{n} \mu_i f_i(\mathbf{x}) - \sum_{j=1}^{N} \alpha_j \Phi_j(\mathbf{x}), \tag{6.3}$$

wherein μ_i corresponds to each objective's weight, f_i to each particular objective function, $\mathbf{x}$ to the vector of design variables to optimise, α_j weights each constraint and Φ_j regards a particular constraint. Moreover, if the objectives have different orders of magnitude, they must be multiplied by a certain parameter which ensures that each objective contributes in a equitable way for the fitness function assessment (normalisation). The constraints related to this particular problem were directly imposed, again, on the range of values suitable for each design variable. Therefore,

the fitness function expression was set to

$$Maximise \;\; FIT^{(2)} = 0.5 \cdot OUT_{ANN} + 0.5 \cdot [-100000 \cdot (h_1 + h_2 + h_3)] - \sum_{j=1}^{N} \alpha_j \Phi_j(\mathbf{x}). \tag{6.4}$$

The two objectives were equally weighted and the one regarding the structure's weight can be seen as an additional constraint as well. As referred in Section 2.6, for this type of multi-objective process, there is only one final solution and not a front of Pareto.

The following constraints were considered:

- balanced stacking sequence, that is, the same number of $-\theta$ and θ plies; and symmetric laminate about the midplane, in order to avoid shear-extension coupling (A_{16}=A_{26}=0) and extension-bending coupling (B_{ij}=0) (see Section 3.2). Those constraints arose from the design provided by the Cardiff School of Engineering (see Figure 5.5);

- contiguity constraint: in order to reduce matrix damage propagation up to a certain thickness, no more than 4 plies of the same orientation must be stacked together. This constraint was enforced by avoiding $\theta_3 = 0$;

- homogeneity constraint: each pair of $+\theta/-\theta$ plies should be located as closely as possible, aiming to minimise the bending-twisting coupling (D_{16}, D_{26}) and to improve the strength behaviour. This constraint is also verified by the initial provided stacking sequence design;

- the outer plies of the skin should always contain at least one set of +/- 45° for damage tolerance requirements and to improve the composite laminate behaviour under in-plane compressive loads [83, 106–108];

- strength constraint: this constraint is used to ensure that damage, either fibre breaking or matrix rupture, does not appear before buckling, not only because damage might lead to the structure's failure before buckling, but also to take damage into account. It was thought to enforce this restriction using the *Tsai-Hill* criteria, due to its conservative nature [2, 128–130]. Ply rupture occurs if

$$\left(\frac{\sigma_1}{X}\right)^2 + \left(\frac{\sigma_2}{Y}\right)^2 - \left(\frac{1}{X^2} + \frac{1}{Y^2}\right)\sigma_1\sigma_2 + \left(\frac{\sigma_6}{S}\right)^2 \geq 1, \tag{6.5}$$

  wherein X, Y and S correspond to the tensile, compressive and shear strengths, respectively, and σ_1, σ_2 and σ_6 to the normal and shear stresses with respect to the material axis system. The failure mechanism of composite materials is much more complex than that related to the isotropic ones due to their intrinsic structural and material complexity. A failure of a certain ply induces the redistribution of stresses along the remaining ones. The lamina failure modes could be fibre dominant failure, matrix dominant failure or interface dominant failure. The several failure criteria regards the first ply failure in order to ensure high design's reliability. If the stresses of the weakest lamina exceeds the allowable stress, it fails. There are several

criteria regarding this design problem, such as the maximum stress theory, in which the stresses acting on a lamina are transformed into normal and shear stresses in the local axes and the failure is predicted in a certain ply if any of the normal or shear stresses in the local axes of a lamina is equal to or exceeds the corresponding ultimate strength; the maximum strain theory, wherein failure is predicted in a lamina, if any of the normal or shearing strains in the local axes of a lamina is equal or exceed the corresponding ultimate strains of the unidirectional lamina; the *Hoffman*'s criteria; the *Tsai-Wu* criteria, which is based on the total strain energy failure theory of *Beltrami* and is more general than the *Tsai-Hill* criteria, because it distinguishes the compressive and tensile strengths of a lamina and the components of its failure condition may be calculated using the five strength parameters of a unidirectional lamina except one which is obtained experimentally by knowing a biaxial stress at which the lamina fails; or the *Tsai-Hill* criteria, based on the distortion energy failure theory of *Von Mises* applied to anisotropic materials [2, 128–130].

The *Hoffman*'s, *Tsai-Wu* and *Tsai-Hill* criterias are based on the following general polynomial and tensorial criteria

$$F_i \cdot \sigma_i + F_{ij} \cdot \sigma_i \cdot \sigma_j + F_{ijk} \cdot \sigma_i \cdot \sigma_j \cdot \sigma_k \geq 1, \tag{6.6}$$

wherein the F_i, F_{ij} and F_{ijk} (i, j, k=1, ..., 6) are related to the lamina strengths in the principal directions and differ according to the selected lamina failure theory [130].

It was performed a FEM simulation for the highest critical buckling load and corresponding stacking sequence among the experimental points, aiming to perceive if the explicit inclusion of this constraint is really necessary, because the optimised value for P_{crit} is certainly placed around that value. Taking into account the structure's mechanical properties and the results from the simulation:

- X= 2000 MPa, Y= 200 MPa and S= 70 MPa;
- FEM simulation: σ_1= 519 MPa, σ_2= 50 MPa, and σ_6= 50 MPa.

Applying the *Tsai-Hill* criteria, there is no weakest ply failure by a large safety margin. Therefore, it was decided to not include the strength constraint, because it would increase the computational time quite extensively due to the necessity to run the FEM model for each population's generation of $\mathbf{GA}^{(2)}$. An alternative would be the construction of an additional artificial neural network to predict the necessary strength values based on another 27 experimental points. However, the additional development time would not compensate. Moreover, the already constructed ANN could be a possibility, integrating these variables as output variables as well. As a consequence, the absolute and relative errors for the prediction of the buckling loads would increase, which would not be acceptable.

The second optimization phase was performed using the ANN's configuration obtained from the first optimization procedure, $\mathbf{P}^{opt}_{ANN}$, and the following genetic parameters: N_{pop}=21; $\%_{elite}$=33

%; $\%_{mutation}$=10 %; N_{gen}=15000. During the evolution process, a certain individual is removed from the population if it has the same genotype for at least 4 out of 6 variables, comparing with another one from the population. The design variables can take a value from the respective intervals: θ_1=±0.7854 rad; $0 \leq \theta_2 \leq 1.5708$ rad; $0.1745 \leq \theta_3 \leq 1.5708$ rad; $0.1 \leq h_1 \leq 0.4$ mm; $0.1 \leq h_2 \leq 0.4$ mm and $0.1 \leq h_3 \leq 0.4$ mm.

The optimised configuration is shown in Table 6.8:

Table 6.8 – Optimised laminate configuration for buckling, considering the layers orientations and thicknesses as design variables.

θ_1 /rad	θ_2 /rad	θ_3 /rad	h_1 /mm	h_2 /mm	h_3 /mm	$FIT^{(2)}$	$P_{1,ANN}$ /N · m^{-1}	$P_{1,FEM}$ /N · m^{-1}
0.7854	0	1.5708	0.1	0.1	0.1	15332.37	60665	60002

According to expression 6.4 and to the obtained values for the plies thicknesses, the required value, maximised critical buckling load, can be calculated from the fitness function value.

The resulted laminate configuration satisfies all constraints and the maximised value is higher than those obtained for the experimental data. Furthermore, the ANN and FEM results are in clear agreement (relative error of 1.1%), which validates the developed optimization framework. The evolution of the fitness function value over the generations is plotted in the figure below, Figure 6.7.

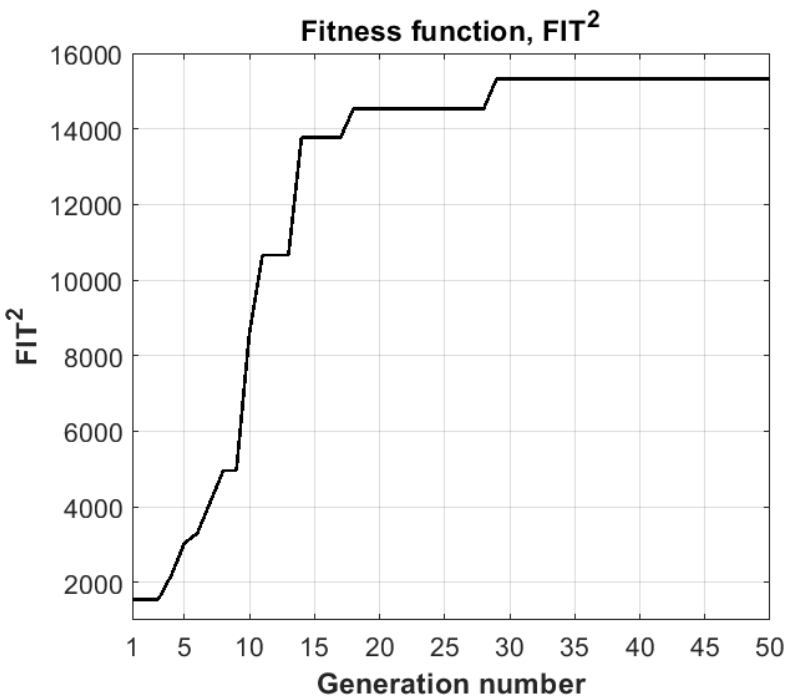

Figure 6.7 – Evolution of the maximised critical buckling load over the generations, having the plies orientations and thicknesses as design variables.

The fitness function value evolves from 1547 to 15332, which is a meaningful improvement.

Due to the low number of variables involved, the algorithm stops evolving since the 28-generation. Overall, there were seven upgrades.

From the intensive study regarding the variation of all genetic-based and ANN's parameters, another "optimal" configuration can be considered. Its composition is exactly the one described above as the reference configuration, that is, the one that corresponds to the lowest values for the absolute and relative errors (see end of Section 6.2). The result of the second optimization phase is presented in the following table:

Table 6.9 – Optimised laminate configuration for buckling considering the other well fitted configuration.

θ_1 /rad	θ_2 /rad	θ_3 /rad	h_1 /mm	h_2 /mm	h_3 /mm	FIT^2	$P_{1,ANN}$ /N $\cdot$ m^{-1}	$P_{1,FEM}$ /N $\cdot$ m^{-1}
0.7854	0.3146	1.5708	0.1	0.1	0.1	14349.32	58699	59857

Only the intermediate layer's orientation angle differs between the two optimized arrangements. The relative error between the ANN and FEM predictions is, for this alternative configuration, 1.9%.

6.4 *Sobol* indices

Here, the relative importance of each design variable on the variance of the critical buckling load response is calculated, again, following the procedure described in subsection 5.2.5, assuming that the input variables are independent, that is, there are no couplings between them. Taking into account the ANN's architecture and genetic parameters which led to the laminate configuration described in Table 6.8, the *Sobol* indices were accordingly obtained.

Table 6.10 – *Sobol* indices regarding the optimization of the structure for buckling, having the plies orientations and thicknesses as design variables.

$\mathbf{N}_f$	$\mathbf{N}_r$	S_2^O	S_3^O	S_4^O	S_5^O	S_6^O	$\sum_{i=2}^{6} \mathrm{S}_i^O$
5	22	0.0021	0.2545	0.0226	0.5996	0.2019	1.0807
5	23	0.0075	0.2297	0.0511	0.5981	0.1341	1.0205
5	24	0.0016	0.3397	0.0703	0.7191	0.1234	1.2541
5	25	0.0081	0.2363	0.0139	0.5876	0.1511	0.9970
5	26	0.0069	0.2567	0.0452	0.4130	0.2090	0.9308
5	27	0.0058	0.2046	0.0322	0.5904	0.2319	1.0649
5	28	0.0023	0.3679	0.0796	0.4443	0.2599	1.1541
		0.0049	0.2699	0.0450	0.5646	0.1873	1.0717

The dimension of the vector $\boldsymbol{\lambda}_{fix}$ was set to 5 and N_r ranged from 22 to 28. These values were selected, because they correspond to the lowest grade of coupling between the design variables, as a result of an exhaustive study. The following average *Sobol* indices were obtained: $\bar{S}_2^O$=0.0049;

$\bar{S}_3^O$=0.2699; $\bar{S}_4^O$=0.0450; $\bar{S}_5^O$=0.5646 and $\bar{S}_6^O$=0.1973. Their sum indicates the existence of a small coupling between the input variables.

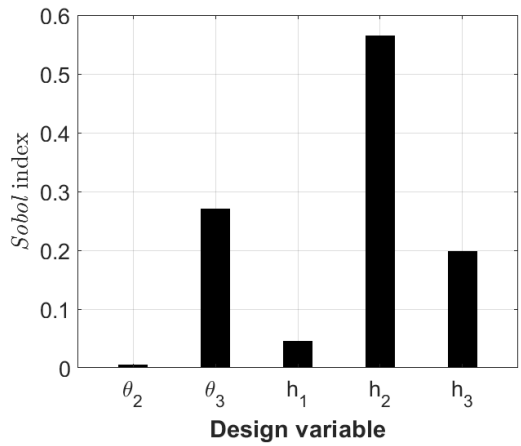

Figure 6.8 – *Sobol* indices corresponding to the P_{crit} maximisation, having the plies orientations and thicknesses as design variables.

The uncertainty about the impact of the position of a certain layer along the composite panel is more evident for the critical buckling load maximisation. From Figure 6.8, the preponderance of the design variables of the innermost layer (θ_3 and h_3) is similar to the contribution of only the thickness variable of the intermediate layer. The outermost layer, with only h_1 as design variable due to the θ_1 prescription, has no significant contribution for the variance of the critical buckling load response.

6.5 Conclusions and final remarks

In this chapter, a multi-objective optimization procedure was developed, which involved the maximisation of the critical buckling load and, at the same time, the minimisation of the stiffened composite panel weight. The implemented artificial neural network predicts the P_{crit} values with a relative error around 3.1%, for the selected configuration. An aggregation method was used in the second genetic algorithm to consider the two objectives in the same scalar function. Moreover, the strength constraint was not explicitly taken into account, because it does not compromise the obtained results by a large safety margin. The following panel's configuration was achieved (θ_1=0.7854 rad, θ_2=0 rad and θ_3=1.5708 rad; h_1=0.1 mm, h_2=0.1 mm and h_3=0.1 mm). The thickness variables assume the lowest value, which enables to conclude about the algorithm's assertiveness. A relative error of 1.1% was obtained between the results from the optimised ANN and finite element model. The maximised P_{crit} value is again higher than those observed among the experimental points (Figure 6.3). The thickness variable of the intermediate layer, h_2, has the bigger influence on the variance of the output response.

Chapter 7

Conclusions and Future Work

7.1 Conclusions

In this dissertation, the airplane wing representative structure is subjected to an optimization procedure in order to maximise its fundamental natural frequency and critical buckling load. The overall structure is composed by two composite panels reinforced by longitudinal and transversal aluminium stiffeners. The connections are ensured by bolts and adhesive joints.

Due to the considered design variables, plies' orientations and thicknesses, and taking into account that the two panels are similar, only a substructure of the representative one provided by the Cardiff School of Engineering was considered. Then, two finite element models were created in order to predict the natural frequencies and buckling loads necessary for the optimization framework. An analytical model based on the *Rayleigh-Ritz* method was approached with the aim of establishing an alternative procedure capable of obtaining the natural frequencies of the stiffened panel. The genetic algorithm was used both for optimising the artificial neural network created for the prediction of the output variables and to achieve the optimised values of the mechanical variables under analysis. This type of evolutionary algorithm was chosen due to the ease of implementation and the lower probability of finding local minima in comparison with the gradient/based optimization algorithms.

Firstly, the structure was optimised with regard to its fundamental natural frequency. Composite structures are often optimised for vibration by either maximising the ω_1 value or the gap between two successive natural frequencies. Therefore, there is sufficient margin for the structure's excitation without being close to the natural frequencies. The amplitude of vibration is proportional to the dynamic amplification factor $\left(\mu = \frac{1}{\sqrt{(1-\beta^2)+(2\xi\beta)^2}}\right)$ in a single degree of freedom system with a damping ratio given by ξ, which increases as $\beta = \frac{\omega}{\omega_n} \rightarrow 1$, particularly for lower-damping structures. Considering only the plies' orientations as design variables, the maximised value was not as accurate as the relative and absolute errors obtained for the establishment of the relationship between the input variables and the output response. The lower number of variables induces both ease of data fitness and premature convergence of the maximised output value. However, similar results were obtained by FEM and ANN for the same composite optimised configu-

ration. The same procedure was accomplished adding the thicknesses as design variables, which augmented the algorithm's complexity and allowed to obtain good results both for the ANN's training and for the second optimization phase. The obtained value is even superior to the ones observed among the experimental points which, according to the Uniform Design Method, are uniformly scattered along the domain, representing it with minimum discrepancy. The optimization procedure is further validated by the fundamental natural frequency resulted from the finite element method. Obviously, the absolute and relative errors in the data representation are bigger than those relative with the problem described above, due to the increase on the input variables, which increases the domain to scan.

Lastly, using the linear aggregation method, the same composite structure was optimised with respect to its critical buckling load and weight. The buckling phenomena generates unpredictable stiffness variations, which compromises the structure's safety and even the people around. It was obtained, again, a higher value for the optimised configuration in comparison with the training dataset.

This dissertation allows to acquire a general knowledge about the different optimization algorithms applicable to composite structures, particularly the genetic algorithm, to understand their main advantages and drawbacks in comparison with the more conventional ones, gradient-based optimization methods, and to perceive their importance upon the design of complex and multidisciplinary structures. Besides that, the understanding and further development of the finite element model already created was an excellent introduction to the Abaqus® software, analysing their main functionalities and developing new skills that enable the creation of more complex models.

7.2 Further Work

In order to farther validate the obtained results or even improve them, several additional studies might be performed:

- Consider the effects of the bolted and adhesive connections on the obtained results, since they are stress-concentration spots;
- Take into account the delamination effect on the modes of vibration and critical buckling loads, because it may cause a significant reduction both in the compressive load-carrying capacity and bending stiffness of the structure;
- Compare the obtained results with others evolutionary algorithms and gradient-based methods, highlighting the advantages and drawbacks of each one of them;
- Add more design variables to the structure, such as the dimensions, shape, number and position of the stiffeners;
- Due to the prescription of the orientation of the outermost layer (size constraint), redo the optimization procedures, considering one less design variable for the training process of the ANN;

- Consider the curvilinear fibres usage in order to better tailor the composite stiffness and strength to the optimal direction;
- Increase the genetic algorithm's complexity, adding more constraints to the system under analysis with the aim of better representing the mechanical behaviour of the composite structure;
- Use other techniques to select the training dataset and compare the obtained results;
- Multi-objective optimization using the dominance concept.

References

[1] Baker A. Composite Materials for Aircraft Structures. AIAA Education Series; American Institute of Aeronautics & Astronautics; 2004. ISBN 9781600860409.

[2] Kaw A. Mechanics of Composite Materials. Mechanical and Aerospace Engineering Series; CRC Press; 2005. ISBN 9781420058291.

[3] Campbell F. Structural Composite Materials. ASM International; 2010. ISBN 9781615031405.

[4] Vinson JR, Sierakowski RL. Joining of Composite Material Structures; chap. 8. Dordrecht: Springer Netherlands. ISBN 978-0-306-48414-8; 2008, p. 333–359. URL: https://doi.org/10.1007/0-306-48414-5_8. doi:10.1007/0-306-48414-5_8.

[5] Beatriz Henriques . Static and Dynamic Analysis of an Airplane Wing Representative Structure for Damage Detection. Master's thesis; Faculty of Engineering of University of Porto; Porto; 2021.

[6] Mouritz AP. Nondestructive inspection and structural health monitoring of aerospace materials; chap. 23. Woodhead Publishing. ISBN 978-1-85573-946-8; 2012, p. 534–557. URL: https://www.sciencedirect.com/science/article/pii/B9781855739468500236. doi:https://doi.org/10.1533/9780857095152.534.

[7] Senthil K, Arockiarajan A, Palaninathan R, Santhosh B, Usha K. Defects in composite structures: Its effects and prediction methods – a comprehensive review. Composite Structures 2013;106:139–149. URL: https://www.sciencedirect.com/science/article/pii/S0263822313002845. doi:https://doi.org/10.1016/j.compstruct.2013.06.008.

[8] Dwivedi SK, Vishwakarma M, Soni P. Advances and researches on non destructive testing: A review. Materials Today: Proceedings 2018;5:3690–3698. URL: https://www.sciencedirect.com/science/article/pii/S2214785317328936. doi:https://doi.org/10.1016/j.matpr.2017.11.620.

[9] Giurgiutiu V. Structural health monitoring (SHM) of aerospace composites; chap. 16. Woodhead Publishing. ISBN 978-0-85709-523-7; 2015, p. 449–507. URL: https://www.sciencedirect.com/science/article/pii/B9780857095237000165. doi:https://doi.org/10.1016/B978-0-85709-523-7.00016-5.

[10] Brevault L, Balesdent M, Morio J. Aerospace System Analysis and Optimization in Uncertainty. Springer Optimization and Its Applications; Springer International Publishing; 2021. ISBN 9783030391287.

[11] Megson T. Chapter 11 - Structural Components of Aircraft. In: Megson T, editor. Introduction to Aircraft Structural Analysis. Boston: Butterworth-Heinemann. ISBN 978-1-85617-932-4; 2010, p. 351–371. URL: https://www.sciencedirect.com/science/article/pii/B9781856179324000117. doi:https://doi.org/10.1016/B978-1-85617-932-4.00011-7.

[12] Megson T. Chapter 23 - Wings. In: Megson T, editor. Aircraft Structures for Engineering Students (Fifth Edition); fifth edition ed. Boston: Butterworth-Heinemann. ISBN 978-0-08-096905-3; 2013, p. 653–686. URL: https://www.sciencedirect.com/science/article/pii/B9780080969053000395. doi:https://doi.org/10.1016/B978-0-08-096905-3.00039-5.

[13] Megson T. Chapter 28 - Wing problems. In: Megson T, editor. Aircraft Structures for Engineering Students (Fifth Edition); fifth edition ed. Boston: Butterworth-Heinemann. ISBN 978-0-08-096905-3; 2013, p. 801–823. URL: https://www.sciencedirect.com/science/article/pii/B9780080969053000371. doi:https://doi.org/10.1016/B978-0-08-096905-3.00037-1.

[14] Boeing . In-flight airplane vibration and flight crew response. https://www.boeing.com/commercial/aeromagazine/aero_16/vibration_story.html; 2019. Accessed: 2022-09-20.

[15] European Cost . Cost Action CA18203 - Optimizing Design for Inspection (ODIN). https://www.cost.eu/actions/CA18203/; 2019. Accessed: 2022-04-10.

[16] Singh P, Kar A, Singh Y, Kolekar M, Tanwar S. Proceedings of ICRIC 2019: Recent Innovations in Computing. Lecture Notes in Electrical Engineering; Springer International Publishing; 2019. ISBN 9783030294069.

[17] Abdolrasol M, Hussain S, Ustun TS, Sarker M, Hannan MA, Mohamed R, Ali J, Mekhilef S, Milad A. Artificial neural networks based optimization techniques: A review. Electronics 2021;10:2689. doi:10.3390/electronics10212689.

[18] Vijay Kanade . What is machine learning? definition, types, applications, and trends for 2022. https://www.spiceworks.com/tech/artificial-intelligence/articles/what-is-ml/; 2022. Accessed: 2022-06-28.

[19] da Silva I, Spatti D, Flauzino R, Liboni L, dos Reis Alves S. Artificial Neural Networks: A Practical Course. Springer International Publishing; 2016. ISBN 9783319431628.

[20] Gupta MM, Homma N, Jin L. Static and Dynamic Neural Networks: From Fundamentals to Advanced Theory. 1st ed.; USA: John Wiley and Sons, Inc.; 2003. ISBN 0471219487.

[21] Trask, Andrew . Grokking Deep Learning. 1st ed.; USA: Manning Publications Co.; 2019. ISBN 1617293709.

[22] Zhang W, Yang G, Lin Y, Ji C, Gupta M. On Definition of Deep Learning. In: 2018 World Automation Congress (WAC). 2018, p. 1–5. doi:10.23919/WAC.2018.8430387.

[23] Chassagnon G, Vakalopolou M, Paragios N, Revel MP. Deep learning: definition and perspectives for thoracic imaging. European radiology 2020;30(4):2021—2030. URL: https://doi.org/10.1007/s00330-019-06564-3. doi:10.1007/s00330-019-06564-3.

[24] Gordan M, Abdul Razak H, Ismail Z, Ghaedi K. Recent developments in damage identification of structures using data mining. Latin American Journal of Solids and Structures 2017;14:2373–2401. doi:10.1590/1679-78254378.

[25] Zhang A, Lipton ZC, Li M, Smola AJ. Dive into Deep Learning. arXiv preprint arXiv:210611342 2021;.

[26] Yang XS. Nature-Inspired Optimization Algorithms: Second Edition. 2020. ISBN 9780128219867.

[27] Civicioglu P. Backtracking search optimization algorithm for numerical optimization problems. Applied Mathematics and Computation 2013;219(15):8121–8144. URL: https://www.sciencedirect.com/science/article/pii/S0096300313001380. doi:https://doi.org/10.1016/j.amc.2013.02.017.

[28] Kalita K, Haldar S, Chakraborty SA. A Comprehensive Review on High-Fidelity and Metamodel-Based Optimization of Composite Laminates; chap. 29. 2022, p. 3305–3340. doi:https://doi.org/10.1007/s11831-021-09699-z.

[29] António CC. Otimização de Sistemas em Engenharia: Fundamentos e algoritmos para o projeto ótimo. Engebook; 2020. ISBN 9789899017344.

[30] Özkaraca O. A Review on usage of Optimization methods in Geothermal Power Generation. Mugla Journal of Science and Technology 2018;:130–136doi:10.22531/muglajsci.437340.

[31] Yang XS. Harmony Search as a Metaheuristic Algorithm. Studies in Computational Intelligence 2010;191. doi:10.1007/978-3-642-00185-7_1.

[32] Das S, Biswas A, Dasgupta S, Abraham A. "Bacterial Foraging Optimization Algorithm: Theoretical Foundations, Analysis, and Applications"; chap. "2". "Berlin, Heidelberg": "Springer Berlin Heidelberg". ISBN "978-3-642-01085-9"; "2009", p. "23–55". URL: "https://doi.org/10.1007/978-3-642-01085-9_2". doi:"10.1007/978-3-642-01085-9_2".

[33] Poli R, Kennedy J, Blackwell T. Particle swarm optimization: An overview. Swarm Intelligence 2007;1. doi:10.1007/s11721-007-0002-0.

[34] Gao W, Liu S, Huang L. A global best artificial bee colony algorithm for global optimization. Journal of Computational and Applied Mathematics 2012;236(11):2741–2753. URL: https://www.sciencedirect.com/science/article/pii/S0377042712000246. doi:https://doi.org/10.1016/j.cam.2012.01.013.

[35] Shareef H, Ibrahim AA, Mutlag AH. Lightning search algorithm. Applied Soft Computing 2015;36:315–333. URL: https://www.sciencedirect.com/science/article/pii/S1568494615004688. doi:https://doi.org/10.1016/j.asoc.2015.07.028.

[36] Rashedi E, Nezamabadi-pour H, Saryazdi S. GSA: A Gravitational Search Algorithm. Information Sciences 2009;179(13):2232–2248. URL: https://www.sciencedirect.com/science/article/pii/S0020025509001200. doi:https://doi.org/10.1016/j.ins.2009.03.004.

[37] Krenker A, Bester J, Kos A. Introduction to the artificial neural networks. In: Suzuki K, editor. Artificial Neural Networks; chap. 1. Rijeka: IntechOpen; 2011, p. 3–18. URL: https://doi.org/10.5772/15751. doi:10.5772/15751.

[38] Sakib S, Ahmed NSS, Kabir AJ, Ahmed H. An overview of convolutional neural network: Its architecture and applications. Preprints 2018;doi:10.20944/preprints201811.0546.v4.

[39] O'Shea K, Nash R. An introduction to convolutional neural networks. 2015. URL: https://arxiv.org/abs/1511.08458. doi:10.48550/ARXIV.1511.08458.

[40] Grossberg S. Recurrent neural networks. Scholarpedia 2013;8(2):1888. doi:10.4249/scholarpedia.1888.

[41] Graves A, Fernández S, Schmidhuber J. Multi-dimensional recurrent neural networks. In: de Sá JM, Alexandre LA, Duch W, Mandic D, editors. Artificial Neural Networks – ICANN 2007. Berlin, Heidelberg: Springer Berlin Heidelberg. ISBN 978-3-540-74690-4; 2007, p. 549–558.

[42] Zhang L, Liang YZ, Jiang JH, Yu RQ, Fang KT. Uniform design applied to nonlinear multivariate calibration by ann. Analytica Chimica Acta 1998;370(1):65–77. URL: https://www.sciencedirect.com/science/article/pii/S0003267098002566. doi:https://doi.org/10.1016/S0003-2670(98)00256-6.

[43] Bishop CM. Neural networks and their applications. Review of Scientific Instruments 1994;65(6):1803–1832. URL: https://doi.org/10.1063/1.1144830. doi:10.1063/1.1144830. arXiv:https://doi.org/10.1063/1.1144830.

[44] Carson JM, Chakshu NK, Sazonov I, Nithiarasu P. Artificial intelligence approaches to predict coronary stenosis severity using non-invasive fractional flow reserve. Proceedings of the Institution of Mechanical Engineers Part H, Journal of Engineering in Medicine 2020;234:1337 – 1350.

[45] Papadrakakis M, Lagaros ND, Tsompanakis Y. Structural optimization using evolution strategies and neural networks. Computer Methods in Applied Mechanics and Engineering 1998;156(1):309–333. URL: https://www.sciencedirect.com/science/article/pii/S0045782597002156. doi:https://doi.org/10.1016/S0045-7825(97)00215-6.

[46] Tu JV. Advantages and disadvantages of using artificial neural networks versus logistic regression for predicting medical outcomes. Journal of Clinical Epidemiology 1996;49(11):1225–1231. URL: https://www.sciencedirect.com/science/article/pii/S0895435696000029. doi:https://doi.org/10.1016/S0895-4356(96)00002-9.

[47] Basheer I, Hajmeer M. Artificial neural networks: fundamentals, computing, design, and application. Journal of Microbiological Methods 2000;43(1):3–31. URL: https://www.sciencedirect.com/science/article/pii/S0167701200002013. doi:https://doi.org/10.1016/S0167-7012(00)00201-3.

[48] Draper NR, Pukelsheim F. An overview of design of experiments. Statistical Papers 1996;37(1):1–32. doi:https://doi.org/10.1007/BF02926157.

[49] Ferreira S, Bruns R, Ferreira H, Matos G, David J, Brandão G, da Silva E, Portugal L, dos Reis P, Souza A, dos Santos W. Box-Behnken design: An alternative for the optimization of analytical methods. Analytica Chimica Acta 2007;597(2):179–186. URL: https://www.sciencedirect.com/science/article/pii/S0003267007011671. doi:https://doi.org/10.1016/j.aca.2007.07.011.

[50] Zhou J, Yu X, Ding C, Wang Z, Zhou Q, Pao H, Cai W. Optimization of phenol degradation by Candida tropicalis Z-04 using Plackett-Burman design and response surface methodology. Journal of Environmental Sciences 2011;23(1):22–30. URL: https://www.sciencedirect.com/science/article/pii/S1001074210603695. doi:https://doi.org/10.1016/S1001-0742(10)60369-5.

[51] Khaw JF, Lim B, Lim LE. Optimal design of neural networks using the taguchi method. Neurocomputing 1995;7(3):225–245. URL: https://www.sciencedirect.com/science/article/pii/092523129400013I. doi:https://doi.org/10.1016/0925-2312(94)00013-I.

[52] Jadid MN, Fairbairn DR. Neural-network applications in predicting moment-curvature parameters from experimental data. Engineering Applications of Artificial Intelligence 1996;9(3):309–319. URL: https://www.sciencedirect.com/science/article/pii/0952197696000218. doi:https://doi.org/10.1016/0952-1976(96)00021-8.

[53] Lachtermacher G, Fuller JD. Back propagation in time-series forecasting. Journal of Forecasting 1995;14:381–393.

[54] Widrow B, Lehr MA. 30 years of adaptive neural networks: perceptron, Madaline, and backpropagation. Proc IEEE 1990;78:1415–1442.

[55] Amazon Machine Learning . Amazon machine learning: Model fit: Underfitting vs. overfitting. https://docs.aws.amazon.com/machine-learning/latest/dg/model-fit-underfitting-vs-overfitting.html; 2022. Accessed: 2022-06-27.

[56] Miller B, Ziemiański L. Optimization of dynamic behavior of thin-walled laminated cylindrical shells by genetic algorithms and deep neural networks supported by modal shape identification. Advances in Engineering Software 2020;147:102830. URL: https://www.sciencedirect.com/science/article/pii/S0965997820300582. doi:https://doi.org/10.1016/j.advengsoft.2020.102830.

[57] Miller B, Ziemiański L. Maximization of Eigenfrequency Gaps in a Composite Cylindrical Shell Using Genetic Algorithms and Neural Networks. Applied Sciences 2019;9(13). URL: https://www.mdpi.com/2076-3417/9/13/2754. doi:10.3390/app9132754.

[58] Honda S, Narita Y, Sasaki K. Discrete optimization for vibration design of composite plates by using lamination parameters. Advanced Composite Materials 2009;18(4):297–314. URL: https://doi.org/10.1163/156855109X434739. doi:10.1163/156855109X434739. arXiv:https://doi.org/10.1163/156855109X434739.

[59] Herencia J, Haftka R, Weaver P, Friswell M. Lay-Up Optimization of Composite Stiffened Panels Using Linear Approximations in Lamination Space. Aiaa Journal - AIAA J 2008;46:2387–2391. doi:10.2514/1.36189.

[60] Liu W, Butler R, Kim HA. Optimization of composite stiffened panels subject to compression and lateral pressure using a bi-level approach. Structural and Multidisciplinary Optimization 2007;36:235–245. doi:10.1007/s00158-007-0156-9.

[61] Abouhamze M, Shakeri M. Multi-objective stacking sequence optimization of laminated cylindrical panels using a genetic algorithm and neural networks. Composite Structures 2007;81(2):253–263. URL: https://www.sciencedirect.com/science/article/pii/S0263822306003175. doi:https://doi.org/10.1016/j.compstruct.2006.08.015.

[62] Mutra D, Reddy B, Reddy V, Surisetty S. Prediction of natural frequency of laminated composite plates using artificial neural networks. Engineering 2012;04:329–337. doi:10.4236/eng.2012.46043.

[63] Mallela UK, Upadhyay A. Buckling load prediction of laminated composite stiffened panels subjected to in-plane shear using artificial neural networks. Thin-Walled Structures 2016;102:158–164. URL: https://www.sciencedirect.com/science/article/pii/S0263823116300258. doi:https://doi.org/10.1016/j.tws.2016.01.025.

[64] Bacarreza O, Aliabadi M, Apicella A. Robust design and optimization of composite stiffened panels in post-buckling. Structural and Multidisciplinary Optimization 2014;51. doi:10.1007/s00158-014-1136-5.

[65] Wang D, Abdalla MM, Zhang W. Buckling optimization design of curved stiffeners for grid-stiffened composite structures. Composite Structures 2017;159:656–666. URL: https://www.sciencedirect.com/science/article/pii/S0263822316311813. doi:https://doi.org/10.1016/j.compstruct.2016.10.013.

[66] Ma X, Wang F, Aage N, Tian K, Hao P, Wang B. Generative design of stiffened plates based on homogenization method. Structural and Multidisciplinary Optimization 2021;64. doi:10.1007/s00158-021-03070-3.

[67] Dähne S, Werthen E. Stringer-Concept Evaluations with Multidisciplinary Gradient Based Optimization of Composite Wing Structures. 6th Aircraft Structural Design Conference 2018;URL: https://www.researchgate.net/publication/328355792_Stringer-Concept_Evaluations_with_Multidisciplinary_Gradient_Based_Optimization_of_Composite_Wing_Structures.

[68] Ding S, Li H, Su C, Yu J, Jin F. Evolutionary artificial neural networks: A review. Artificial Intelligence Review - AIR 2013;39. doi:10.1007/s10462-011-9270-6.

[69] Erzurum Cicek ZI, Kamisli Ozturk Z. Optimizing the artificial neural network parameters using a biased random key genetic algorithm for time series forecasting. Applied Soft Computing 2021;102:107091. URL: https://www.sciencedirect.com/science/article/pii/S1568494621000144. doi:https://doi.org/10.1016/j.asoc.2021.107091.

[70] Chattopadhyay S, Marik A, Pramanik R. A Brief Overview of Physics-inspired Metaheuristic Optimization Techniques. CoRR 2022;abs/2201.12810. URL: https://arxiv.org/abs/2201.12810. arXiv:2201.12810.

[71] Biswas A, Mishra K, Tiwari S, Misra A. Physics-Inspired Optimization Algorithms: A Survey. Journal of Optimization 2013;2013:16 pages. doi:10.1155/2013/438152.

[72] Todoroki A, Haftka RT. Stacking sequence optimization by a genetic algorithm with a new recessive gene like repair strategy. Composites Part B: Engineering 1998;29(3):277–285. URL: https://www.sciencedirect.com/science/article/pii/S1359836897000309. doi:https://doi.org/10.1016/S1359-8368(97)00030-9.

[73] Sivanandam S, Deepa S. Genetic Algorithms; chap. 2. Berlin, Heidelberg: Springer Berlin Heidelberg. ISBN 978-3-540-73190-0; 2008, p. 15–37. URL: https://doi.org/10.1007/978-3-540-73190-0_2. doi:10.1007/978-3-540-73190-0_2.

[74] Park CH, Lee WI, Han WS, Vautrin A. Improved genetic algorithm for multidisciplinary optimization of composite laminates. Computers and Structures 2008;86(19):1894–1903. URL: https://www.sciencedirect.com/science/article/pii/S004579490800062X. doi:https://doi.org/10.1016/j.compstruc.2008.03.001.

[75] Chehouri A, Younes R, Perron J, Ilinca A. A Constraint-Handling Technique for Genetic Algorithms using a Violation Factor. Journal of Computer Science 2016;12(7):350–362. URL: https://doi.org/10.3844%2Fjcssp.2016.350.362. doi:10.3844/jcssp.2016.350.362.

[76] Deb K. An efficient constraint handling method for genetic algorithms. Computer Methods in Applied Mechanics and Engineering 2000;186(2):311–338. URL: https://www.sciencedirect.com/science/article/pii/S0045782599003898. doi:https://doi.org/10.1016/S0045-7825(99)00389-8.

[77] Mirjalili S. Genetic Algorithm; chap. 4. Cham: Springer International Publishing. ISBN 978-3-319-93025-1; 2019, p. 43–55. URL: https://doi.org/10.1007/978-3-319-93025-1_4. doi:10.1007/978-3-319-93025-1_4.

[78] Shukla A, Pandey HM, Mehrotra D. Comparative review of selection techniques in genetic algorithm. In: 2015 International Conference on Futuristic Trends on Computational Analysis and Knowledge Management (ABLAZE). 2015, p. 515–519. doi:10.1109/ABLAZE.2015.7154916.

[79] Soni N, Kumar T. Study of various mutation operators in genetic algorithms. 2014. URL: http://www.ijcsit.com/docs/Volume%205/vol5issue03/ijcsit20140503404.pdf.

[80] Safe M, Carballido J, Ponzoni I, Brignole N. "On Stopping Criteria for Genetic Algorithms". In: Bazzan ALC, Labidi S, editors. "Advances in Artificial Intelligence – SBIA 2004". Berlin, Heidelberg: Springer Berlin Heidelberg. ISBN 978-3-540-28645-5; 2004, p. 405–413.

[81] Liu B, Haftka R, Akgun M. Composite wing structural optimization using genetic algorithms and response surfaces. 7th AIAA/USAF/NASA/ISSMO Symposium on Multidisciplinary Analysis and Optimization 1998;URL: https://arc.aiaa.org/doi/abs/10.2514/6.1998-4854. doi:10.2514/6.1998-4854. arXiv:https://arc.aiaa.org/doi/pdf/10.2514/6.1998-4854.

[82] Narita Y, Robinson P. Maximizing the fundamental frequency of laminated cylindrical panels using layerwise optimization. International Journal of Mechanical Sciences 2006;48(12):1516–1524. URL: https://www.sciencedirect.com/science/article/pii/S0020740306001305. doi:https://doi.org/10.1016/j.ijmecsci.2006.06.008.

[83] Nagendra S, Jestin D, Gürdal Z, Haftka R, Watson L. Improved genetic algorithm for the design of stiffened composite panels. Computers and Structures 1996;58(3):543–555. URL: https://www.sciencedirect.com/science/article/pii/004579499500160I. doi:https://doi.org/10.1016/0045-7949(95)00160-I.

[84] Jia-qing Z, Wang L. Center Based Genetic Algorithm and its application to the stiffness equivalence of the aircraft wing. Expert Systems with Applications 2011;38(5):6254–6261. URL: https://www.sciencedirect.com/science/article/pii/S0957417410013448. doi:https://doi.org/10.1016/j.eswa.2010.11.106.

[85] Ben Rahmoune M, Hafaifa A, Mouloud G. Neural network monitoring system used for the frequency vibration prediction in gas turbine. In: 2015 3rd International Conference on Control, Engineering & Information Technology (CEIT). 2015, p. 1–5. doi:10.1109/CEIT.2015.7233185.

[86] Dey S, Mukhopadhyay T, Spickenheuer A, Gohs U, Adhikari S. Uncertainty Quantification in Natural Frequency of Composite Plates - An Artificial Neural Network Based Approach. Advanced Composites Letters 2016;25:43–48. doi:10.1177/096369351602500203.

[87] Shakeri M, Yas M, Gol M. Optimal Stacking Sequence of Laminated Cylindrical Shells Using Genetic Algorithm. Mechanics of Advanced Materials and Structures 2005;12:305–312. doi:10.1080/15376490590898501.

[88] António CC, Hoffbauer LN. Uncertainty assessment approach for composite structures based on global sensitivity indices. Composite Structures 2013;99:202–212. URL: https://www.sciencedirect.com/science/article/pii/S0263822312005880. doi:https://doi.org/10.1016/j.compstruct.2012.12.001.

[89] António CC, Hoffbauer LN. Uncertainty propagation in inverse reliability-based design of composite structures. Int J Mech Mater Des 2010;6:89–102. doi:10.1007/s10999-010-9123-5.

[90] Coello CC. A Comprehensive Survey of Evolutionary-Based Multiobjective Optimization Techniques. Knowledge and Information Systems 1 1999;:269–308URL: https://link.springer.com/article/10.1007/BF03325101#citeas. doi:https://doi.org/10.1007/BF03325101.

[91] Coello Coello CA. Recent Trends in Evolutionary Multiobjective Optimization; chap. 2. London: Springer London. ISBN 978-1-84628-137-2; 2005, p. 7–32. URL: https://doi.org/10.1007/1-84628-137-7_2. doi:10.1007/1-84628-137-7_2.

[92] Halffmann P, Schäfer LE, Dächert K, Klamroth K, Ruzika S. Exact algorithms for multiobjective linear optimization problems with integer variables: A state of the art survey. Journal of Multi-Criteria Decision

Analysis 2022;URL: https://onlinelibrary.wiley.com/doi/abs/10.1002/mcda.1780. doi:https://doi.org/10.1002/mcda.1780. arXiv:https://onlinelibrary.wiley.com/doi/pdf/10.1002/mcda.1780.

[93] Audet C, Bigeon J, Cartier D, Le Digabel S, Salomon L. Performance indicators in multiobjective optimization. European Journal of Operational Research 2021;292(2):397–422. URL: https://www.sciencedirect.com/science/article/pii/S0377221720309620. doi:https://doi.org/10.1016/j.ejor.2020.11.016.

[94] Irisarri FX, Bassir DH, Carrere N, Maire JF. Multiobjective stacking sequence optimization for laminated composite structures. Composites Science and Technology 2009;69(7):983–990. URL: https://www.sciencedirect.com/science/article/pii/S0266353809000074. doi:https://doi.org/10.1016/j.compscitech.2009.01.011.

[95] Ehsani A, Dalir H. Multi-objective optimization of composite angle grid plates for maximum buckling load and minimum weight using genetic algorithms and neural networks. Composite Structures 2019;229:111450. URL: https://www.sciencedirect.com/science/article/pii/S0263822319316393. doi:https://doi.org/10.1016/j.compstruct.2019.111450.

[96] Seyyedrahmani F, Khandar Shahabad P, Serhat G, Bediz B, Basdogan I. Multi-objective optimization of composite sandwich panels using lamination parameters and spectral Chebyshev method. Composite Structures 2022;289:115417. URL: https://www.sciencedirect.com/science/article/pii/S0263822322002112. doi:https://doi.org/10.1016/j.compstruct.2022.115417.

[97] Kheirikhah M. Multi-objective genetic algorithm optimization of composite sandwich plates using a higher-order theory. Journal of the Brazilian Society of Mechanical Sciences and Engineering 2020;42:523. doi:10.1007/s40430-020-02596-9.

[98] Manickam R, Kalita K. Weighted sum multi-objective optimization of skew composite laminates. Structural Engineering and Mechanics 2019;69:21–31. doi:10.12989/sem.2019.69.1.021.

[99] Narayanan G, Ragavendran U, Kalita K, Jain P, Gao XZ. Multi-Objective High-Fidelity Optimization Using NSGA-III and MO-RPSOLC. Computer Modeling in Engineering and Sciences 2021;129:1–22. doi:10.32604/cmes.2021.014960.

[100] An H, Chen S, Huang H. Multi-Objective Optimization of a Composite Stiffened Panel for Hybrid Design of Stiffener Layout and Laminate Stacking Sequence. Struct Multidiscip Optim 2018;57(4):1411–1426. URL: https://doi.org/10.1007/s00158-018-1918-2. doi:10.1007/s00158-018-1918-2.

[101] Murugesan Ph.D. M, Kang BS, Lee K. Multi-Objective Design Optimization of Composite Stiffened Panel Using Response Surface Methodology. Composites Research 2015;28:297–310. doi:10.7234/composres.2015.28.5.297.

[102] António CC. Local and Global Pareto Dominance Applied to Optimal Design and Material Selection of Composite Structures. Structutal Multidisciplinary Optimization 2013;48(1):73–94. URL: https://doi.org/10.1007/s00158-012-0878-1. doi:10.1007/s00158-012-0878-1.

[103] António CC, Hoffbauer LN. Bi-level dominance GA for minimum weight and maximum feasibility robustness of composite structures. Composite Structures 2016;135:83–95. URL: https://www.sciencedirect.com/science/article/pii/S0263822315008557. doi:https://doi.org/10.1016/j.compstruct.2015.09.019.

[104] Carneiro G, António CC. A RBRDO approach based on structural robustness and imposed reliability level. Structural and Multidisciplinary Optimization 2018;57. doi:10.1007/s00158-017-1870-6.

[105] António CC, Hoffbauer LN. Optimal design of composite shells based on minimum weight and maximum feasibility robustness. International Journal of Mechanics and Materials in Design 2017;13. doi:10.1007/s10999-015-9329-7.

[106] Smith PJ, Wilson RD. Damage Tolerant Composite Wing Panels For Transport Aircraft. Langley Research Center under Contract NAS 1-16863 1985;URL: https://ntrs.nasa.gov/citations/19890005816.

[107] Byers BA. Behavior of damaged graphite/epoxy laminates under compression loading. CONTRACT NASI-151Q07 1980;URL: https://ntrs.nasa.gov/citations/19820024544.

[108] Liu W, Butler R. Buckling Optimization for Composite Panels with Elastic Tailoring. 49th Structures, Structural Dynamics, and Materials Conference 2008;doi:10.2514/6.2008-2125.

[109] Ribeiro PL. Composite laminated plates. Plates and Shells 2021;.

[110] Reddy J. Mechanics of Laminated Composite Plates and Shells: Theory and Analysis (2nd ed.). CRC Press; 2003. ISBN 9780429210693.

[111] Gibson R. Principles of Composite Material Mechanics. Mechanical Engineering; CRC Press; 2016. ISBN 9781498720724.

[112] Matthews F, Rawlings R. Stiffness of unidirectional composites and laminates. In: Matthews F, Rawlings R, editors. Composite Materials; chap. 7. Woodhead Publishing Series in Composites Science and Engineering; Woodhead Publishing. ISBN 978-1-85573-473-9; 1999, p. 223–250. URL: https://www.sciencedirect.com/science/article/pii/B9781855734739500102. doi:https://doi.org/10.1016/B978-1-85573-473-9.50010-2.

[113] Matthews F, Rawlings R. Stiffness, strength and related topics. In: Matthews F, Rawlings R, editors. Composite Materials; chap. 6. Woodhead Publishing Series in Composites Science and Engineering; Woodhead Publishing. ISBN 978-1-85573-473-9; 1999, p. 206–222. URL: https://www.sciencedirect.com/science/article/pii/B9781855734739500096. doi:https://doi.org/10.1016/B978-1-85573-473-9.50009-6.

[114] Sayyad AS, Ghugal YM. On the free vibration analysis of laminated composite and sandwich plates: A review of recent literature with some numerical results. Composite Structures 2015;129:177–201. URL: https://www.sciencedirect.com/science/article/pii/S0263822315002779. doi:https://doi.org/10.1016/j.compstruct.2015.04.007.

[115] Ventsel E, Krauthammer T. Thin Plates and Shells: Theory: Analysis, and Applications. CRC Press; 2001. ISBN 9780203908723. URL: https://books.google.pt/books?id=nvny90yqgOYC.

[116] Aydogdu M, Timarci T. Free Vibrations of Antisymmetric Angle-Ply Laminated Thin Square Composite Plates. Turkish Journal of Engineering and Environmental Sciences 2007;31:243–249.

[117] Messina A, Soldatos KP. Vibration of completely free composite plates and cylindrical shell panels by a higher-order theory. International Journal of Mechanical Sciences 1999;41(8):891–918. URL: https://www.sciencedirect.com/science/article/pii/S0020740398000691. doi:https://doi.org/10.1016/S0020-7403(98)00069-1.

[118] Qing G, Qiu J, Liu Y. Free vibration analysis of stiffened laminated plates. International Journal of Solids and Structures 2006;43(6):1357–1371. URL: https://www.sciencedirect.com/science/article/pii/S002076830500123X. doi:https://doi.org/10.1016/j.ijsolstr.2005.03.012.

[119] Xue J, Wang Y. Free vibration analysis of a flat stiffened plate with side crack through the Ritz method. Archive of Applied Mechanics 2019;89. doi:10.1007/s00419-019-01565-6.

[120] Alanbay B, Singh K, Kapania R. Vibration of Curvilinearly Stiffened Plates Using Ritz Method With Orthogonal Jacobi Polynomials. Journal of Vibration and Acoustics 2019;142:1–49. doi:10.1115/1.4045098.

[121] Systèmes D. Getting Started with Abaqus: Interactive Edition. Dassault Systèmes; 2013. URL: http://130.149.89.49:2080/v6.13/books/gsa/default.htm?startat=ap03.html.

[122] Ramesh SS, Wang C, Reddy J, Ang K. A higher-order plate element for accurate prediction of interlaminar stresses in laminated composite plates. Composite Structures 2009;91(3):337–357. URL: https://www.sciencedirect.com/science/article/pii/S0263822309002050. doi:https://doi.org/10.1016/j.compstruct.2009.06.001.

[123] Burlayenko V, Altenbach H, Sadowski T. An evaluation of displacement-based finite element models used for free vibration analysis of homogeneous and composite plates. Journal of Sound and Vibration 2015;358:152–175. URL: https://www.sciencedirect.com/science/article/pii/S0022460X15006616. doi:https://doi.org/10.1016/j.jsv.2015.08.010.

[124] Paiva R, António CC, da Silva LFM. Optimal design of adhesive composition in footwear industry based on creep rate minimization. The International Journal of Advanced Manufacturing Technology 2016;84. doi:10.1007/s00170-015-7746-2.

[125] Oktem H, Erzurumlu T, Erzincanli F. Prediction of minimum surface roughness in end milling mold parts using neural network and genetic algorithm. Materials & Design 2006;27(9):735–744. URL: https://www.sciencedirect.com/science/article/pii/S0261306905000336. doi:https://doi.org/10.1016/j.matdes.2005.01.010.

[126] António CC, Davim JP, Lapa V. Artificial neural network based on genetic learning for machining of polyetheretherketone composite materials. The International Journal of Advanced Manufacturing Technology 2008;39:1101–1110. doi:10.1007/s00170-007-1304-5.

[127] Ewins D. Modal Testing: Theory, Practice and Application. Engineering dynamics series; Wiley; 2000. ISBN 9780863802188. URL: https://books.google.pt/books?id=Z4QoAQAAMAAJ.

[128] Ray C, Satsangi SK. Laminated Stiffened Plate-A First Ply Failure Analysis. Journal of Reinforced Plastics and Composites 1999;18(12):1061–1076. URL: https://doi.org/10.1177/073168449901801201. doi:10.1177/073168449901801201. arXiv:https://doi.org/10.1177/073168449901801201.

[129] Satish Kumar Y, Srivastava A. First ply failure analysis of laminated stiffened plates. Composite Structures 2003;60(3):307–315. URL: https://www.sciencedirect.com/science/article/pii/S0263822302003501. doi:https://doi.org/10.1016/S0263-8223(02)00350-1.

[130] Camanho PP. Failure criteria for fibre-reinforced polymer composites. In: FEUP. Secção de Mecânica Aplicada. 2002, p. 1–11.